I-125-labeled Triplex-Forming-oligonucleotides: Studies on intracellular distribution, cytotoxicity and on gene expression alterations of target genes

Inaugural-Dissertation

zur

Erlangung des Doktorgrades

Dr. rer. nat.

der Fakultät für

Biologie

an der

Universität Duisburg-Essen

Standort Essen

vorgelegt von

Volker Dahmen

aus Düren

März, 2013

Die der vorliegenden Arbeit zugrunde liegenden Experimente wurden am Institut für Sicherheit und Strahlenschutz des Forschungszentrums Jülich GmbH durchgeführt.

1. Gutachter: Prof. Dr. Georg Iliakis
2. Gutachter: PD Dr. Jürgen Thomale

Vorsitzender des Prüfungsausschusses: Prof. Dr. Hemmo Meyer

Tag der mündlichen Prüfung: 11.09.2013

Danksagung

Herrn Prof. Dr. George Iliakis danke ich für die Bereitstellung des interessanten Themas und für die Übernahme des Gutachtens.

Besonderer Dank gilt Herrn Dr. Ralf Kriehuber für die umfassende und lehrreiche Betreuung meiner Promotion. Ebenso danken möchte ich ihm für viele motivierende und inspirierende Gespräche.

Außerdem möchte ich meiner Kollegin und Sitznachbarin Frau Dr. Katja Knops sehr danken, die immer ein offenes Ohr für wissenschaftliche und auch weltliche Fragen und Probleme hatte und meine Zeit im Labor sehr bereichert hat.

Frau Dr. Sabine Schäfer, Herrn Dr. Martin Ostapczuk und Frau Christiane Federlin-Dahmen möchte ich für das Korrekturlesen der Arbeit und so manchem aufbauenden Gespräch danken.

Weiterhin bedanken möchte ich mich bei Marcel von Ameln, Dominik Oskamp, Dr. Sabine Schmitz, Marcus Unverricht-Yeboah und allen weiteren Mitarbeitern der AG Strahlenbiologie für fachliche Unterstützung und insbesondere für eine tolle Arbeitsatmosphäre, die den morgendlichen Weg zur Arbeit stets einfach gemacht hat.

Herrn Dr. Burkhard Heuel-Fabianek und Dr. Ekkehard Pomplun möchte ich für ihre Unterstützung und die Möglichkeit danken meine Arbeit in den Laboren des Instituts für Sicherheit und Strahlenschutz durchzuführen.

Mein ganz besonderer Dank gilt meiner Frau Christiane für ihre immer währende Unterstützung und Rückhalt insbesondere in den sehr schwierigen Abschnitten dieser Arbeit.

Ebenfalls besonders danken möchte ich meinen Eltern für die fortwährende Unterstützung während meines Studiums, der Promotion und darüber hinaus. Sie haben diese Arbeit erst möglich gemacht.

Abbreviations

A	Adenine
AEE	Auger-electron emitter
APS	Ammonium persulfate
ATM	Ataxia Telangiectasia Mutated
ATR	Ataxia Telangiectasia and RAD3 Related Kinase
C	Cytosine
CdR	2´-Deoxycytidine hydrochloride
Cdk	Cyclin-dependent kinase
Chk1	Checkpoint kinase 1
Chk2	Checkpoint kinase 2
G	Guanine
dATP	2´-deoxyadenine-5´-triphosphate
dCTP	2´-deoxycytidine-5´-triphosphate
DDR	DNA Damage Response
dGTP	2´-deoxyguanine-5´-triphosphate
dNTP	2´-deoxynucleoside-5´-triphosphate
dTTP	2´-deoxythymidine-5´-triphosphate
DMSO	Dimethyl sulfoxide
DNA	Deoxyribonucleic Acid
DSB	Double-Strand Break
EMSA	Electrophoretic Mobility Shift Assay
FBS	Fetal Bovine Serum
FUdR	5-Fluoro-2´-deoxyuridine
FITC	Fluorescein
FSC	Forward Scatter
IdU	5-Iodo-2´-deoxyuridine
MBR	Major Breakpoint Region
MBS	Multi-Binding-Site
Mdm2	Murine double minute 2
MDS	Multiply Damaged Site
MEM	Minimal Essential Medium Eagle

MN	Micronuclei
mRNA	messenger RNA
PPG	6-aminopyrazolo[3,4-*d*]pyrimidine-4(*3H*)-one-(8-aza-7-deazaguanine)
PQS	Putative Quadruplex Sequence
QFO	Quadruplex-Forming-Oligonucleotide
RBE	Relative Biological Effectiveness
RNA	Ribonucleic Acid
ROS	Reactive Oxygen Species
ROX	5-carboxy-X-rhodamine
RT	room temperature
7-AAD	7-aminoactinoymycin D
SBS	Single-Binding-Site
SSC	Side Scatter
T	Thymine
TFO	Triplex-Forming-oligonucleotide
Tm	Melting temperature
Tris	Tris-(hydroxymethyl)-aminomethan
TTS	Triple-Helix Target Site

Contents

List of Figures

List of Tables

Abstract

Purpose: Triplex-forming-oligonucleotides (TFOs) are able to bind DNA in a sequence-specific manner and are a promising tool to manipulate genes or gene regulatory units in a cellular environment. TFOs posses also a therapeutic potential e.g. as a carrier molecule for Alpha- or Auger-electron-emitter (AEE) to target specific DNA sequences in tumor cells. A method for the effective labeling of TFOs with the AEE iodine-125 (I-125) was established and the ability of I-125-labeled TFOs to induce site-specific double-strand breaks (DSB) in DNA was investigated. Moreover analysis of the influence of I-125-labeled TFOs in transfected SCL-II cells with regard to cell survival, DNA damage and the induction of cell cycle arrest were performed. Furthermore the ability of I-125-labeled TFOs to alter gene expression of targeted genes was examined.

Methods: For that purpose two groups of TFOs were designed – TFOs specific for single targets in the genes *BCL2*, *BRCA1* and *GAPDH* and multi-binding TFOs with several thousand binding sites in the whole genome. The cellular distribution and persistence of TFOs was analyzed via flow cytometry and the I-125 labeling was performed using a modified primer extension method. Cell survival was analyzed with the colony forming assay. DNA DSB were determined using the 53BP1 assay and the micronucleus assay. The analysis of cell cycle was done after 7-aminoactinomycin D (7-AAD) cell staining by flow cytometry. Gene expression alteration of targeted genes was tested via quantitative Real-Time PCR with RNA isolates from transfected SCL-II cells.

Results: A persistence of intact TFOs in a cellular environment for at least 72 h could be confirmed. For all tested I-125-labeled TFOs an increased cytotoxicity and DNA damaging potential was detected. Moreover, the degree of cytotoxicity seemed to depend on target localization as well as on target quantity. A pronounced induction of cell cycle arrest in G_2/M-phase 8 h post-transfection could also be detected. The gene-specific binding of I-125-labeled TFOs led to a significant down-regulation of *GAPDH* and an almost 2-fold up-regulation of *BCL2* gene expression. The *BRCA1* gene expression did not show any alteration.

Conclusions: The magnitude of an I-125-labeled TFO induced cytotoxic effect can be influenced by the total number of targets as well as by the distinct location of a single target. Therefore targeting many non-crucial targets can be as cytotoxic as targeting one single, but crucial target and vice versa. Additionally, single gene targeting can alter gene expression in a gene-specific manner.

1. Introduction

1.1. Discovery of DNA Triplex Structures

Since the end of the 19th century it has been known that cells contain nucleic acids, discovered by Friedrich Miescher in 1869, who isolated various phosphate-rich chemicals from leukocyte nuclei [22] and named them nuclein. The role of DNA as the source of genetic information was discovered not until 1944 by O. T. Avery [6] and thereafter it took almost further ten years, when Watson and Crick discovered, in 1953, the double-helix structure of the DNA [140]. In 1957 Felsenfeld at al. were able to show that DNA does not exclusively appear in a double-helix structure, when they detected a DNA structure composed of three polynucleotide strands, forming a triplex structure in the presence of divalent cations [33]. This structure consists either of one polypurine strand and two polypyrimidine strands or one polypyrimidine and two polypurine strands [108, 78]. Thereby the two complementary strands form a DNA double-helix and the third strand is located in the major groove of the DNA double-helix, associated via non-Watson-Crick hydrogen bonds [33, 13]. The respective hydrogen bonds are nowadays known as Hoogsteen hydrogen bonds [55]. Within the following two decades not much effort was dedicated to DNA triplex research. Only in the late 1980s the discoveries of several groups generated new impetus for DNA triplex related research. In 1986 Le Doan et al. could show that homopyrimidine oligonucleotides are able to form stable complexes with homopurine-homopyrimidine sites on duplex DNA in a sequence-specific manner [72]. Moreover a novel DNA conformation, in supercoiled plasmids, was discovered, whose major structural element was a triplex structure. This DNA formation was named H-DNA [86, 91]. It was not until 1994 when Panyutin et al. [96] introduced triplex-forming-oligonucleotides (TFOs) as possible carrier molecules for radionuclides, which were able to deliver the radionuclides in a sequence-specific manner into close proximity to the DNA and induce DNA double-strand breaks in specified genes. With that they lay the foundations for what was established in the first decade of the 21st century as the antigene radiotherapy [100, 119, 98].

1.2. Structure of the DNA Triple Helix

The basic unit of a triple helix structure is a construct of three bases, called a triplet. Two of these bases form a classical Watson-Crick base pair consisting of two complementary bases connected by two (Adenine - Thymine) or three (Guanine - Cytosine) Watson-Crick hydrogen bonds. The third base is connected to the base pair via non-Watson-Crick hydrogen bonds, called Hoogsteen hydrogen bonds [55]. The third base can only bind to the purine already engaged in the Watson-Crick base pair. All combinations of base triplets, important for the present work, are displayed in *Figure 1.1* and were first investigated and described by Letai et al. in the third strand binding code [75].

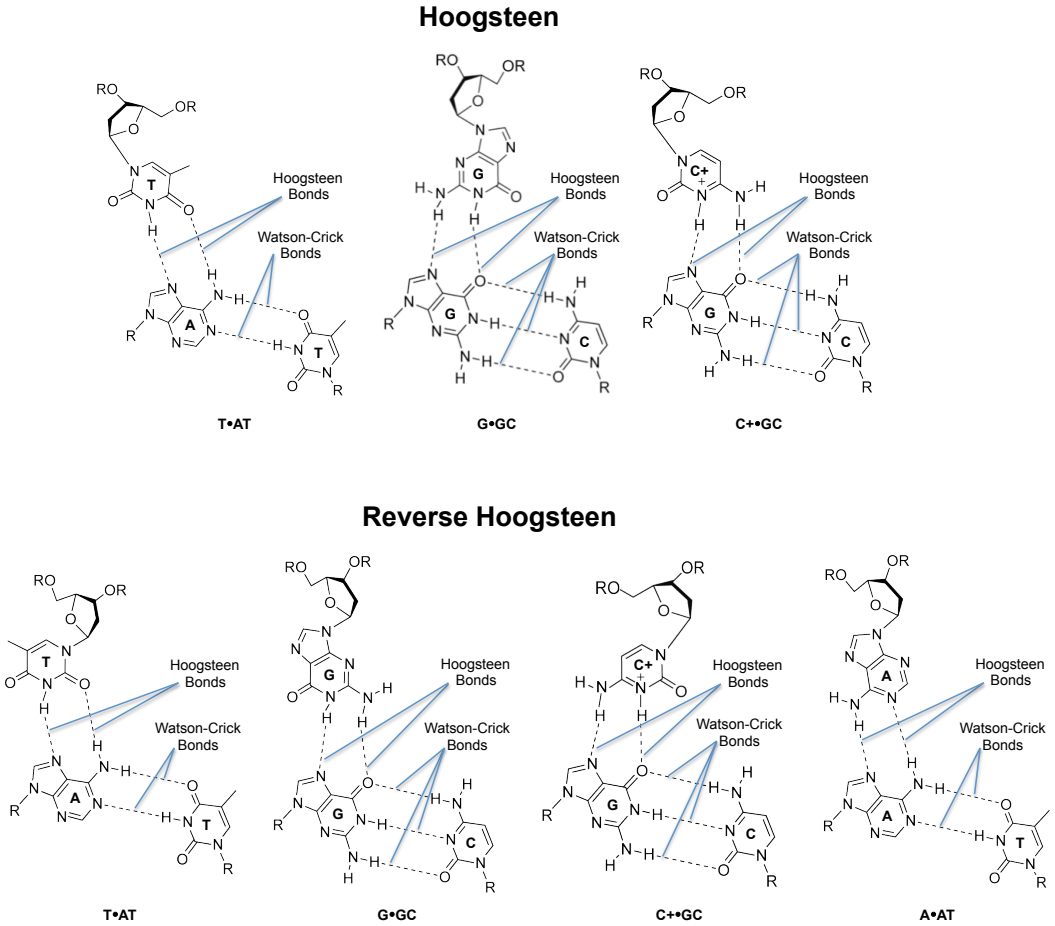

Figure 1.1.: Base triplets consisting of Watson-Crick A-T and G-C base pairs bound to T, G and protonated C in Hoogsteen conformation (upper picture) and to T, G, A and protonated C in reverse Hoogsteen conformation (lower picture). (Figure modified according to Copyright© ATDBio Ltd. 2005-2012)

Binding of the third base to the purine is possible in two different conformations. The first conformation is conform to the structure discovered by Hoogsteen [55] and is therefore called Hoogsteen conformation. In the second conformation the third base

is twisted by 180° and is therefore called reverse Hoogsteen conformation. The bases guanine, thymine and cytosine are able to bind in both orientations whereas adenine can only attach to the purine base in reverse Hoogsteen conformation [75]. An oligonucleotide can only form a triple helix when being located in the major groove of a double-helix [37, 55] and when all bases of the third strand can adopt the same conformation. The conformation of the third strand leads to a dedicated 5´- 3´orientation in relation to the homopurine strand of the DNA target strand. If the bases in the third strand are in Hoogsteen conformation, this corresponds to a parallel orientation of the third strand in relation to the homopurine strand of the DNA target strand [72] (*Figure 1.2*). A reverse

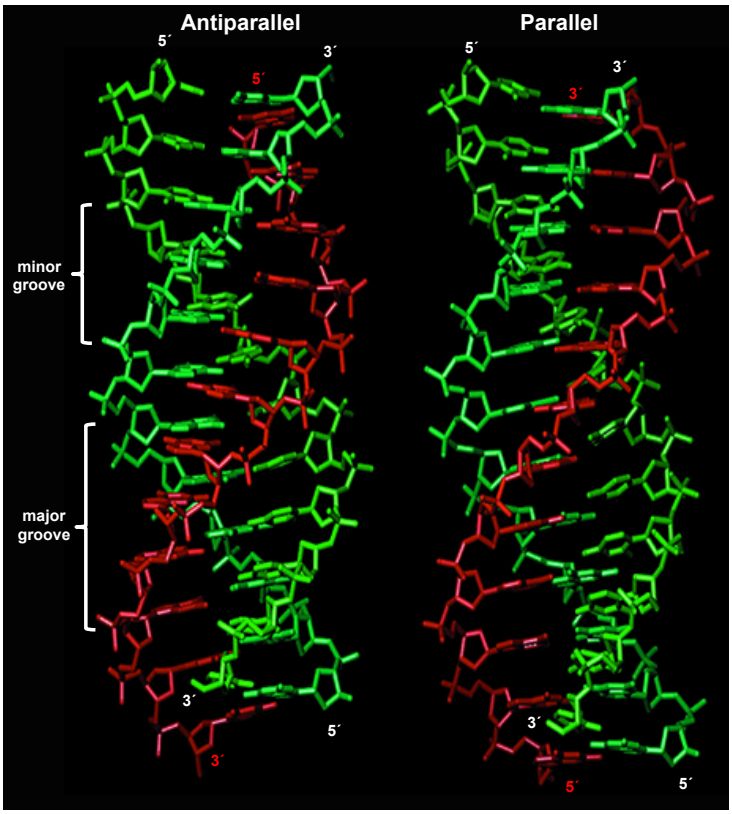

Figure 1.2.: Model of the X-ray crystal structure of a triplex-forming-oligonucleotide (red) located in the major groove of a DNA target strand (green) in antiparallel (left) and parallel (right) orientation. (Figure modified according to Vlieghe et al. [136]).

Hoogsteen conformation corresponds to an antiparallel orientation of the third strand [8] (*Figure 1.2*). Universally, oligonculeotides able to form a triple helix are termed as triplex-forming-oligonucleotides (TFOs).

1.3. Triplex-Forming-oligonucleotides

TFOs are able to bind complementary DNA sequences, by forming triple helices, in a sequence-specific manner according to the third-strand binding code [75]. This means that only if the bases of the TFO match the double-strand base sequence, corresponding to the triplet combinations shown in *Figure 1.1*, the formation of a triple helix can occur. Triple helices almost exclusively form at homopurine-homopyrimidine sequences in the DNA, with all purines located on one strand [72]. A purine sequence switching once between the two strands does not inhibit triplex formation on principle but makes a modification of the corresponding TFO necessary [24]. Homopurine-homopyrimidine sequences of adequate length are so-called triple-helix target sites (TTSs). TTSs appear at a high frequency in the human genome especially in promoter regions [44, 45]. The adequate length of a target region and accordingly the length of a TFO necessary for the specific recognition of a unique DNA sequence depends on the size of the genome. In case of the human genome, consisting of $\sim 3x10^9$ base pairs, a minimum of approximately 17 base pairs must be recognized by the TFO for a specific binding [15]. However, when designing a TFO it has to be taken into account that the binding capabilities of the TFO are not determined by the base composition and the orientation only. The bond-angles, bond-lengths and the binding strength of the different base triplets are also of importance when designing a TFO [9, 131].

1.3.1. Design of Triplex-Forming-oligonucleotides

1.3.1.1. Bond-Angles and Bond-Lengths of Base Triplets

The bond-angles and -lengths of base triplets refer to the C1-atom of the nucleotides in the third strand, when the C1-atoms of the Watson-Crick base pair are used as fixed points. If the angles and lengths of two triplet structures are equal the triplets are termed as isomorphous. Shown in *Figure 1.3* are the bond-angles and -lengths of the potential triplets. When a TFO binds within the major groove of a double-strand a minimal deformation of the TFO backbone is necessary. To fascilitate this structural adaption the angles and lengths of the TFO triplets should be as isomorphic as possible. The lower the degree of isomorphism the more deformation of the TFO backbone is needed to enable a triplex formation. As visible in *Figure 1.3* only two triplets are truly isomorphous. Solely T*A·T and C^{+}*G·C[1] in Hoogsteen conformation show similar

1 A Hoogsten bond is indicated by a "*" and a Watson-Crick bond by a "·".

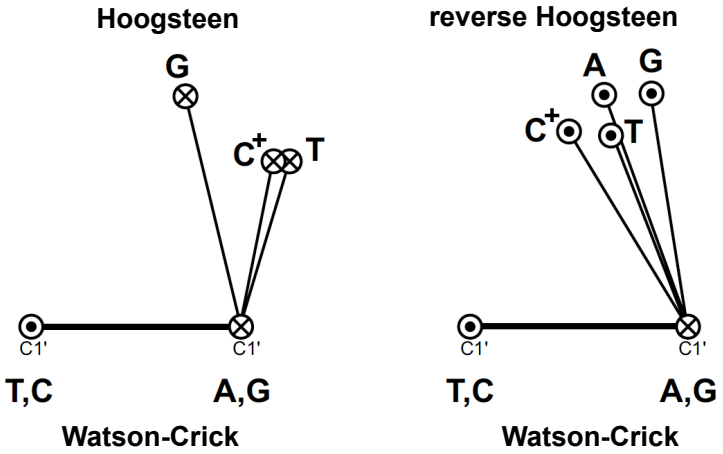

Figure 1.3.: Angles and lengths of base triplets. The angle refers to the C1-atom of the third strand nucleotide in relation to the C1-atoms of the Watson-Crick base pair located at fixed positions. The bond length is the distance between the C1-atom of the purine base engaged in the Watson-Crick base pair and the C1-atom of the third base. The C1-atoms of the third strand base are shown in either the Hoogsteen or the reverse Hoogsteen conformation. (Figure modified according to Thuong and Hélène [131])

bond-angles and -lengths. The combination of non-isomorphous triplets in a triple helix leads to a stronger distortion of the DNA helix backbone in order to minimize the effect of the non-isomorphism, leading to a reduced stability of the triple helix [131]. However, non-isomorphous triplet combinations are nonetheless able to form triple helices with homopurine-homopyrimidine DNA sequences. TFOs containing G and T [20], G and A [8] or G, T and C [42] have been shown to form triple helices as well.

1.3.1.2. Bond Stability of Single Base Triplets

In thermal denaturation and affinity cleaving experiments it could be shown that the most stable triplets are A*A·T, G*G·C and T*A·T in reverse Hoogsteen conformation. Triplet formation could also be shown for the triplet combinations C*A·T, A*G·C and T*C·G but with an almost 50% reduced bond stability in comparison to the strongest triplets [9]. A special case represents cytosine when engaged as the third base in a C*G·C triplet. Cytosine does built strong triplets but it can only form a triplet when protonated at the N3 nitrogen. Therefore, triplex formation of cytosine containing TFOs is rather pH dependent with a reduced stability at physiological and higher pH values [131].

1.3.2. Types of Triplex-Forming-oligonucleotides

The multiple characteristics of the basic TFO units, the triplets, lead to a multitude of different TFO combinations within the performed studies. In most of the early works TFOs were composed of thymine and cytosine [50]. Mainly because of their isomorphous structure facilitating the binding of the TFO in the major groove of the double-helix. However, the reduced binding abilities of cytosine containing TFOs at physiological or higher pH led to further investigations and the use of TFOs consisting of guanines and adenines, which built also strong hydrogen bonds and were mostly pH independent [8]. The guanine, adenine TFOs were first used in parallel orientation to the duplex purine strand but triplex formation could not be confirmed . Only when used in antiparallel orientation the triplex formation could be realized [8]. Furthermore Beal et al. [8] could show that replacing adenine with thymine leads to increased triplex stability. Finally, two basic types of TFOs evolved. The pyrimidine type TFOs binding with reverse Hoogsteen bonds in antiparallel orientation to the double-helix, and the purine type TFOs binding with reverse Hoogsteen bonds in antiparallel orientation. Both types show different characteristics and abilities with regard to pH dependance, available ions or formation of secondary structures. Therefore, the TFO type of choice depends on the desired application.

1.3.2.1. Pyrimidine Type

A TFO of the pyrimidine type consists always of T*A·T and C*G·C base triplets thus the TFO sequence is fully determined by the sequence of the duplex. Cytosine and thymine are the only isomorphous bases and can therefore form a regular backbone conformation of the third strand [129]. In order to form a triplex the cytosine needs to be protonated at the N3 nitrogen. This limits pyrimidine type TFOs to the use in acidic conditions. Referring to the base triplet conformations both bases are able to adopt the Hoogsteen as well as the reverse Hoogsteen conformation. However, Beal et al. [8] reported that TFOs of the pyrimidine type can only form a triple helix in reverse Hoogsteen conformation.

1.3.2.2. Purine Type

In contrast to the pyrimidine TFOs whose third strand sequence is completely determined by the sequence of the duplex, the situation is different for purine TFOs. A purine

TFO can consist of the bases guanine, cytosine and thymine allowing the following combinations: G*G·C, A*A·T and T*A·T. The triplex formation with a purine type TFO is almost pH independent and is therefore preferred for triplex formation under physiological conditions [38]. However, purine type TFOs need the presence of divalent cations like magnesium, whereas monovalent cations like potassium inhibit the triplex formation. The cellular concentration of magnesium is sufficient but the high concentration of potassium in turn induces an inhibitory effect on the triplex formation [109, 18]. The inhibitory effect of monovalent cations is particularly obvious in purine type TFOs engaging guanine and adenine. Moreover these tend to form self-associated dimers (homoduplexes), inhibiting the triplex formation [94]. This effect is less pronounced when the adenine is replaced with thymine and the TFOs bind in reverse Hoogsteen conformations [8]. A further cation-linked effect, appearing in both purine type TFOs, is the formation of secondary structures such as G-quartetts. These G-Quartetts are mainly formed by TFOs containing repetitive sequence tracks of four or more guanines in a row [106]. Modification of the guanines were developed for the minimization of the G-quartett appearance, e.g. replacing all or some of the guanines in the TFO with 2´-deoxy-6-thioguanosines, was clearly shown to reduce G-quartett formation [106]. Notwithstanding the fact that thymine is a pyrimidine, these TFOs are nevertheless counted among the purine type TFOs. On the basis of their bond stability and ability to form triplices under physiological conditions, most of the TFOs employed in the present work are guanine, thymine TFOs binding in reverse Hoogsteen conformation.

1.4. Applications for TFOs

What makes TFOs an interesting tool for a multitude of cellular applications is their capability of site-specific recognizing DNA sequences in the duplex DNA and to remain at their point of action for long enough to efficiently interfere in a direct or indirect manner with DNA related processes [16, 118]. TFOs binding to specific regions of the DNA in a cellular environment are able to inhibit replication, modulate transcription and induce site directed mutagenesis and recombination [16].

A way to inhibit DNA replication is the usage of a TFO targeting the region upstream of the initiation site [47], where the TFO of action inhibits the binding of the DNA polymerase to the DNA double-strand. Another mode is the blockage of the progressing replication fork with a TFO binding downstream of the initiation site, though requiring a modification of the TFO to increase the binding strength, which is often achieved with a psoralen induced cross-link [111, 27]. A comparable approach can be used for the

TFO based modulation of transcription. A TFO positioned within the promotor region of a specific gene is able to block the binding of transcription factors and thereby inhibiting the transcription initiation [105]. Inhibition of the transcriptional elongation can be achieved by a TFO that binds tightly within the coding region and blocks the progression of the RNA-polymerase [144]. TFOs can also be used for the site-specific induction of DNA damage, thereby increasing the frequency of mutation and recombination. Therefore TFOs are most often coupled to mutagenic agents, which are then juxtaposed by the TFO to site-specific regions of the DNA. A frequently used mutagenic agent is psoralen which is activated by UVA radiation and then intercalates with DNA and covalently cross-links thymines on both DNA strands [130]. The psoralen induced cross-link does not only lead to an increased mutation frequency [138] but also enhances recombination and gene conversion at the targeted site [32]. The basic term for the TFO based gene modulation is "antigene strategy", which also involves the special field of "antigene radiotherapy" (1.5). The antigene radiotherapy is the generic term for damaging selected genes by a high dose of radiation from radionuclides delivered to this gene by specific DNA-binding molecules [99]. In antigene radiotherapy TFOs are employed as carrier systems for radiochemicals. They mediate the highly precise positioning of the carried compounds at their point of action along with a decline of non-specific side effects [99].

1.5. Antigene Radiotherapy

The antigene radiotherapy represents an alternative therapeutic approach in radiation based tumor therapy, compared to conventional radiotherapy. One severe disadvantage of conventional radiotherapy are the pronounced side effects on non-cancerous tissues due to dose delivery to normal cells. Thus a major task in radiotherapy is the minimization of radio-damage to the surrounding normal tissues while maximizing the radiation dose delivered to the tumor. For external irradiation this task is very complicated to accomplish. Selected radionuclides induced directly into tumorous tissue improve somehow the restraints of conventional therapy. A more promising approach is the use of TFOs as a carrier system for short-range particle emitting radionuclides, which is the basis of the antigene radiotherapy. Radiolabeled TFOs are able to target selected genes with high specificity, and thereby locate the carried radionuclide in close proximity to the DNA [100]. The specificity of the TFO enables the targeting of sequences exclusively appearing in cancerous cells and not in normal cells, reducing possible side-effects [98]. Moreover the closeness of the radionuclide to its target enables the use of radionuclides with special characteristics that again reduce the side-

effects to the surrounding tissue. These characteristics shall include that the radiation primarily emitted has low energy and therefore a very limited range in tissue or employs particles with short track lengths in tissue such as α-particles. A consequence of using radionuclides emitting low energy electrons is, that most of the energy will be deposited in a very small volume around the decay site. The considered nuclide shall have a half-life matching the pharmacokinetics of the carrier molecule in the cell. The most promising radionuclides for this approach is the group of Auger-electron emitting radionuclides (AEE) (1.6). Suitable AEE for the antigene radiotherapy include In-111 (67 h)[2], I-123 (13.2 h) or Br-77 (57 h). For *in vitro* experiments the most convenient AEE is I-125 (60 d). Within a first approach Sedelnikova et al. and Panyutin et al. were able to induce specific DSBs in the human *mdr1* gene by using a I-125-labeled TFO transfected into purified nuclei, digitonin permeabelized cells and in intact cells [119, 99]. However, the DNA DSB induction per decay was reduced by a factor of $\sim$ 10, when compared to targeting isolated DNA.

1.6. Auger-Electron Emitters

1.6.1. Auger Electrons

Auger electrons were discovered by Pierre Victor Auger in 1923. He reported that the irradiation of a cloud chamber with X-ray photons resulted in the appearance of multiple electron tracks. He concluded that these electrons originated in correlation to the ejection of inner shell electrons from the irradiated atoms [5].

1.6.2. The Generation of Auger Electrons

The emission of Auger electrons is correlated with inner shell electron vacancies. Processes leading to an inner shell vacancy are electron capture[3] (EC), internal conversion[4] (IC) or irradiation of nuclides with low energy X-ray photons (photoelectric effect[5]) [29, 51]. These vacancies are rapidly filled by a transition of an higher shell electron, which in turn creates another vacancy that is again filled by the transition of an even

2 In parentheses is the half-life in hours (h) or days (d).
3 An electron from an inner shell is captured by the nucleus, converting a proton into a neutron and a neutrino is emitted.
4 The γ-quant released by the excited atomic nucleus interacts with an electron in one of the lower atomic shells, causing the emission of the electron.
5 The emission of electrons from material as a result of being struck by photons.

higher shell electron. Each transition results in the emission of either a characteristic atomic X-ray photon or an Auger, Coster-Kronig, or super Coster-Kronig low-energy electron [21], collectively termed as Auger electrons (*Figure 1.4*). Like that, one single decay event can lead to the emission of a cascade of Auger electrons, and creates a highly positive charged daughter atom [62].

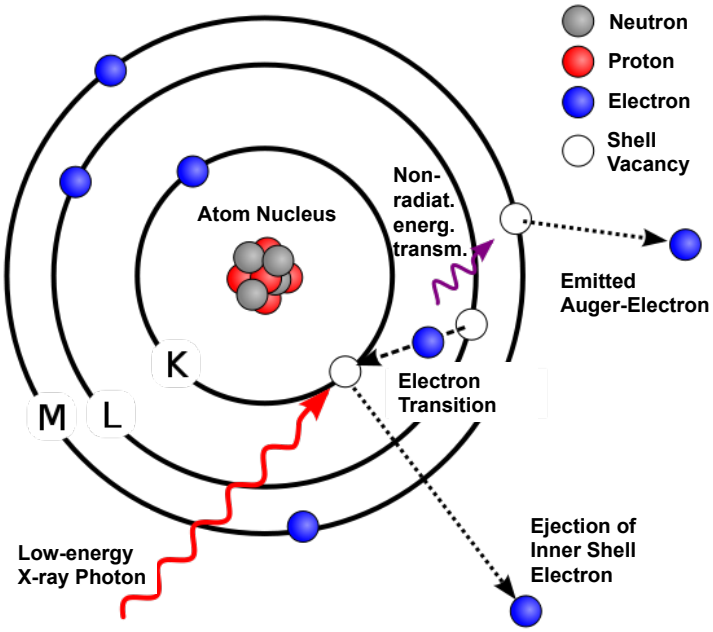

Figure 1.4.: Schematic presentation of the Auger effect as a result of the photoelectric effect. (Figure modified according to http://de.wikipedia.org/wiki/Augerelektronenspektroskopie/Auger-Effekt)

1.6.3. Characteristics of Auger Electrons

Auger electrons are low energy and short-range electrons released by EC or IC decay processes [62]. During the decay of an Auger emitter up to about 30 Auger electrons are emitted, depending on the isotope, with energies ranging between few eV to several keV [63]. Most Auger electrons posses low energies of $\sim$ 20 - 500 eV [57]. As all electrons, Auger electrons do not travel linearly in matter but in contorted paths and their range in water totals, due to their low energies, between few nanometers and 0.5 μm. Therefore most of the energy is deposited in a very small volume around the decay site. Since one decay produces multiple Auger electrons a high density of ionizations is produced in a few nanometer sphere around the decay site [62].

1.6.4. Radiobiological Effects of Auger Electrons

The deposition of high energies in a small volume make Auger-electron emitting radioisotopes very interesting as DNA damaging agents [70, 68], provided they are in close proximity to their DNA target. It could be demonstrated that I-125, which is one of the most extensively investigated Auger electron emitters (AEE), incorporated in nuclear DNA possesses a high DNA damaging potential, whereas the damage to the cellular environment was found to be only minor [81]. Most of the induced damage is displayed in the form of single-strand breaks (SSB), double-strand breaks (DSB), base damage, DNA-protein-cross-links, and locally multiply damaged sites (LMDS)[6]. The majority of these damages is accurately repaired by the cell except for DSB and LMDS, whose repair is more difficult and frequently erroneous [63, 139, 48]. These features are accountable for the high relative biologic effectiveness (RBE)[7] of Auger emitters. However, the observed effects are not only caused by the "high local deposition of radiation energy from short-range Auger electrons (the radiation component)" [82] but depend also on the influence of hydrogen radicals generated by radiolysis of the surrounding water [137] and the neutralization effect of the highly positive charged daughter atom [82]. The neutralization by charge transfer from the surrounding bases can lead to destabilization and damage of the bases due to the so-called Coulomb explosion [104].

1.6.5. DNA Damaging Effect of Auger Electrons

Due to the low energies and short track lengths of Auger electrons, they dissipate most of their energy in a few nanometer sphere around the decay site [65, 62]. Therefore, the damage induced by Auger electrons in DNA highly depends on the localization of the Auger electron emitter (AEE) e.g. I-125 in relation to the target [81, 64]. Schmidt and Hotz could show that one decay of I-125 incorporated in DNA as the thymidine analog I-125-iododeoxyuridine ((I-125)IdU), leads on average to one DSB per decay [114]. Additionally Martin and Haseltine [89] could determine that more than 70% of the induced breaks by DNA incorporated I-125 occur in a sphere of 5 bp around the decay site. Although DNA damage could be observed up to 7 nm of the decay site they postulated that for the maximum efficiency of DSB induction the distance of I-125 to the

6 **Def. LMDS:** "Any of a wide variety of complex lesions, including base damage as well as double-strand breaks, produced by "spurs" and "blobs" from a high-LET track." [48]

7 **Def. RBE:** "The RBE of some test radiation (r) compared with X-rays (250 keV) is defined by the ratio D_{250}/D_r, where D_{250} and D_r are, respectively, the doses of X-rays and the test radiation required for equal biological effect." [48]

DNA should not exceed 2 nm [89]. This postulation was confirmed by Kassis et al. who showed that the DSB induction of I-125 positioned in close vicinity of the DNA (<1 nm) by usage of the minor groove binder I-125-iodo-Hoechst 33342 led to a similar Decay-DSB ratio of 1.08 DSB/decay as observed after DNA-incorporation of I-125 [64]. With further increasing distance of I-125 to the DNA, using modified Hoechst derivatives, the DSB yield decreased (0.52 - 0.10 DSB/decay) inversely proportional to increasing distance [7]. The usage of a major groove binding TFO, which positions the I-125 further away from the DNA than Hoechst 33342, a DSB ratio of 0.46 DSB/decay was reported [101], which is in good agreement with the observed coherence of distance and DSB induction by Balagurumoorthy et al. [7] and Kassis et al. [64]. Additionally the delivery via TFO allows the sequence-specific positioning of the I-125, respectively, the targeted induction of DSB at a defined positions in the DNA, whereas (I-125)IdU and I-125-iodo-Hoechst derivates are randomly distributed in the DNA. Adelstein at al. [2] postulated that there are two mechanisms for DSB production by Auger emitters in DNA, packed as chromatin. A direct effect at the immediate site of decay and one indirect effect at many bases away from the decay site. However, the indirect effect was significantly decreased experimentally in the presence of DMSO whereas no effect could be observed on the direct effect. That led to the assumption that the scavenging effect of DMSO reduced the effect of reactive oxygen species (ROS) created by the Auger decay and the subsequent radiolysis of water [2]. Since the focus of the present work was on the site specific damaging potential of I-125-TFOs, all experiments in cells were performed in the presence of DMSO. Hence it can be assumed that all observed effects are due to the postulated direct effect of AEE.

1.6.6. Cytotoxicity of Auger Electrons

One measure of radiotoxicity is the fraction of cells having lost their infinite capability to reproduce after exposure to ionizing radiation. Consequently, cells still able to reproduce infinitely is represented by the survival fraction. In general cell survival data are plotted as the logarithm of the survival fraction as a function of applied radiation dose. The mathematical modeling of survival curves produces individual shaped curves characteristic for certain radiation qualities. There are two basic shapes of cell survival curves. The exponential survival curve, which reflects cell killing by high-LET or densely ionizing radiation and the linear quadratic shape, corresponding to low-LET or sparsely ionizing radiation [12] (*Figure 1.5*).

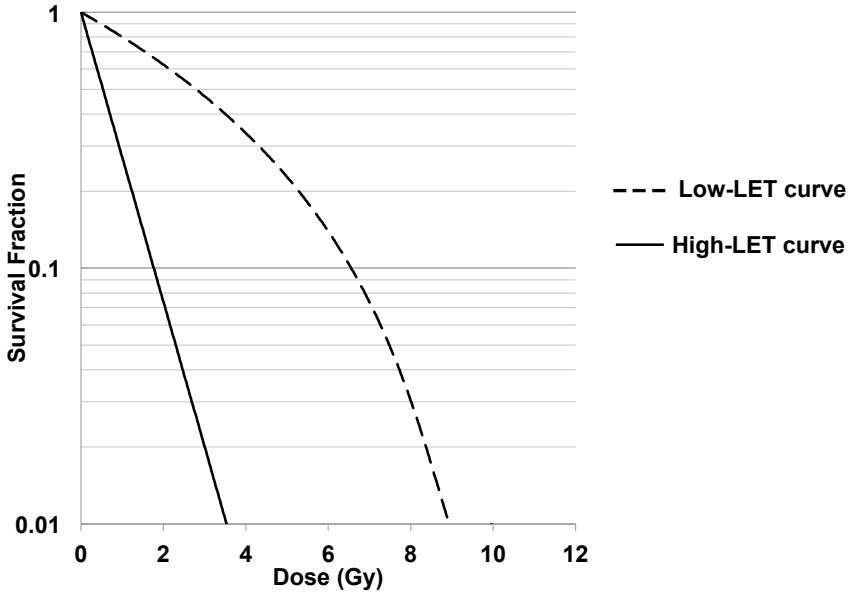

Figure 1.5.: Cell survival of mammalian cells after high- or low-LET irradiation. The high-LET survival curve reflects the straight exponential cell killing model of densely ionizing radiation. The low-LET survival curve reflects the linear-quadratic model of cell killing of sparsely ionizing radiation.

Sparsely ionizing radiation e.g. X-rays or β-radiation produce especially at lower doses repairable sublethal damage. The effects of this damage are reflected in the characteristic shoulder of the curve in the low dose range. With increasing dose the sublethal damage accumulates and leads to lethal damage and a more exponential decrease of the survival fraction (single-target, two hits model [127]). In contrast, for densely ionizing radiation it is assumed that each decay or hit of the target produces a lethal damage and is therefore called single-target, single-hit model [127]. In consequence, the survival fraction diminishes in an straight exponential way with increasing dose. The damage produced by Auger electron emitter (e.g. I-125) when incorporated or covalently bound to DNA is highly cytotoxic. Decays, sufficiently close to the relevant target, are supposed to cause lethal hits and thereby cause an exponential reduction of cell survival. Therefore Auger electron emitter causes high-LET like survival curves in mammalian cells [62, 69].

1.6.7. Cell-Cycle Arrest caused by Auger Decay

The delay of the cell cycle and the arrest in a cell cycle phase after irradiation is a well documented phenomenon and is part of a signaling network, known as the DNA damage response (DDR). The main role of the DDR is to maintain genomic integrity after DNA damage [87, 124]. The eukaryotic cell cycle consists of four distinct phases: G_1-, S-, G_2 and M-phase. Traverse between the phases is regulated by Cyclins and Cyclin-

dependent kinases (Cdks). Cyclins are proteins that are able to bind and activate Cdks, which in turn phosphorylate further substrates that regulate cell cycle progression. After irradiation and subsequent DNA damage, particularly DSB formation, the cell cycle progression is interrupted in order to signal and repair damaged DNA. An interruption is initiated by the activation of cell cycle checkpoints, which arrest normal cell cycle progression at different cell cycle phases (*Figure 1.6*). These checkpoints exist at the G_1/S, G_2/M boundary and in the S-phase [123, 46, 25].

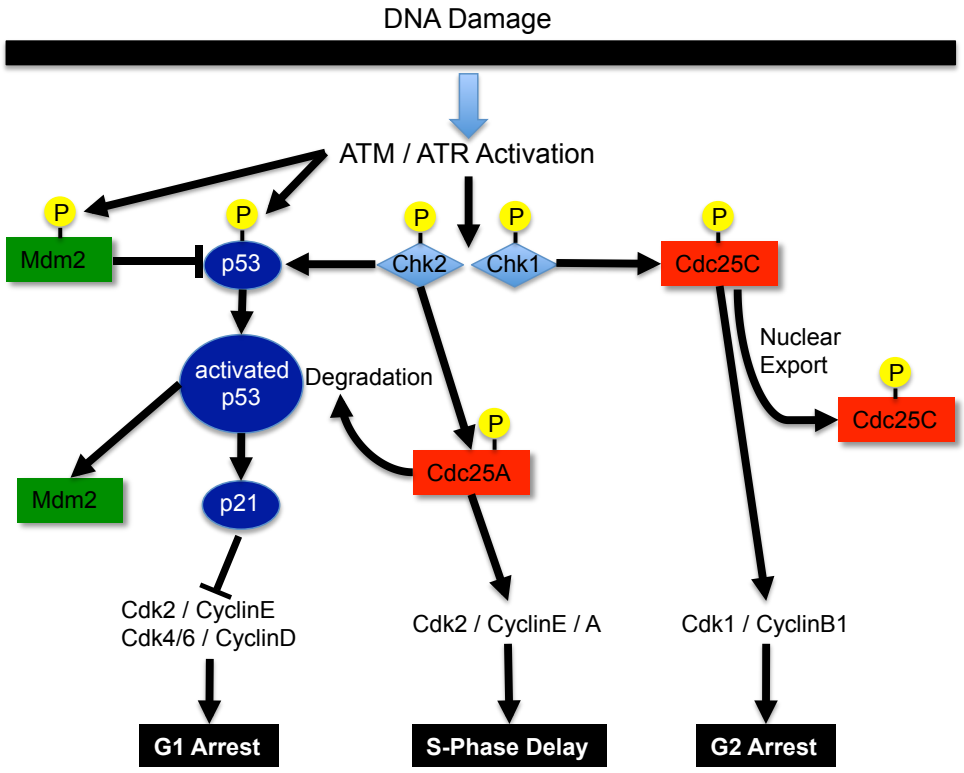

Figure 1.6.: Mammalian cell cycle checkpoint pathways. Figure modified according to http://www.rndsystems.com/MiniReview_MR03_DNADamageResponse.aspx

The G_1/S checkpoint was shown to be activated in many cell lines after irradiation with increasing intensity as a function of both LET and dose [40]. However, the G_1-phase block does not appear in most p53 deficient tumor cell lines [67]. The transition from the G_1- to the S-phase is regulated by two complexes, CyclinD/Cdk4/6 and CyclinE/Cdk2. Initiation of the G_1/S1 checkpoint leads to the ataxia telangiectasia mutated (ATM) mediated phosphorylation of p53. Also phosphorylated are murine double minute 2 (Mdm2) and checkpoint kinase 2 (Chk2) causing the activation of p53. p53 in turn up-regulates the gene expression of p21 whose protein is an inhibitor of CyclinD/Cdk4/6 as well as CyclinE/Cdk2 thusly inhibiting the G_1/S transition. Additionally, the phosphorylated Chk2 inhibits Cdc25A, which is an activation phosphatase for CyclinE/Cdk2 keeping this complex in an inactivated state. The latter pathway reacts more quickly to DNA damage (< 1 h) than the slower (2-3 h) p53 dependent pathway [25, 61].

In contrast to the G_1/S and the G_2/M checkpoints, the activation of the S-phase checkpoint leads only to a delay and not to an arrest of the cell cycle [66]. Ionizing radiation induced DNA DSBs activate the S-phase checkpoint, leading to the ATM mediated phosphorylation of Chk2, which in turn dephosphorylates Cdc25A. The subsequent degradation of Cdc25A prevents the activation of Cdk2 keeping the CyclinE A/Cdk2 complex in an inactive state. That results in a transient inhibition of replicon initiation [66].

The G_2/M checkpoint is activated in almost all eukaryotic cells in response to irradiation. The duration of the subsequent arrest corresponds to the applied dose and rarely to the radiation quality when applied at equitoxic doses [143, 11, 40]. The main control mechanisms for the G_2/M transition is the CyclinB1/Cdk1 complex, which has to be activated by Cdc25C mediated dephosphorylation of Cdk1. In case of DNA damage, ATM and ataxia telangiectasia and RAD3 related kinase (ATR) phosphorylate Chk1 and Chk2, which, in turn, phosphorylate Cdc25C. Consequently, Cdc25C is translocated to the cytoplasm, preventing the activation of the CyclinB1/Cdk1 complex [1]. The CyclinB1/Cdk1 complex is further kept in an inactivated state by a second slowly activated, p53-dependent pathway [85, 25]. The transition from late G_2 cells to M-phase is inhibited and the cells are arrested in late G_2.

1.6.8. The Auger Electron Emitter I-125

The Auger Electron Emitter I-125 has a half life of 60.5 days [63]. The I-125 decay is induced by electron capture mostly from the K-shell and can be divided into two stages (*Figure 1.7*). In the first stage the nucleus decays to an excited metastable state of the

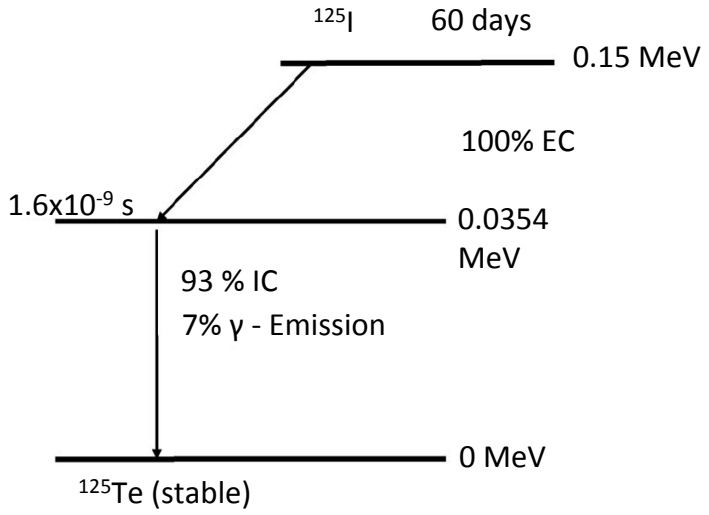

Figure 1.7.: Decay scheme for I-125. (Data after Lederer et al. [73])

tellurium-125 (Te-125) daughter by capture of an inner shell electron accompanied by the emission of a neutrino. The thereby inner shell vacancy is filled by the transition of an higher shell electron. The energy from the electron transition is transferred onto a higher shell electron, which is then ejected as an Auger electron [5]. Alternatively the energy can be emitted as an X-ray photon, which is then said to be a radiative transition. In the second stage, the metastable Te-125 state decays to the Te-125 ground state either by internal conversion (93%) or by γ-emission (7%). Internal conversion creates again an inner shell vacancy by transferring the available energy (35.4 keV) to an inner shell electron which escapes as a conversion electron from the atom. As a consequence of this vacancy a second Auger cascade runs off, leading to the emission of further conversion electrons [93]. On average I-125 releases $\sim$ 15 Auger electrons per decay [103] with the majority having energies of < 500 eV [56]. Shown in *Table 1.1* are the electron emissions from I-125.

Table 1.1.: Auger, Coster-Kronig (CK) and Internal Conversion (IC) electrons from the decay of I-125. Data after Adelstein et al. [2]

Transition	Average Energy (MeV)	Range (μm)
IC 1 K	3.65E-03	4.98E-01
IC 1 L	3.06E-02	1.86E101
IC M,N	3.41E-02	2.31E101
Auger KLL	2.24E-02	1.08E101
Auger KLX	2.64E-02	1.43E101
Auger KXY	3.02E-02	1.82E101
CK LLX	2.19E-04	1.02E-02
Auger LMM	3.05E-03	3.73E-01
Auger LMX	3.67E-03	5.04E-01
Auger LXY	4.34E-03	6.62E-01
CK MMX	1.27E-04	6.43E-03
Auger MXY	4.61E-04	2.25E-02
CK NNX	2.99E-05	1.15E-03
Auger NXY	3.24E-05	1.97E-03
CK OOX	6.00E-06	1.50E-04

1.7. G-Quadruplex Forming Oligonucleotides as an Alternative Carrier-System

TFOs as a carrier system for radioisotopes are very promising due to their high specificity and stability, but nevertheless TFOs are also limited to targets consisting of polypurine repeats. Recently, there is evidence that oligonucleotides are able to be part of quadruplex structures in guanine rich sequences [95]. The basic unit of a quadruplex is a structure consisting of four guanosin-5´-monophosphates arranged in a square coplanar array. Each base is connected to its neighbours by two Hoogsteen hydrogen bonds (*Figure 1.8* a). These basic units are termed G-Quartetts. These arranged in two or more stacks build up a so called "G-Quadruplex structure" (*Figure 1.8* b) [125].

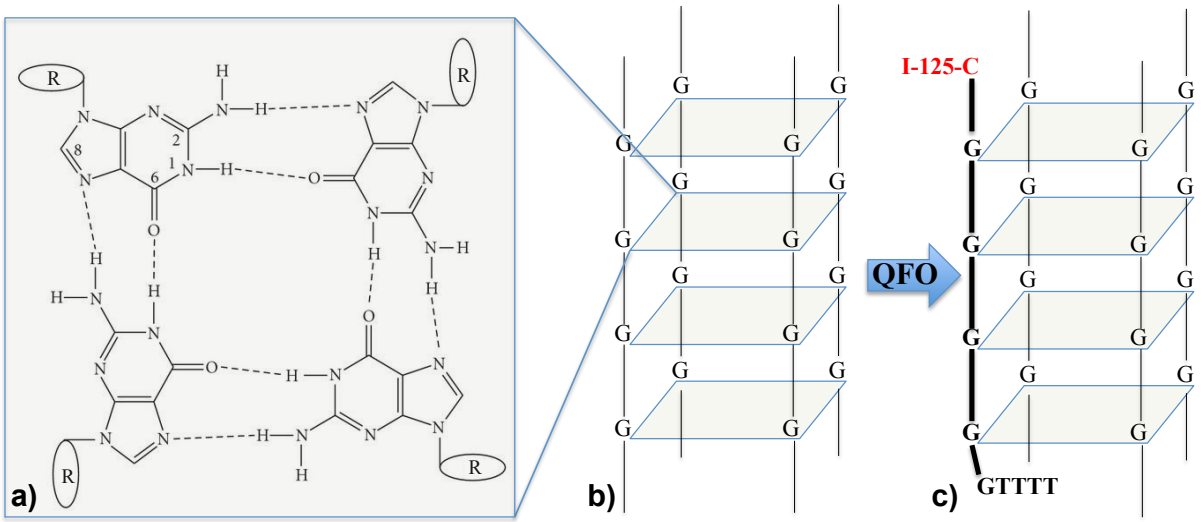

Figure 1.8.: Schematic representation of the G-Quartett; (a) and the structure of a G-Quadruplex consisting of four G-Quartett units; (b). G-Quadruplex with one strand replaced by a I-125-Oligonucleotide (QFO, bold); (c). (Figure modified according to Diculescu et al. [26].)

This G-Quadruplex in turn can be built of one, two or four guanine strands with each strand building one of the G-Quadruplex corners.

We assume that one or more of the involved strands could be a TFO like oligonucleotide, carrying an AEE (*Figure 1.8* c), inducing damage to the subsequent G-quadruplex structure during decay. These G-quadruplex structures appear at high frequencies in the human genome and form at so-called quadruplex sequences. A genome wide survey by Todd et al. [133] identified 375,157 putative quadruplex sequences (PQS) in the human genome and Huppert et al. [59] identified 14,769 PQS in the promotor region of 19,268 known human genes. The overall number of PQS and especially the amount of PQS in promotor regions harbors a great potential of "quadruplex-forming-oligonucleotides" (QFO) as additional carriers for radionuclides. However, we must be

aware of the fact that a labeled QFO will not posses the sequence specificity of a TFO due to its limitation to guanine repeats, but the number of targets by one QFO would be considerably high and outnumber the few binding sites of a sequence-specific TFO.

2. Aim of the Work

The major aim of the present study was to establish a TFO based carrier system, which allows the site directed delivery of the AEE I-125 to specific DNA target sequences in the cell. On this basis the cyto- and genotoxic potential of I-125-labeled TFOs should be investigated *in vitro*.

To accomplish this task it was mandatory to establish a robust and efficient labeling procedure of TFOs while the TFO binding capabilities should be remained unaffected.

Of equal importance was to characterize the target sequence specific binding of various TFOs, to investigate the DNA double-strand break capacity and the cell killing properties of I-125-labeled TFOs.

The cyto- and genotoxic potential of I-125-labeled TFOs should be analyzed in respect to the number and the quality of the targeted sequences.

Additionally, the biokinetics and intracellular distribution of TFOs should be characterized with regard to time dependent localization and their overall persistence in the cellular environment. Also the effects of I-125-labeled TFOs on gene expression of targeted genes will be studied in order to elucidate the possibility of directed gene expression manipulation by I-125-TFOs.

3. Materials and Methods

3.1. Materials

3.1.1. SCL-II Cell Line

The squamous carcinoma cell line II (SCL-II) is derived from a undifferentiated squamous epithelium carcinoma of a 91-year-old male patient [132]. SCL-II cells grow adherent and confluent in cell culture flasks with unlimited proliferation capacity. They show an epithelial growing pattern, a polygonal to round shape and their cytoplasm is largely filled by the nucleus. The cell size is approximately 11 μm in diameter. In cell culture with increased cell density they do not grow in strict monolayers but occasionally in few stacked layers.

3.1.2. Oligonucleotides

All oligonucleotides used in this work were provided by Metabion international AG (Martins-ried, Germany) with exception of the fluorochrome labeled TFOs (Alexa488), which were delivered by TIB Molbiol GmbH (Berlin, Germany).

Table 3.1.: Triplex-Forming-oligonucleotides

Name	Sequence (5´- 3´)	Target-sequence (5´- 3´)	Gene (locus)	Reference
TFO-MBS	gag aga gag aga gag aga gag aga gag aga gag c	gag aga gag aga gag aga gag aga gag aga gag g	multi binding sites	[121]
TFO-V1	ggt ttg gtg gtt ggg tgt gtg	gga aag gag gaa ggg aga gag	*cdkn2a* (21995579)	this work
TFO-V2	ttt gtt ggg tgg tgg gtt ggt tgt gtt	aag aga agg aag gga gga ggg aag aaa	*cdkn2a* (21969523)	this work
TFO-V3	ggg ggt tgg ggt gtg gtg ggg	ggg gcg gag atg ggc agg ggg	*cdkn2a* (21994442)	this work
TFO-V6	ttg tgg gtg tgg tgg ggt tt	aaa ggg gag gag agg gag aa	*cdk4* (58148139)	this work

Table 3.1.: Continuation Triplex-Forming-oligonucleotides

Name	Sequence (5´- 3´)	Target-sequence (5´- 3´)	Gene (locus)	Reference
TFO-V7	gtt gtg gtt gtg gtt ggg	ggg aag gag aag gag aag	*cdk4* (58148122)	this work
TFO-V8	ggt gtt ggt tgg ttg ttt tgg tgg tgg gg	ggg gag gag gaa aag aag gaa gga aga gg	*bcl2* (60874077)	this work
TFO-BCL2	gtg ttt gtt ttt gtt ggg tgg tgt ggg gc	ggg gga gag gag gga aga aaa aga aag ag	*bcl2* (60796002)	this work
TFO-BCL2-Alexa488	Alexa488-gtg ttt gtt ttt gtt ggg tgg tgt ggg gg	ggg gga gag gag gga aga aaa aga aag ag	*bcl2* (60796002)	this work
TFO-BCl2-Alexa594	Alexa594-gtg ttt gtt ttt gtt ggg tgg tgt ggg gg	ggg gga gag gag gga aga aaa aga aag ag	*bcl2* (60796002)	this work
TFO-BRCA1	tgg gtg tgt gtt ggt gtg ttg ttc c	gga aga aga gag gaa gag aga ggg a	*brca1* (41203138)	this work
TFO-V12	ggg tgg tgt ggg tgg gtt ttt ttt	aaa aaa aag gga ggg aga gga ggg	*chk2* (29133020)	this work
TFO-V13	ggg ttt ttt gtg ggg gtg ttg	gaa gag ggg gag aaa aaa ggg	*chk2* (29099560)	this work
TFO-GAPDH	ggg ggt ggg gtt tgt ttg ttt c	g aaa gaa aga aag ggg agg ggg	*gapdh* (6643235)	this work
TFO-QRT	aaa aac ccc cct ttt tgg ggg ctc	unknown	multi binding sites	this work

For the Primer-Extension Method (3.2.8) special precursor stages (preTFOs) of the TFOs shown in ***Table 3.1*** and biotinylated template oligonucleotides were used. The preTFOs and oligonculeotides are displayed in ***Table 3.2.***

Table 3.2.: Biotinylated Oligonucleotide Templates and preTFOs used for the Primer Extension Method

Name	Sequence preTFO (5´- 3´)	Sequence Template (5´- 3´)
preTFO-MBS	gag aga gag aga gag aga gag aga gag aga gag	aaa gct ctc tct ctc tct ctc tct ctc tct ctc tct c-Biotin
preTFO-BCL2	gtg ttt gtt ttt gtt ggg tgg tgt ggg g	gcc cca cac cac cca aca aaa aca aac act ctt ctt-Biotin
preTFO-BRCA1	tgg gtg tgt gtt ggt gtg ttg tt	gga aca aca cac caa cac aca ccc att ctt ct-Biotin
preTFO-GAPDH	ggg ggt ggg gtt tgt ttg ttt	ctc gaa aca aac aaa ccc cac ccc ctt ctt-Biotin
preTFO-QRT	aaa aac ccc cct ttt tgg ggg ct	ctg agc ccc caa aaa ggg ggt ttt ttt c-Biotin

Table 3.3.: Primer Sequences for amplification of target DNA fragments

Name	Sequence (5´- 3´)	Binding TFO	Fragment Size	Reference
BCL2 212 fwd.	agc tcc cac cag ggc caa act	TFO-BCL2	212 bp	this work
BCL2 212 rev.	ttc tga agg tgc cca ggc tgc			this work
BCL2 1695 fwd.	aca gga acc ctc cct ctg tt	TFO-BCL2	1695 bp	this work
BCL2 1695 rev.	ccc ttg act gac caa atg ct			this work
GAPDH 1695 fwd.	tcc cac cgt gtg ccc aag	TFO-GAPDH	1695 bp	this work
GAPDH 1695 rev.	ctc ctg ttt ctg ggg ac			this work
GAPDH 1202 fwd.	tct gcc ctc cta cca gaa ga	TFO-GAPDH	1202 bp	this work
GAPDH 1202 rev.	aag aag atg cgg ctg act gt			this work

Table 3.4.: Primer Sequences for amplification of Southern-Blot probes

Name	Sequence (5´- 3´)	Binding TFO	Fragment Size	Reference
GAPDH F1 fwd.	cat gga aag cga atc tct gtt t	TFO-GAPDH	400 bp	this work
GAPDH F1 rev.	gcc tat ctg ggc cac aag t			this work
GAPDH F2 fwd.	ggc cat gat tca gaa acc ac	TFO-GAPDH	595 bp	this work
GAPDH F2 rev.	tca aga cca gcc tgg aaa gt			this work

Table 3.5.: Primer Sequences for qRT-PCR

Name	Sequence (5´- 3´)	Gene	Fragment Size	Reference
ACTA fwd.	gca aat gct tct aga cac act cca c	*ACTIN*	126 bp	this work
ACTA rev.	cag caa cgg aag ttg tta caa aga a			this work
BCL2 fwd.	act cct gat tca ttg gga agt ttc a	*BCL2*	121 bp	this work
BCL2 rev.	gca tga tcc tct gtc aag ttt cct t			this work
BRCA1 fwd.	gat tgg ttc ttc caa aca aat gag g	*BRCA1*	137 bp	this work
BRCA1 rev.	gaa tcc atg ctt tgc tct tct tga t			this work
GAPDH fwd.	gac cac ttt gtc aag ctc att tcc t	*GAPDH*	134 bp	K. Knops
GAPDH rev.	tct ctc ttc ctc ttg tgc tct tgc t			K. Knops

3.1.3. Culture Media

Table 3.6.: Culture Media

Medium	Company
Dulbecco´s modified Eagle medium: Nutrient Mixture F-12 (DMEM: F12) with L-Glutamin, 15 mM Hepes, 1.2 g/l $NaCO_3$	PAN^{TM} Biotech GmbH, Aidenbach, Germany
L-15 Leibowitz´s medium	Invitrogen, Darmstadt, Germany
Minimum essential medium Eagle (MEM) with L-Glutamine	PAA Laboratories GmbH, Cölbe, Germany

3.1.4. Antibodies and Enzymes

Table 3.7.: Antibodies and Enzymes

Substance	Company
53BP1 (H-300): sc-22760	Santa Cruz Biotechnology, Inc., Heidelberg, Germany
goat anti-rabbit IgG-TR: sc-2780	Santa Cruz Biotechnology, Inc., Heidelberg, Germany
Klenow Fragment (-Exo)	Fermentas, St. Leon-Rot, Germany
Taq DNA Polymerase	Fermentas, St. Leon-Rot, Germany

3.1.5. Buffer and Solutions

If not otherwise indicated all Buffer and Solutions in ***Table 3.8*** are solved in deionized water.

Table 3.8.: Buffer and Solutions

Buffer/ Solution	Composition
Denaturation-Solution	1.5 M NaCl, 0.5 M NaOH
Developing-Solution	300 mM Na_2CO_3, 0.05% Formaldehyde (37%)
Freezing medium (RPE-1 cells)	10% Dimethy sulfoxide, 20% DMEM solved in FBS
Freezing medium (SCL-II cells)	10% Dimethyl sulfoxide solved in FBS
Gel-Preserving-Solution	5% Glycerol, 35% Methanol
Klenow-Buffer (x1)	500 mM Tris-HCl, pH 8.0, 50 mM $MgCl_2$, 10 mM DTT
Loading Dye (x10)	50% Glycerol, 0.25% Bromphenolblue
Microscopy-Buffer	2.6 mM Na_2HPO_4 $2H_2O$, 3 mM KH_2PO_4, pH 6.8
Mounting medium	Sigma-Aldrich, Steinheim, Germany
Neutralization-Solution	1.5 M NaCl, 0.5 M Tris-HCl, pH 7.0
Nuclei-Extraction Buffer	320 mM Sucrose, 10 mM HEPES, 5 mM $MgCl_2$, 1% Triton X-100, pH 7.4
Nuclei-Wash Buffer	320 mM Sucrose, 10 mM HEPES, 5 mM $MgCl_2$, pH 7.4
PBS-Buffer	17 mM NaH_2PO_4, 27 mM BaCl, 70 mM Na_2HPO_4
SSC-Transfer Buffer (x20)	3 M NaCl, 0.3 M $Na_3C_6H_5O_7$, pH 7.0
Stop-Solution	3% Acetic acid (glacial)
TAE-Buffer	40 mM Tris-Base, pH 8.0, 20 mM acetic acid, 1 mM EDTA
TBE-Buffer	89 mM Tris-Base, pH 8.0, 89 mM boric acid, 2 mM EDTA
TBP-Buffer	0.2% Triton X-100, 1% bovine serum albumine solved in PBS
TEN_{100} Binding Buffer	10 mM Tris-HCl, pH 7.5, 1 mM EDTA, 100 mM NaCl
TEN_{1000} Wash Buffer	10 mM Tris-HCl, pH 7.5, 1 mM EDTA, 1 M NaCl
TFO-Binding Buffer	10 mM $MgCl_2$, 10 mM Tris-HCl, pH 5.8
TFO-Binding Buffer B	10 mM $MgCl_2$, 10 mM Tris-HCl, pH 5.8, 16 μM Coralyne chloride hydrate
Washing Solution 1	10% SSC-Transfer Buffer (x20)
Washing Solution 2	10% SSC-Transfer Buffer (x20), 0.1% SDS
Washing Solution 3	0.005% SSC-Transfer Buffer (x20), 0.1% SDS

3.1.6. Disposable Products

Table 3.9.: Disposable Products

Product	Company
Casy® Cups	Schärfe System, Reutlingen, Germany
Cell culture flasks	TPP Techno Plastic Products AG, Trasadingen, Switzerland
Centrifuge tubes 15 ml , 50 ml	Sarstedt, Nümbrecht, Germany
Folded Filters (Grade 3 hw)	Sartorius, Göttingen, Germany
Freezer vials	VWR International, Darmstadt, Germany
Glass coverslips	Menzel GmbH, Braunschweig, Germany
Glass Bottom Dishes (35 mm)	MatTek corp., Ashland, USA
Microscope slides	Menzel GmbH, Braunschweig, Germany
Nylon transfer membrane	GE Water & Process Technology, Herentals, Belgium
Optical Adhesive Cover	Applied Biosystems, Darmstadt, Germany
Pipette tips 10 μl, 100 μl, 1000 μl	Eppendorf, Hamburg, Germany
Round Bottom Tubes 5 ml	BD Bioscience, Heidelberg, Germany
Syringe Filter (20 μm)	Millipore, Billerica, USA
Tubes 0.2 ml, 0.5 ml, 1.5 ml, 2 ml	Eppendorf, Hamburg, Germany
Whatman paper	Carl Roth, Karlsruhe, Germany

3.1.7. Chemical Reagents

The chemicals used in this work (*Table 3.10*) were of analytical grade.

Table 3.10.: Chemical Reagents

Chemical	Company
Acetic acid (glacial)	Carl Roth, Karlsruhe, Germany
Agarose low EEO	AppliChem, Darmstadt, Germany
Albumin, from bovine serum	Sigma-Aldrich, Steinheim, Germany
Ammoniumpersulfate (APS)	Bio-Rad, Munich, Germany
β-Mercaptoethanol	Sigma-Aldrich, Steinheim, Germany
Blotting Grade Blocker Non-Fat Dry Milk	Bio-Rad, Munich, Germany
Boric acid	Carl Roth, Karlsruhe, Germany
Bromphenolblue (BPB)	Sigma-Aldrich, Steinheim, Germany
Casy®Ton	Schärfe System, Reutlingen, Germany
Coralyne chloride hydrate	Sigma-Aldrich, Steinheim, Germany
Cytochalasin B	Thermo Fisher Scientific, Geel, Belgium
2´-Deoxycytidine hydrochloride (CdR)	Fluka, Buchs, Switzerland
Dimethyl sulfoxide (DMSO)	Carl Roth, Karlsruhe, Germany
Disodiumhydrogenphosphate, dihydrate (Na_2HPO_4, $2H_2O$)	Merck KGaG, Darmstadt, Germany
dNTP-Mix, 25 mM each	Fermentas, St. Leon-Rot, Germany

Table 3.10.: Continuation Chemical Reagents

Chemical	Company
Dulbecco´s phosphate buffered saline (PBS)	PAA GmbH, Paschingen, Austria
Ethanol (absolut)	Merck KGaG, Darmstadt, Germany
Ethidium bromide (EtBr)	Sigma-Aldrich, Steinheim, Germany
Ethylenediaminetetraacetic acid (EDTA)	Merck KGaA, Darmstadt, Germany
Ethyleneglycoltetraacetic acid (EGTA)	Merck KGaA, Darmstadt, Germany
Fetal Bovine Serum (FBS)	Biochrome, Berlin, Germany
Fluorescein-dCTP (FITC-dCTP)	Perkin-Elmer GmbH, Rodgau, Germany
5-Fluoro-2´-deoxyuridine (FUdR)	Fluka, Buchs, Switzerland
Formaldehyde 37% (CH_2O)	Optichem GmbH, Inzlingen, Germany
GeneRuler™ 10 bp DNA ladder	Fermentas, St. Leon-Rot, Germany
GeneRuler™ 100 bp DNA ladder	Fermentas, St. Leon-Rot, Germany
GeneRuler™ 500 bp DNA ladder	Fermentas, St. Leon-Rot, Germany
Glycerol	Serva, Heidelberg, Germany
Glycine	Merck KGaA, Darmstadt, Germany
HEPES	Merck KGaA, Darmstadt, Germany
Hoechst 33342	Sigma-Aldrich, Steinheim, Germany
Hygromycine B	Invivogen, Toulouse, France
5-[I-125]Iodo-2´-deoxycytidine-5´-triphosphate (I-125-dCTP)	Hartmann Analytic, Braunschweig, Germany
5-[I-125]Iodo-2´-deoxyuridine ((I-125)IdU)	Perkin-Elmer GmbH, Rodgau, Germany
Immun-Star™ AP Substrate	Bio-Rad, Munich. Germany
Methanol absolut	Merck KGaA, Darmstadt, Germany
Nitric acid (HNO_3)	Merck KGaA, Darmstadt, Germany
Nuclease-Free dH_2O	Qiagen, Hilden, Germany
α-P-32-dATP	Hartmann Analytic, Braunschweig, Germany
Potassium chloride (KCl)	Merck KGaA, Darmstadt, Germany
ProLong Goldantifade reagent with DAPI	Invitrogen, Darmstadt, Germany
7-aminoactinomycin D (7-AAD)	BD Pharmingen™, Heidelberg, Germany
Silver nitrate ($AgNO_3$)	Santa Cruz Biotechnology, Inc., Heidelberg, Germany
Sodium acetate (NaAc)	Merck KGaA, Darmstadt, Germany
Sodiumdihydrogenphpsphate, monohydrate (NaH_2PO_4, H_2O)	Merck KGaA, Darmstadt, Germany
Sodium carbonate (Na_2CO_3)	Merck KGaA, Darmstadt, Germany
Sodium chloride (NaCl)	Merck KGaA, Darmstadt, Germany
Sodium dodecyl sulfate (SDS)	Sigma-Aldrich, Steinheim, Germany
Sodium hydrogen carbonate ($NaHCO_3$)	Merck KGaA, Darmstadt, Germany
Sodium ortho vanadate (Na_3V_4O)	Sigma-Aldrich, Steinheim, Germany
Streptavidin Magnetic Particles	Roche Applied Science, Mannheim, Germany
Sucrose	Sigma-Aldrich, Steinheim, Germany
Tetramethylethylenediamine (TEMED)	Bio-Rad, Munich, Germany
Tris-Base	Merck KGaA, Darmstadt, Germany
Tris-HCl	Merck KGaA, Darmstadt, Germany

Table 3.10.: Continuation Chemical Reagents

Chemical	Company
Trisodium citrate ($Na_3C_6H_5O_7$)	Merck KGaA, Darmstadt, Germany
Triton X-100	Carl Roth, Karlsruhe, Germany
Trypsin-EDTA	PAA GmbH, Paschingen, Austria

3.1.8. Commercial Kits

Table 3.11.: Commercial Kits

Kit	Company
Cell Line Nucleofector® Kit V	Lonza GmbH, Basel, Switzerland
DecaLabel™ DNA Labeling Kit	Fermentas, St. Leon-Rot, Germany
DNeasy™ Blood & Tissue Kit	Qiagen, Hilden, Germany
FITC Annexin V Apoptosis Detection Kit I	BD Pharmingen™, Heidelberg, Germany
Power SYBR® Green RNA-to-C_T™ 1-Step Kit	Applied Biosystems, Darmstadt, Germany
QIAquick™ PCR Purification Kit	Qiagen, Hilden, Germany
RNA 6000 Nano Kit	Agilent Technologies Deutschland GmbH, Waldbronn, Germany
RNeasy™ Mini Kit	Quagen, Hilden, Germany
Transcriptor High Fidelity cDNA Synthesis Kit	Roche Applied Science, Mannheim, Germany

3.1.9. Laboratory Apparatus

Table 3.12.: Laboratory Apparatus

Apparatus	Company
Agilent Bioanalyzer 2100	Agilent Technologies Deutschland GmbH, Waldbronn, Germany
BD FACS Canto™ II	BD Bioscience, Heidelberg, Germany
Casy® Cell Counter	Scärfe System, Reutlingen, Germany
Centrifuge 5415 R	Eppendorf, Hamburg, Germany
Centrifuge Multifuge 1s-r	Heraeus, Hanau, Germany
ChemiDoc™ XRS+	Bio-Rad, Munich, Germany
Concentrator 5301	Eppendorf, Hamburg, Germany
Gamma Counter 1480 Wizard™ 3	Perkin-Elmer GmbH, Rodgau, Germany
Gel-Chamber	Peqlab Biotechnologie GmbH, Erlangen, Germany
Hamilton Syringe (10 μl, 50 μl)	Hamilton Bonaduz AG, Switzerland
Hybridization Chamber	Sheldon Manufacturing, Cornelius, USA
Imaging System FLA-5000	Fujifilm, Düsseldorf, Germany
Imaging Plates BAS 2325	Fujifilm, Düsseldorf, Germany

Table 3.12.: Continuation Laboratory Apparatus

Apparatus	Company
Incubator MCO-20 AIC	Sanyo, Bad Nenndorf, Germany
Laser Scan Microscope Axio Observer. Z1 LSM 700	Zeiss GmbH, Göttingen, Germany
Magnetic Stirrer RCT basic IKAMAG®	IKA® Werke GmbH & Co. KG, Staufen, Germany
Microscope Axioplan 2	Zeiss GmbH, Göttingen, Germany
Mini-Protean™ II electrophoresis cell	Bio-Rad, Munich, Germany
NanoDrop® ND-1000 UV-VIS	Peqlab Biotechnologie GmbH, Erlangen, Germany
Nucleofector Device I	Lonza GmbH, Basel, Switzerland
Protean™ II electrophoresis cell	Bio-Rad, Munich, Germany
pH-Meter Orion Star	Thermo Scientific, Meiningen, Germany
POWER PAC 3000	Bio-Rad, Munich, Germany
Real Time PCR System 7500	Applied Biosystems, Darmstadt, Germany
TProfessional Basic Thermocycler Gradient	Biometra, Göttingen, Germany
Vivatome Axio Observer. Z1	Zeiss GmbH, Göttingen, Germany
Vortexer	VWR International, Langenfeld, Germany

3.1.10. Software

Table 3.13.: Software

Software	Company
FACSDiva Software	BD Biosciences, Heidelberg, Germany
Metafer 4 Metacyte Software	Metasystems, Altlusheim, Germany
Primerdesign	http://frodo.wi.mit.edu/primer3/
Quantity One® Version 4.2.1	Bio-Rad, Munich, Germany
Sequence Detection Software 1.3.1	Applied Biosystems, Darmstadt, Germany
TFO Target Sequence Search	http://spi.mdanderson.org/tfo/about.php

3.2. Methods

3.2.1. Cell Line Culture and Storage Conditions

SCL-II cells were grown in MEM with L-Glutamine, supplemented with 16% FBS in a water-saturated atmosphere of 5% CO_2 at 37°C. SCL-II cells grow adherent and therefore were passaged by removal of medium, one wash step with PBS and addition of 1 ml trypsin/EDTA for 5 min at 37°C. 5 ml of medium was added. Subcultivation of cells was done three times a week in a ratio of 1:2 to 1:4 as needed. When used for live cell imaging SCL-II cells were incubated in a microscope incubation chamber which did not allow CO_2 gassing. Therefore the cells were kept in L-15 Leibowitz´s medium, which is commonly used in CO_2 free systems. Before the cells were used for live cell imaging they had to be subcultivated for at least two weeks in L-15 Leibowitz´s medium for adaption.

For storage SCL-II cells were grown in T25 or T75 cell culture flasks to 70 - 80% confluency, then trypsinized by addition of 1 ml Trypsin-EDTA for 5 min and resuspended in at least 4 ml MEM with 16% FBS. After determination of the cell number via Casy® Cell Counter the cell suspension was centrifuged for 5 min at 300 x g and the supernatant discarded. The cell pellet was resuspended in freezing medium (FBS + 10% DMSO) to a concentration of $1x10^6$ cells/ml and aliquoted in freezer vials at 1 ml per vial. For pre-cooling the vials were kept at -80°C for three days and then transferred to -150°C for long time storage.

3.2.2. γ-Irradiation of SCL-II Cells

For the gamma irradiation, $1x10^6$ SCL-II cells were cultivated in T25 cell culture flasks for 24 h. Thereafter cells were gamma irradiated in a Cs-137 radiation chamber (0.7 Gy/min) with 1, 2, 3, 4, 6, 8 and 10 Gy. For the irradiation procedure cells were kept in the culture flasks. As negative controls served unirradiated SCL-II cells, elsewise treated as the irradiated cell samples. After irradiation cells were trypsinized by the addition of 1 ml Trypsin-EDTA per flask, incubtated for 5 min at 37°C and finally resuspended in at least 4 ml MEM supplemented with 16% FBS. After that cells were counted on a Casy® Cell Counter and the appropriate number was plated in 6-well plates.

3.2.3. Polymerase Chain Reaction

The Polymerase Chain Reaction (PCR) is a way to amplify DNA sequences between two short flanking regions of known sequence. For the standard PCR reaction is needed a DNA template, two oligonucleotide Primer, didesoxynucleotides (dNTPs) and a heat stable DNA-polymerase (Taq-Polymerase) (*Table 3.14*). The standard PCR consists of 5 steps, whereupon the steps 2 - 4 are repeated in 25 to 35 cycles:

1. **initial Denaturation**, 95°C, 2 - 4 minutes. DNA template gets completely denatured to single stranded DNA.
2. **Denaturation**, 95°C, 30 - 60 seconds. Double-stranded DNA template and Template-Primer hybrids are separated.
3. **Annealing**, 30 - 60 seconds. The annealing temperature depends on the T_m of the used Primers and were determined using a gradient PCR reaction. In this step the Primer hybridize with the DNA template.
4. **Elongation**, 72°C. The duration of the steps depends on the length of the amplified sequence, estimating that 1 kbp (kilo base pairs) is synthesized per minute. In this step the template DNA is amplified, starting at the Template-Primer hybrid.
5. **final Elongation**, 5 - 10 minutes, Temperature as in step 4 indicated. Ensures that any remaining single-stranded DNA is fully extended.

A gradient PCR is a standard PCR reaction performed in a gradient Thermal Cyler which allows to apply a temperature gradient, of approximately 10°C, on the thermal element of the cycler within the annealing step. Along this gradient several positive control samples are positioned and amplified. The efficiency of the amplification, screened by agarose gel electrophoresis (**3.2.4**), is an indication for the ideal annealing temperature.

Table 3.14.: Standard PCR-Mix; x, the volume depends on the DNA concentration

Reagent	Volume
Taq Polymerase [5u/μl]	0.5 μl
10 x Taq Buffer $(NH_4)_2SO_4$	5 μl
dNTP-Mix [2 mM]	2.5 μl
Primer-fwd. [10 μM]	2 μl
Primer-rev.[10 μM]	2 μl
$MgCl_2$ [25 mM]	4 μl
DNA-Template	x μl
dem. Aqua	ad 50 μl

3.2.4. Agarose Gel Electrophoresis

Agarose gel electrophoresis is a method to separate a mixed population of DNA fragments on the basis of their mobility along an electric field through an agarose gel matrix. Shorter fragments are able to move faster through the pores of the matrix than larger molecules [90]. Separation of DNA fragments was performed in submerged horizontal electrophoresis gel chambers filled with agarose gels of different concentrations ranging from 1% to 1.5% depending on the DNA-fragment lengths. The running conditions were set to a constant voltage of 90 V in TAE-Buffer for 60 to 90 min. For size estimation of the separated DNA-fragments a DNA ladder was loaded on the gel as well. After electrophoresis the agarose gels were incubated in a concentrated ethidium bromide solution [10μg/ml] for 20 min on a rocking platform followed by a washing step in deionized water for further 20 min. The ethidium bromide molecules intercalate with the DNA and fluoresce with an orange color when exposed to ultraviolet light (λ = 256 nm) and can be therefore used as an fluorescent tag for DNA [74]. The visualization of the stained agarose gel was performed on a UV-table combined with a video documentation dock site (ChemiDoc^{TM} XRS+).

3.2.5. Electrophoretic Mobility Shift Assay

The Electrophoretic Mobility Shift Assay (EMSA) is a method for the electrophoretic separation of DNA fragments interacting with other molecules like single stranded DNA, RNA or proteins. In comparison to non-interacting DNA fragments of the same size these fragments move slower in an electric field through a polyacrylamide gel matrix as the mobility is determined by size, charge and shape. This effect is called a band shift [41]. In the present work the EMSA was used as a verification method for the binding of a TFO to its specific double-strand DNA target sequence. The polyacrylamide gels were cast in a vertical gel chamber with a length of 20 cm in concentrations ranging from 12% to 20% (*Table 3.15*), depending on the size of the DNA target fragments.

Table 3.15.: Non-denaturing Polyacrylamide gels. The quantities refer to a volume of 40 ml/gel.

Reagent	**12%**	**20%**
deionized water	15.6 ml	4.8 ml
$MgCl_2 \cdot 6H_2O$	0.17 g	0.17 g
5 x TBE-Buffer	8 ml	8 ml
30% BIS/Acrylamide	16 ml	26.8 ml
10 % (w/v) APS	400 μl	400 μl
TEMED	40 μl	40 μl

The gels were installed in the electrophoresis chamber and the central cooling core was connected to a recirculating water bath, set to a temperature of 10°C. The electrophoresis tank was filled with TBE-Buffer and each gel slot was additionally jetted with TBE-Buffer. Before loading the samples a pre-run of the gel at 100 V for 10 min was done. The samples were mixed with 10 x Loading Dye and loaded in the gel slots with a 50 μl Hamilton syringe. On both outer slots a DNA ladder (range depending on sample size) was loaded. The running conditions were set to 150 V for 20 h at 10°C. After the run, the gel was removed from between the electrophoresis plates, placed in a glass dish and rinsed with deionized water as a preparation for the silver staining procedure. All following steps were performed under slight shaking on a rocking platform. The DNA in the gel was fixed by incubation in 10% ethanol for 10 min and then rinsed in deionized water. Incubation in 1% nitric acid for exactly 3 min followed by two rinsing steps in deionized water and two additional wash steps in deionized water for 5 min. Incubation in 0.2% silver nitrate for 15 min. The gel was rinsed three times in deionized water and additionally incubated for 2 min in deionized water. The Developing-Solution was added and slightly shaken until a brown precipitate forms in the solution. The old solution was decanted and replaced by fresh Developing-Solution. The incubation was continued until the desired intensity of the band and background was reached. The reaction was stopped by decanting the Developing-Solution and the addition of Stop-Solution for 5 min. If a longer storage of the gel was needed, an overnight incubation in Gel-Preserving-Solution was done and then stored in transparency film at 4°C.

3.2.6. TFO Screening and Design

The screening for TFO target sequences in the human genome was done with the "TFO Target Sequence Search" online tool (http://spi.mdanderson.org/tfo/about.php). The screening settings were set according to the following criteria: - minimum length of 15 bp, - guanine content minimum 50%, - no pyrimidine interrupts allowed and the purine sequence located on one strand. The TFO sequences were designed in a complementary manner to the target sequences consisting of guanines (binding guanine) and thymines (binding adenine) in a reverse Hoogsteen conformation. A maximum of two cytosines was allowed but only in terminal position of the TFO.

3.2.7. *In Vitro* Triplex Formation and Binding Assay

All designed TFOs were additionally tested *in vitro* for their triplex forming abilities with their DNA target sequences. For this testing short DNA fragments containing the specific target sequence were synthesized. The fragments were 6 base pairs longer on each side of the contained target sequence and were the exact duplicates of the target regions in the genome. The target DNA fragment [1 pmol/μl] and the specific TFO [10 pmol/μl] were mixed with TFO Binding Buffer B to a total volume of 24 μl in a 0.2 ml tube (*Table 3.16*). For each sample two controls were prepared. One containing the DNA fragment (Negative Control) only and an other one containing the tested TFO and a non-complementary DNA fragment (Non-sense).

Table 3.16.: Reaction-mix for Triplex Formation Assay

Reagent	**Volume**	
	TFO/Non-sense	Negative Control
10 x TFO Binding Buffer B	2.4 μl	2.4 μl
Target DNA fragment (1 pmol/μl)	2 μl	2 μl
TFO (10 pmol/μl)	2.4 μl	-
deionized water	17.2 μl	19.6 μl

The samples were incubated at 37°C for 20 - 24 h. After the incubation all samples were analyzed in an EMSA (**3.2.5**). If the specific triplex formation of the tested TFOs with their target sequences could be confirmed by EMSA these TFOs were utilizable for further experiments. First step was the labeling with I-125 by the Primer Extension Method (**3.2.8**).

3.2.8. Primer Extension Method

The Primer Extension Method is a procedure invented by Sanger and Coulson [112] which allows the defined elongation of an oligonucleotide with a defined number of labeled deoxynucleoside triphosphates (dNTPs). In the present work a modified version of the Primer Extension Method was used according to the proceedings of Panyutin and Neumann [97] to label the used TFOs with I-125. In the first step biotinylated oligonucleotide template and preTFO (sequences shown in *Table 3.2*) were mixed with Klenow-Buffer in 0.2 ml tubes and annealed by incubation at 95°C for 10 min followed by slow cooling (1°C/min) to room temperature.

Table 3.17.: Annealing Mixture for Primer Extension Method

Reagent	Volume
Oligonucleotide Template [10 pmol/μl]	0.5 μl
preTFO [10 pmol/μl]	0.5 μl
10 x Klenow Buffer	1 μl
deionized water	7.5 μl

The primer extension reaction was carried out in the presence of 2.5 units of exonuclease-free Klenow fragment and 2.5 MBq I-125-dCTP in a total volume of 10 μl. After 15 min the reaction was stopped by heating to 75°C for 10 min, followed by slow cooling (1°C/min) to room temperature. The duplex-DNA product was resuspended in TEN_{100} Binding Buffer. Before the labeled duplex-DNA could be bound to Streptavidin Magnetic Particles, the particles were prepared by three wash steps in TEN_{100} Binding Buffer (500 μl each) and finally resuspended in 30 μl of TEN_{100} Binding Buffer. The Streptavidin magnetic particles were mixed with the labeled duplex-DNA and incubated for 15 min at room temperature. To keep the magnetic particles from settling, slight shaking is recommended. The incubation was followed by two wash steps with TEN_{1000} Wash Buffer and one more wash step in deionized water (150 μl each). The magnetic particles were resuspended in 20 μl 0.15 M NaOH and incubated for 5 min at room temperature for denaturation of the DNA-duplex. The magnetic particles were removed with a magnet and the supernatant containing the I-125-labeled TFOs was collected. Further 2.2 μl of 10 x TFO-Binding Buffer and 2 μl 1.25 M acetic acid were added and mixed with a pipet. At this step the amount of incorporated I-125-dC was determined by activity measurement using a 1480 Automatic Gamma-Counter. Before further use or storage at -80°C the labeled TFO have to be heated to 95°C for 5 min and directly chilled on ice for the denaturation of TFO dimers or secondary structures.

After the labeling reaction the I-125-labeled TFO have to be tested once again for their triplex forming ability. This is necessary to exclude any unwanted modification of the TFO due to the labeling reaction, that might inhibit the triplex formation. The testing was done in accordance to the settings of the *in vitro* triplex formation and binding assay described in **3.2.7**, only differing in TFO and DNA target fragment amount. For this, 18 - 20 kBq of I-125-labeled TFO were mixed, under binding conditions, with DNA fragments containing the corresponding target sequence. The target fragments lengths ranged between 200 to 1700 bp. The fragments were PCR amplificates from SCL-II cell DNA isolates and added to the triplex reaction mix (**3.16**) in varying concentrations (0.4 μg - 5 μg). After incubation the reaction mix was loaded on polyacrylamidgels (concentration depending on DNA target size) and analyzed via EMSA and autoradio-

graphy. The EMSA analysis is only possible for fragments shorter than 300 bp. For longer fragments the triplex induced band shift is not distinct enough for visualization.

3.2.9. Calculation of I-125 Labeling Efficiency

The labeling efficiency of the primer extension method was calculated on the base of the amount of preTFO loaded in the primer extension reaction mix (**3.2.8**) in relation to the amount of I-125-labeled TFO at the end of the reaction. Thereby all preTFOs used in the present work were labeled with a single I-125-dC per TFO. The calculations were done according to the following formulas:

$$\text{Specific Activity of I-125} = 81.4\ \text{kBq/pmol}$$

$$\text{Amount I-125-labeled TFO [pmol]} = \frac{\text{Activity labeled TFO [kBq]}}{81.4\ \text{kBq}} \tag{3.1}$$

$$\text{Labeling Efficiency [\%]} = \frac{\text{preTFO [pmol]}}{\text{I-125-labeled TFO [pmol]}} \tag{3.2}$$

3.2.10. Calculation of Accumulated I-125 Decays

The calculations of accumulated I-125- decays were done according to the following formulas, created by Dr. E. Kümmerle.

$$\lambda = \frac{ln(2)}{t_{1/2}} \tag{3.3}$$

λ = decay constant
$t_{1/2}$ = half life

$$A = A_0 \times e^{(-\lambda \times t)} \tag{3.4}$$

t = time in (h)
A = Remaining decays after time (t)
A_0 = Initial value of decays

$$\begin{aligned} A_{acc} = &\Big[(t-(t-0.25)) \times 1800 \times (A_0 \times e^{(-\lambda \times (t-0.25))}) + (A_0 \times e^{(-\lambda \times t)})\Big] + \\ &\Big[((t-0.25)-(t-0.5)) \times 1800 \times (A_0 \times e^{(-\lambda \times (t-0.5))}) + (A_0 \times e^{(-\lambda \times (t-0.25))})\Big] \end{aligned} \tag{3.5}$$

A_{acc} = Accumulated decays after t

The initial value of decays A_0 was determined at 22 - 24 h post transfection, for decays measured per whole cell. A measurement of DNA bound I-125-TFO only was not performed since the formed triplex structures do not remain intact throughout an DNA isolation process. After the accumulation storage (t) at -150°C samples were thawed and incubated for 24 h. Decays that took place within this second incubation period were not added to the final dose, since these decays accounted on average for less than 9% of the total dose.

3.2.11. Amplification of Target DNA Fragments from DNA Isolates of SCL-II Cells

DNA isolation from SCL-II cells was performed with the DNeasy™ Blood & Tissue Kit according to the manufacturers guidelines. Typically the SCL-II cells were cultured as

described in **3.2.1** and trypsinized with 1 ml Trypsin-EDTA for 5 min and then resuspended in 4 ml MEM. A maximum number of 5x10^6 cells was used for the isolation. The elution step was done with 100μl of Buffer AE for an increased DNA concentration as indicated by the manufacturer.

PCR Primer sets (*Table 3.3*) were designed for the amplification of DNA fragment, isolated from SCL-II cells, containing the specific target sequence for the I-125-labeled TFO. The fragment lengths varied from 200 bp to 1700 bp and the amplification was carried out in a TProfessional Gradient Cycler as described in **3.2.3**. After the amplification the samples were added up to 100 μl with deionized water and transferred in a 1.5 ml tube. After addition of 10 μl NaAc [3 M] and 250 μl ethanol the solution was mixed by vortexing and centrifuged at 15,000 x g for 25 min. The supernatant was discarded and 400 μl of ethanol (70%) were added. After a further centrifugation at 15,000 x g for 5 min the supernatant was discarded and the DNA pellet dried at 37°C for 20 min. The pellet was resuspended in 20 μl of deionized water.

3.2.12. P-32-labeling of Southern-Blot Probes

The probes used for the southern-blot were PCR-amplified fragments of the up- and downstream TFO target region. The primers used for the amplification are shown in *Table 3.4* and were amplified in a standard PCR reaction (**3.2.3**). After the amplification the DNA was purified with the QIAquick™ PCR Purification Kit according to the manufacturer´s guidelines and resolved in deionized water. P-32 labeling of the probes was performed with the DecaLabel™ DNA Labeling Kit according to the manufacturer´s guidelines with α-P-32-dATP.

3.2.13. Double-Strand Break Analysis via Southern Blotting

The Southern Blotting is a method for the detection of specific DNA sequences in DNA samples with radioactive or fluorescent labeled probes. It was named and evolved by Edwin Southern [126]. A Southern Blot can basically be divided into the following steps. At first the desired DNA sample is restriction digested[1], separated in a polyacrylamide gel and then transferred and fixated on a nylon or cellulose membrane. In the last step the fixed DNA fragments are stained with radioactive labeled RNA or DNA probes

1 Restriction digestion was not necessary in the given setting as the target DNA was a PCR amplificate of the required size.

which are specific for the fragments of interest [126]. In the present work the Southern Blotting was used for the detection of breakage fragments resulting from the decay of I-125-TFO bound to a DNA fragment containing its target sequence.

Approximately 100 kBq I-125-TFO (~ 1.2 pmol) were added to ~ 700 ng (~ 0.6 pmol) of the specific target DNA in TFO-Binding Buffer B to a total volume of 20 μl, equaling in a molar ratio of 2:1 (TFO:DNA Target). The sample mixture was incubated at 37°C for 24 h. At this point a part of the mixture was used for verification of triplex formation via autoradiography. The remaining mixture was stored for at least 60 days (1 half-life of I-125) at -80°C for decay accumulation. After the accumulation period the samples were thawed and loaded on a 1% agarose gel and ran at 90 V for 90 min at room temperature. The gel was ethidium bromide stained and photographed with a scale of length aside. Then washed twice in 10 x volume Denaturation-Solution for 20 min and twice in 10 times volume Neutralization-Solution for 20 min. After that the gel was placed on a Nylon transfer membrane in a downward capillary blot assembly (*Figure 3.1*). For the the downward capillary transfer a stack of paper towels, slightly wider than the gel, was placed in a glass dish and covered with four pieces of Whatman paper. A fifth paper was soaked in 20 x SSC-Buffer (transfer-buffer) and put on top. Before placing the membrane (as wide as the gel) on top it had to be equilibrated in deionized water for 3 min. Bubbles were removed with a pipet. Then the gel and three pieces of Whatman paper (soaked in transfer-buffer) with the same size as the gel are placed on top. At least two large Whatman papers are soaked in transfer-buffer and placed on top as shown in *Figure 3.1* acting as a bridge between the gel and the transfer-buffer reservoir. A glass plate on top of the stack can help reducing evaporation. Blotting was performed for 1 h.

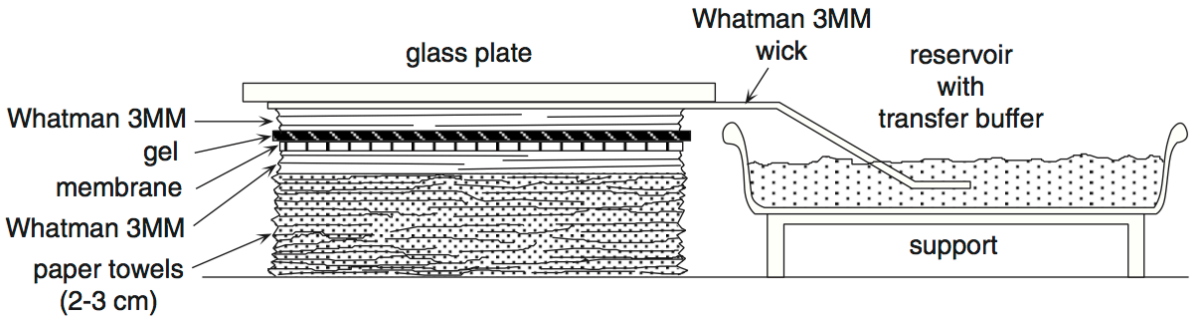

Figure 3.1.: Transfer pyramid setup for Southern blotting via downward capillary transfer [14].

After that the blotting apparatus was removed and the membrane was dried at room temperature for 30 min. Cross-Linking of the membrane was done on the UV-table of an ChemiDoc™ XRS+ for 2 min. Thereafter the membrane was rolled up with the top facing in and placed in a 50 ml Falcon tube. 15 ml of CHURCH Buffer (**3.2.14**) were

added followed by a prehybridisation at 65°C for 4 h in a slow agitating hybridization chamber. After the prehybridisation the buffer was replaced with fresh CHURCH Buffer and the P-32-labeled probes (**3.2.12**). The hybridization was performed at 65°C for 20 h in the hybridization chamber under slow agitation. Thereafter the buffer and probes were discarded and 20 ml of prewarmed (65°C) Washing Solution 1 was added for 10 min at 65°C (all following washing steps were performed at 65°C in the hybridization chamber under slow agitation). Then Washing Solution 1 was removed and replaced with 20 ml of Washing Solution 2 for 10 min. Washing Solution 2 was discarded and the membrane was washed twice in Washing Solution 3 for 20 min each. The membrane was taken out of the tube and dried at room temperature before being exposed to an MS Imaging Plate for 20 min. Visualization was performed on a FLA-5000 Imaging System.

3.2.14. CHURCH Buffer Preparation

The preparation of CHURCH Buffer is divided into two steps. At first the preparation of the Sodium Phosphate Buffer consisting of two hydrogenphosphate solutions and then in the second step the addition of the remaining ingredients for the CHURCH Buffer.

1. Preparation of Sodium Phosphate Buffer (0.5 M, pH 7.2)

Solution A:

Na_2HPO_4, $2H_2O$ (1 M)	177,9 g
deionized water	ad 1 l

Solution B:

NaH_2PO_4, H_2O	137,99g
deionized water	ad 1 l

The Sodium Phosphate Buffer is prepared by mixing both solution as follows:

Solution A	342 ml
Solution B	158 ml
deionized water	500 ml

2. Preparation of CHURCH Buffer

Sodium Phosphate Buffer (0.5 M, pH 7.2)	500 ml
EDTA (0.5 M)	2 ml
BSA	10 g
SDS	70 g

The BSA has to be dissolved in small amounts (per 1g) in 50 ml deionized water at room temperature. The SDS must also be dissolve in small amounts in 400 ml of

deionized water while stirring and heating. All ingredients were added to the Sodium Phosphate Buffer while slow stirring at room temperature followed by filtration with a 0.2 μm pore size syringe filter.

3.2.15. Transfection Procedure

Transfection via electroporation is a method for the permeabilization of cell membranes to insert DNA into eucaryotic cells. The basic principle is the "temporary increase of the membrane permeability due to reversible electrical breakdown of the plasma membrane upon application of external high-intensity field pulses of very short duration" [147]. The transfection method used in the present work was the Lonza Nucleofector system which is a system that combines the electroporation principle with cell type specific solutions. It permits the transfer of DNA or oligonucleotides directly into the nucleus of a living cell with a high efficiency (http://www.lonza.com/). This characteristic made it applicable for our needs. The transfection of the cell lines in the present work was done on the Lonza Nucleofector Device I combined with the Nucleofector® Kit V according to the manufacturer´s guidelines.

3.2.15.1. Transfection of SCL-II Cells

SCL-II cells were grown in T25 cell culture flasks (as described in **3.2.1**) to 70 - 80% confluency, then trypsinized by addition of 1 ml Trypsin-EDTA for 5 min and finally resuspended in at least 4 ml MEM with 16% FBS. The cells were counted on a Casy® Cell Counter and the required number (2x10^6) was transferred into a 15 ml Falcon tube and centrifuged for 10 min at 90 x g. The supernatant was removed and the cell pellet was resuspended in 100 μl Nucleofector Solution. The required amount of TFO was added and the solution was transferred into the transfection cuvette (supplied with the Nucleofector® Kit V). The electroporation reaction was performed on the Nucleofector Device I employing transfection program L-013. Immediately after the reaction 500 μl pre-equilibrated MEM with 16% FBS were added and the cell solution was transferred into a T25 cell culture flask (final volume of 10 ml media per flask) or aliquoted into a 6-well plate (final volume of 1.5 ml media per well), and incubated at 37°C.

3.2.16. SCL-II Cell Treatment for (I-125)IdU Incorporation

Deoxyuridine is a base analogue to deoxythymidine and is incorporated into cellular DNA during replication. In the present work the I-125-labeled deoxyuridine (I-125)IdU works as a carrier and enables the incorporation of I-125 into the DNA. To maximize the (I-125)IdU incorporation cells were synchronized in G_1-phase by contact inhibition as the added (I-125)IdU is only incorporated during the replication in the following S-phase. Moreover the cellular pyrimidine synthesis was blocked by the addition of FUdR, to minimize the inhibitory effect of intracellular thymidine on the incorporation of the added (I-125)IdU. As the cytosine synthesis is also affected by the FUdR blockage CdR had to be added as a substitute

SCL-II cells were grown in T75 cell culture flasks for 5 days. A cell confluency of 100% should be reached as a synchronization of cells due to contact inhibition was intended. After that the cells were trypsinized by addition of 1 ml Trypsin-EDTA for 5 min and resuspended in 20 ml MEM with 16% FBS. The cells were kept in the same culture flask and further incubated for 3 more days. After that the cells were trypsinized resuspended in MEM with 16% FBS and aliquoted in T10 cell culture flasks at 1x10^6 per flask and incubated for 10 h. Thereafter 100 pmol/μl FUdR, 100 pmol/μl CdR and 1 kBq/ml (I-125)IdU were added (total volume 3 ml) and incubated for 20 h. Negative controls were treated the same way but instead of (I-125)IdU 100 pmol/μl non-radioactive IdU was added. After the incubation the cells were washed twice with PBS, trypsinized and resuspended in MEM with 16% FBS. Before centrifugation at 300 x g for 5 min the cell number was counted on a Casy® Cell Counter. After centrifugation the cells were resuspended in freezing medium (FBS + 10% DMSO) and stored in freezer vials. Before storage at -150°C for decay accumulation the specific activity of each vial was determined on a Gamma Counter 1480 Wizard™ 3.

3.2.17. Flow Cytometry

The flow cytometry is an application based on the analysis of cells flowing at high speed past a beam of exciting light. Different detectors are positioned at the point where the cells pass the light beam. The detector located in line with the beam is the Forward Scatter (FSC) whose signals correlate with the cells volume, perpendicular to the beam is the location of the Side Scatter (SSC) measuring the scattered light as a degree for the cytoplasmic granularity or membrane roughness of the cells. Additional fluorescence detectors allow the discrimination of different fluorescent stains which can

be used for staining of whole cells or cellular structures [39]. The flow cytometer used for the following analysis was a BD FACS Canto™ II equipped with two laser beams for 488 nm and 523 nm.

3.2.17.1. Cell Cycle Analysis of SCL-II Cells

In the present work the cell cycle analysis was done by flow cytometry after permeabilisation and 7-aminoactinomycin D (7-AAD) staining of SCL-II cells. 7-AAD is a fluorescent DNA intercalator which enables the relative quantification of DNA in cells. On the basis of the DNA content the different cell cycle phases can be distinguished as the DNA content differs between the phases [71].

The aim of the cell cycle analysis in the present work was to study the influence of I-125-labeled and unlabeled TFOs in SCL-II cells on the duration of the different cell cylce phases. For this purpose SCL-II cells were transfected as described in **3.2.15.1** with $\sim$ 100 kBq of I-125-TFO or 5 pmol of unlabeled TFO and incubated in T25 cell culture flasks for 22 h at 37°C. After the incubation the cells were trypsinized and stored in freezing medium (FBS + 10% DMSO) at -150°C for decay accumulation. After the accumulation period the cell samples were thawed and each sample was aliquoted on several T25 cell culture flasks at 5x10^5 cells per flask and cultured at 37°C. Each of the flasks was used for one measurement time point which were set after 0 h, 8 h, 16 h, 24 h, 32 h, 40 h and 48 h. At each time point the cells were trypsinized, resuspended in MEM, and transferred into a 15 ml falcon tube. After centrifugation (5 min, 400 x g, RT) the cell pellet was resuspended in 1ml PBS and transferred into a 2 ml tube. After a further centrifugation (5 min, 400 x g, RT) and one additional wash step in PBS the sample was centrifuged (5 min, 400 x g, RT) and fixed by the addition of 300 μl PBS and 700 μl Ethanol (100%). The 7-AAD stain was performed as follows. At first the cells were washed twice in PBS and then resuspended in 100 μl PBS + 5 μl 7-AAD staining solution. After staining for 25 min at RT 500 μl PBS were added and then analyzed in a BD FACS CANTO™ II flow cytometer.

3.2.17.2. Biokinetic of TFOs in SCL-II Cells

In the following assay the kinetic behavior of Alexa488-labeled TFOs in SCL-II cells was analyzed, focusing on localization, stability and retention time of the TFOs in the cells. The Alexa488 fluorochrome shows excitation/emission maxima at 495/519 nm. SCL-II cells were transfected with 100 pmol of Alexa488-labeled TFO-BCL2 (**3.2.15.1**) and

incubated in two 6-well plates (3x10^5 cells/well) at 37°C. After 1, 6, 12, 18, 24, 30, 48 and 72 h the medium in one well was discarded, the cells were washed with PBS and subsequently trypsinized with Trypsin-EDTA and resuspended in 2 ml MEM with 16% FBS. The cell solution was transferred in 5 ml round bottom tubes and centrifuged for 5 min at 300 x g at room temperature (all following centrifugation steps were performed with these settings). The supernatant was discarded and the cell pellet washed twice in PBS and finally resuspended in 500 μl PBS. After the addition of 5 μl propidium iodide the samples were incubated for 15 min at RT. Thereafter the cells were analyzed up to a maximum of 10,000 events in the flow cytometer. The fraction of apoptotic and necrotic cells, respectively, was determined on basis of the measured propidium iodide signal. Beside the analysis of whole cells also isolated cell nuclei were tested. Therefore the cells were further processed following a nucleic isolation protocol. At first the cells were resuspended in Nuclei-Extraction Buffer by vortexing for 10 sec and incubation for 10 min on ice. After centrifugation the supernatant was discarded and the pellet washed two times in 2 ml Nuclei-Wash Buffer. Prior to the flow cytometric analysis the isolated nuclei were resuspended in 500 μl Nuclei-Wash Buffer. Sham transfected cells were used as negative controls and were also treated as previously described. The fluorescence measured in the negative controls displayed the background signal and was used to set the threshold for TFO positive samples.

3.2.18. Live Cell Imaging of SCL-II Cells

Live cell imaging is a technique that allows the microscopical monitoring of cellular dynamics and physiological processes. The study of these processes needs live imaging over time which in turn requires special imaging equipment that provides the necessary conditions for living cells. That means a constant temperature of 37°C, provided by a microscopic heating chamber, and if possible a CO_2 gassing. The CO_2 gassing can be omitted if the cells are kept in L-15 Leibowitz´s medium, which does not require a controlled atmosphere. Moreover the cells have to be cultivated in cell dishes with coverslip bottoms (glass bottom dishes). The imaging was performed on a Zeiss Vivatome combined with a Axio Observer. Z1 fluorescence microscope, driven by the AxioVision software, which allows surveilance of multiple cells throughout the whole testing period.

In the present work live cell imaging was used to monitor the biokinetics of Alexa594-labeled TFOs in SCL-II cells. Alexa594 shows excitation/emission maxima at 590/617 nm and was used due to its greater photo stability in comparison to Alexa488, which

was used for flow cytometric analysis. At first SCL-II cells were grown in L-15 Leibowitz´s medium[2] and transfected with 100 pmol of Alexa594-labeled TFO-BCL2. After transfection the cells were transferred into glass bottom dishes and incubated in the microscopic heating chamber until they settled and got adherent to the glass surface. Thereafter 20 solitary growing, adherent cells were chosen and tracked for the next 16 h at an interval of 2 h. For imaging a Plan-Apochromat 100x/1.40 Oil DIC oil immersion objective was used combined with a Texas red T7 filter for fluorescent imaging. For each image a DIC and a fluorescent picture was taken and finally merged. The focus position was set so that the nucleus was clearly visible, with a Z-stack diameter of 0.5 μm. Though a focus drift due to thermal expansion could not be excluded, the focus was manually refocused at each time point.

3.2.19. RNA Isolation from SCL-II Cells

The RNA isolation from SCL-II cells was performed with the RNeasy™ Mini Kit according to the manufacturere´s guidlines. The RNA purity was determined using a NanoDrop® photometer whereas the values for 260/280 nm (protein contamination) and 260/230 (organic solvent contamination) had to be in the range of 2.0 ± 0.2 to be usable for further applications. The RNA quality was analyzed with a lab-on-a-chip system using the RNA 6000 Nano Kit in the Bioanalyzer 2100. Determining for the RNA quality was the RIN-Value (RNA Integrity Number) which shows the relation of 18S- to 28S ribosomal RNA (rRNA). RIN-Values range from 1 to 10 whereas 1 reflects a totally degraded RNA and 10 completely intact RNA. For further applications only RNA with a RIN-Value of at least 8 were used. The RNA isolates were stored for further use at -80°C.

3.2.20. Quantitative Real-Time PCR

The quantitative Real-Time PCR (qRT-PCR) is a method for quantification of nucleic acids. It is based on the standard PCR reaction as described in **3.2.3** but additionally allows the monitoring of the amplification process in real time. The basic principle is the detection of a fluorescent DNA intercalator (EtBr, SYBR-Green) which signals intensity increases in proportion to the progressing DNA amplification [52]. The qRT-PCR can

2 The use of Leibowitz´s medium was necessary as the provided microscopic heating chamber did not allow CO_2 gassing.

also be used to quantify messenger RNA (mRNA) or non-coding RNA when combined with a reverse transcriptase PCR.

In the present work the quantification of mRNA was used to determine the expression of specific genes in SCL-II cells after the transfection with gene specific binding I-125-TFOs. The SCL-II cells were transfected as described in **3.2.15.1** with ~ 100 kBq of I-125-TFO or the analog but unlabeled TFO [5 pmol], incubated for 20 - 23 h at 37°C and then stored in freezing medium at -150°C for decay accumulation. After the accumulation period the cells were thawed and cultured for 20 - 23 h at 37°C in T25 cell culture flasks. Thereafter the cells were trypsinized and an RNA isolation was done as described in **3.2.19**. The effect of three different TFOs was tested, which were designed to bind within one of the following genes, *BRCA1*, *BCL2* or *GAPDH*. As endogenous control or housekeeping genes *GAPDH* (for *BCL2* and *BRCA1*) and *ACTIN* were used. The housekeeping gene expression was determined for each sample. Before starting the qRT-PCR, primer sets (*Table 3.5*) specific for the selected genes were designed. The primer were constructed in accordance with the following characteristics. A product length between 100 bp to 150 bp, annealing temperature 59°C and the melting temperature (Tm) within a range of 65°C to 85°C but ideally at 75°C. Before use the primer sets were tested for their specificity in a standard PCR (**3.2.3**) with a template originating from a whole RNA isolate transcribed into cDNA via cDNA synthesis (**3.2.21**). For the qRT-PCR the Power SYBR® Green RNA-to-C_T™ 1-Step Kit was used. Shown in *Table 3.18* is the component mix for one sample of a qRT-PCR.

Table 3.18.: Component Mixture for one qRT-PCR sample

Reagent	Volume
Primer fwd. [10 μM]	1 μl
Primer rev. [10 μM]	1 μl
RT-Enzyme Mix (x125)	0.16 μl
RT-PCR Mix (x2)	10 μl
RNA-Template [30 ng/μl]	1 μl
nuclease free dH_2O	6.84 μl

Each I-125-TFO was tested in three biological replicates, prepared in independent transfection reactions. Each replicate was loaded on a 96-well plate in three technical replicates that were automatically averaged by the software. In the first step of the qRT-PCR the Master Mix (without RNA-Template) was prepared and loaded on a cooled 96-well plate. In the second step the RNA-Template was added and the 96-well plate was covered with an optical adhesive cover and centrifuged (1 min, 300 x g,

4°C). Subsequently the plate was placed in a qRT-PCR cycler and the qRT-PCR was performed using the program shown in *Table 3.19*.

Table 3.19.: qRT-PCR Program

Step	Temperature	Time	
cDNA-Synthesis	50°C	30 min	
initial Denaturation	95°C	15 min	
Denaturation	94°C	15 sec	
Hybridisation	59°C	30 sec	**x40**
Elongation	72°C	40 sec	

After the qRT-PCR the specificity of the amplificated product was measured using a melting curve analysis, starting at 59°C and increasing stepwise up to 95°C. The evaluation of the results was done with the Sequence Detection Software. The software integrated the technical replicates per sample, allowed the normalization of the detected signals on the basis of the passive reference dye ROX, and calculated the expression of the measured sample in comparison to untreated controls (relative expression). The basis for the calculations were as follows:

1. Normalization in relation to the endogenous control (*GAPDH, ACTIN*)
   Ct Sample - Ct endogenous control (*GAPDH, ACTIN*) = ∆Ct Sample/ Calibrator

2. Normalization to Calibrator (negative control)
   ∆Ct Sample - ∆Ct Calibrator (negative control) = ∆∆Ct

3. Substituted in the formula
   $\mathbf{2}^{-\Delta\Delta\mathbf{Ct}}$

The ∆∆Ct values were further analyzed with Microsoft Excel. That comprised the integration of the biological replicates and the calculation of the significance using the Student´s *t*-test.

3.2.21. cDNA Synthesis

To test the specificity of the qRT-PCR primer (**3.5**) first of all a whole RNA isolate from SCL-II cells (**3.2.19**) was transcribed into cDNA in a reverse transcription synthesis. For this, the Transcriptor High Fidelity cDNA Synthesis Kit was used, which contained all necessary reaction components. At first the Template-Primer Mix (*Table 3.20*) was

prepared in a 0.2 ml tube, heated for 10 min to 65°C and transferred on ice to ensure denaturation of RNA secondary structures. Thereafter the Reverse Transcription Mix (*Table 3.20*) was added and the cDNA synthesis performed for 30 min at 55°C. For inactivation of the reverse transcriptase the sample was heated to 85°C for 5 min and then placed on ice. For further use the samples were stored at -20°C.

Table 3.20.: Component mixture for cDNA synthesis (Transcriptor High Fidelity cDNA Synthesis Kit); x, volume appropriate for 50 ng of total RNA was added

Template Primer Mix	
Reagent	**Volume**
Anchored-oligo$(dt)_{18}$ Primer [50 pmol/μl]	1 μl
total RNA	x
deionized water	ad 11.4 μl
Reverse Transcription Mix	
Reagent	**Volume**
Reverse Transcriptase Reaction Buffer (x5)	4 μl
Protector RNase Inhibitor [40 U/μl]	0.5 μl
Deoxynucleotide Mix [10 mM each]	2 μl
DTT	1 μl
Reverse Transcriptase	1.1 μl

3.2.22. The 53BP1 Foci Assay

The 53BP1 assay performed in the present work is an immunostaining method using a 53BP1 antibody for the visualization of nuclear foci that are localized at sites of DNA DSBs [115].

The SCL-II cells were transfected as described in **3.2.15.1** with ~ 100 kBq of I-125-TFO, incubated for 20 - 23 h at 37°C and then stored in freezing medium at -150°C for decay accumulation. As negative controls served SCL-II cells which were transfected with the analog but unlabeled TFO [5 pmol], and further treated as the active transfected cell samples. After the accumulation period the cells were thawed and the appropriate number (5 x 10^4 cells/well) was plated in 6-well plates and grown on sterilized glass coverslips for 20 - 23 h. Thereafter the cells were rinsed three times with PBS-Buffer and fixed with 4% paraformaldehyde (solved in PBS) for 20 min at room temperature. Then rinsed two times with TBP-Buffer. The coverslips were covered with 1% Triton X-100 (solved in PBS) for 20 min at room temperature and then rinsed two times with TBP-Buffer. Blocking was done in 5% goat serum (solved in PBS) for 1 h at room temperature followed by two washing steps with TBP-Buffer. The primary antibody (53BP1, H-300: sc-22760) was added in a 500-fold dilution in TBP-Buffer for 1 h at

room temperature followed by three washing steps with TBP-Buffer and incubation for 45 min with the second antibody (1:700 in TBP-Buffer, goat anti-rabbit IgG-TR: sc-2780). The coverslips were then washed two times in TBP-Buffer, once in PBS-Buffer and finally rinsed in deionized water and kept at room temperature for drying. For microscopy the monolayers were mounted with ProLong Goldantifade reagent with DAPI on glass slides. The analysis was performed on a Zeiss LSM700 Observer Z1 microscope. For each sample 100 randomly selected cells were analyzed and the average number of foci was calculated.

3.2.23. Colony Forming Assay

The Colony Forming Assay (CFA) is a method to determine the ability of a cell to proliferate indefinitely, whilst retaining its reproductive ability to form a large colony or a clone [92]. It is frequently used to measure the effect of ionizing radiation or chemotherapeutic agents on the reproductive ability of cells [53].

In the present work the CFA was performed with SCL-II cells after gamma irradiation (**3.2.2**), (I-125)IdU incorporation (**3.2.16**) and after the transfection with $\sim$ 100 kBq I-125-TFOs (**3.2.15.1**) binding to single or multiple targets in the human genome. The transfected cell samples were cultured for 20 - 23 h at 37°C, trypsinized and then stored in freezing medium for decay accumulation at -150°C. For gamma irradiated cells, storage was not necessary. As negative controls served SCL-II cells which were transfected with the analog but unlabeled TFO [5 pmol], respectively, IdU or unirradiated, and further treated as the active transfected or irradiated cell samples. After the accumulation period the cells were thawed, centrifuged (5 min, 300 x g, RT; unless specified all centrifugation steps were performed with this program) and the cell pellet was resuspended in MEM. The appropriate number of cells (500 cells/well) was plated in a 6-well plate, filled with 3 ml MEM each, and incubated for 12 days. Cell culture medium was renewed after 6 days. After 12 days the culture medium was removed and the cells were washed with 2 ml PBS. Then the cells were fixed by the addition of methanol and incubated for 10 min at -20°C. Thereafter the methanol was discarded and the cells dried at room temperature for 10 min. After one more wash step with PBS 10% Giemsa stain (preparation see **3.2.23.1**) (1 ml/well) was added for 15 min at room temperature. Finally the Giemsa stain was discarded and the cells were washed twice in deionized water and then dried at room temperature. For the interpretation each colony consisting of 50 or more cells was counted as survivor. The total num-

ber of colonies divided by the total number of colonies of controls was defined as the surviving fraction, which was then plotted against the accumulated decays per cell.

3.2.23.1. Preparation of Giemsa Stain

The Giemsa staining solution was prepared as follows. The desired amount of Giemsa stock solution was mixed with Microscopy Buffer to the desired concentration and thereupon the solution was filtered through a folded filter (grade 3 hw).

3.2.24. Micronucleus Assay

The micronucleus assay is a method for the quantification of chromosomal damage resulting from genotoxic compounds like chemical agents or ionizing radiation. The standard for the chromosomal damage used in this assay is the formation of micronuclei which are small cytoplasmic bodies containing a part or a whole chromosome. The formation of micronuclei occurs after chromosomal damage within the anaphase, when these chromosomal fragments or chromosomes are not carried to the opposite poles. The micronuclei are also surrounded by a nuclear membrane and appear after cytokinesis as small nuclei (micronuclei) in one of the daughter cells [49].

In the present work the micronucleus assay was used to determine the genotoxic potential of I-125-TFOs in SCL-II cells. Therefore SCL-II cells were transfected, as described in **3.2.15.1**, with $\sim$ 100 kBq of the desired I-125-TFO or 5 pmol of the analog unlabeled TFO serving as negative control. The transfected cells were cultured for 20 - 23 h at 37°C, trypsinized and then aliquoted at 5x10^5 cells per freezer vial in freezing medium. The samples were stored at -150°C for decay accumulation. After the accumulation period the cells were thawed, centrifuged (5 min, 300 x g, RT; unless specified all centrifugation steps were performed with this program) resuspended in MEM + Cytochalasin B [1 μg/ml] and cultured for 24 h at 37°C. Thereafter the cells were washed twice with PBS, trypsinized and resuspended in 1.5 ml MEM. The cell solution was transferred into a 2 ml tube and centrifuged. The supernatant was discarded and the cell pellet washed twice in PBS. For fixation the cells were resuspended in a Methanol/ Acetic acid (3:1) solution and were stored at 4°C for further use. For micronucleus analysis 10 - 20 μl of the fixed cells were dropped with a pipet on microscope slides and allowed to dry at RT. After that the slides were incubated in a Hoechst 33342 staining solution [1 μg/ml] for 1 min at RT and then transferred successively in

two deionized water baths for 1 min each. After drying at RT the cells were embedded in mounting medium on the microscope slide and covered with coverslips. The samples were analyzed on a Zeiss Axioplan 2 microscope with the Metafer 4 Metacyte Software.

3.2.25. Statistical Analysis

Results are expressed as the mean and the standard error of the mean (SEM) from at least three (in exceptions two) independent experiments. Statistical analyses were performed with Student´s two-tailed paired (or unpaired) t-test. Values of $p < 0.05$ were considered statistically significant.

4. Results

4.1. *In Vitro* DNA Triplex Formation and Binding Assay

A total of 26 TFOs were tested for their triplex forming ability *in vitro* with their specific target sequence. These TFOs were designed as described in **3.2.6** complementary to their target sequences. The verification of the triplex formation was performed with EMSA (**3.2.5**).

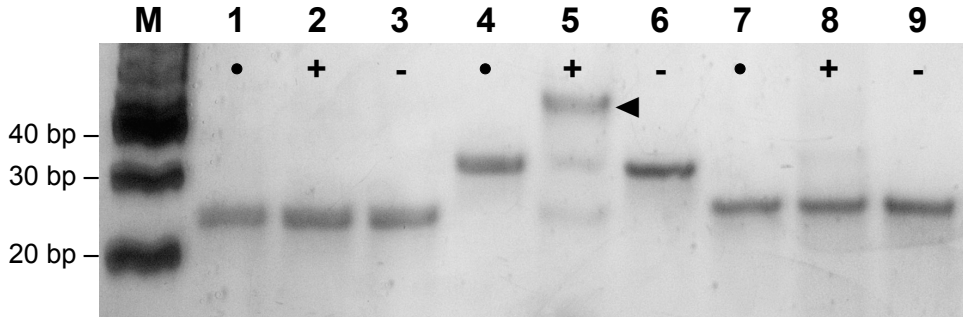

Figure 4.1.: Triplex formation *in vitro* visualized with the electrophoretic mobility shift assay (EMSA). Silver staining. 20% native polyacrylamid gel. •: Non-sense samples containing the target sequence with a non-complementary TFO as control; **lanes 1, 4** and **7**. **+**: TFOs with their specific target sequences; **lanes 2, 5** and **8**. **-**: Negative controls containing the specific TFO target fragment only; **lanes 3, 6** and **9**. **M**: Marker. A band shift reflects a DNA triplex formation (◄).

Of all tested TFOs (*Table 4.1*) having a suitable sequence to form a DNA triplex with their specific DNA targets about 58% failed to form a triplex in the EMSA *in vitro*. Succesful DNA triplex formation could be verified for 42% and was indicated by a clear band-shift of the Target/TFO construct as shown on *Figure 4.1* (lane 5, ◄) when compared to the target sequence only (*Figure 4.1*, lane 6). The triplex formation with non-complementary (non-sense) TFOs as a proof for the specificity of the specific TFO and its target sequence was also analyzed. As expected all non-sense TFOs failed to form DNA triplices (*Figure 4.1*, lane 1, 4 and 7).

Table 4.1.: Triplex-Forming-oligonucleotides tested in the present work. TFO with confirmed triplex formation are marked in gray.

Name	Sequence (5´- 3´)
TFO-V1	ggt ttg gtg gtt ggg tgt gtg
TFO-V2	ttt gtt ggg tgg tgg gtt ggt tgt gtt aag aaa
TFO-V3	ggg ggt tgg ggt gtg gtg ggg
TFO-V4	ggg ggt tgt ggt ttg tgg ttg ttg
TFO-V5	ggtt gtg tgt gtg tgt gtg
TFO-V6	ttg tgg gtg tgg tgg ggt tt
TFO-V7	gtt gtg gtt gtg gtt ggg
TFO-V8	ggt gtt ggt tgg ttg ttt tgg tgg gga aga gg
TFO-BCL2	gtg ttt gtt ttt gtt ggg tgg tgt ggg gc
TFO-BRCA1	tgg gtg tgt gtt ggt gtg ttg ttc cgg ga
TFO-V11	tgg gtg gtg ggt gtt tgt tgt g
TFO-V12	ggg tgg tgt ggg tgg gtt ttt ttt ggg
TFO-V13	ggg ttt ttt gtg ggg gtg ttg
TFO-V14	ttg tgc ttt ggt tgt
TFO-V15	ttg tgc ttt ggt tgt
TFO-V16	ttg gtt cgg gtt gg
TFO-V17-Cyt-17	tgg tgg ttt gtg ggt tc
TFO-GAPDH	ggg ggt ggg gtt tgt ttg ttt c
TFO-V19-Cyt-1423	tgt ttt ggg ttg gct tgt tgg tcg
TFO-V20-Cyt-12	ggt ggt tgg ttc ggt tgg t
TFO-V21-Cyt-20	ttt tgt ggt gtt gtt ttg gcg tt
TFO-V23-Cyt-81729	ttg tgt tcg ttt gtt gcg ttt gtg ggt tct
TFO-V25-Cyt-18	ggg ggt ttg tgg ttt ttc
TFO-V26-Cyt-19	ggg tgg ttg gtt ggg ttg c
TFO-V27	ttt ggt ttt ggg ggg ttt ggt tgg
TFO-V28	gtg ttg ttt gtg ggt tgt ggg t

4.2. I-125 Labeling of TFOs

After having examined the triplex forming capabilities of the unlabeled TFOs (**4.1**) the next major step was to establish the I-125-labeling of the TFOs. The labeling reaction was performed with a modified version of the Primer Extension Method published by Panyutin et al. [97]. However, several delicate steps in the labeling reaction, which are thoroughly described in this chapter, had to be adapted and improved.

4.2.1. Denaturation

During the first two steps of the labeling reaction the biotin template and preTFO were annealed and the preTFO was elongated with a single I-125dCTP (**3.2.8**). In order to isolate the now I-125-labeled TFO from the biotin template, the TFO-Template complex had to be denatured. For denaturation the most common method is heating to a temperature above the melting temperature (Tm) of the TFO. Denaturation can also be achieved by applying alkaline conditions through the addition of NaOH. To determine the best denaturation conditions the primer extension was performed with FITC-dCTP, and thereafter the FITC-labeled TFO-Template-Biotin complex (*Figure 4.2*), bound to streptavidin magnetic particles, was successively heated and brought to alkaline conditions for different periods of time.

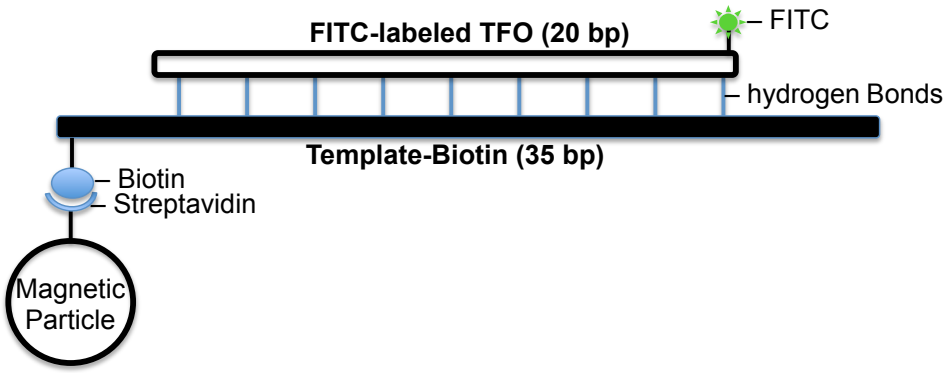

Figure 4.2.: Schematic diagram of the FITC-labeled TFO-Template-Biotin complex bound to a streptavidin magnetic particle.

After each denaturation step the magnetic particles were sedimented with a magnet and the supernatant was collected and loaded on a 20% polyacrylamidgel. Before the next denaturation the magnetic particles were resuspended in deionized water respectively NaOH solution. After the gel run the apparent running height of the EtBr stained fragments revealed the efficiency of the applied denaturation conditions (*Figure 4.3*). The FITC-labeled TFO-Template complex was expected to run at approximately 35

bp whereas the FITC-labeled TFO alone should be detectable at ~ 20 bp. Thus an EtBr- and FITC-signal at 35 bp indicated a breakup of the streptavidine-biotin bond and therefore TFO-template complex could be detected in the supernatant. An EtBr- and FITC-signal at 20 bp was evidence for the efficient detachment of the TFO from the template.

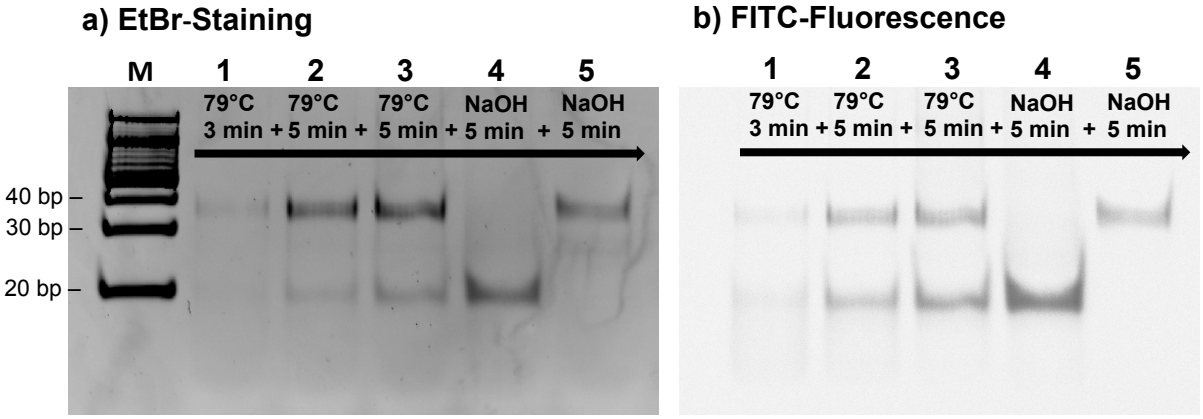

Figure 4.3.: Polyacrylamidgel-electrophoresis of FITC-labeled TFO-Template complex samples after treatment at different denaturation conditions; **lanes 1 - 5**. **M**: Marker. The same sample was successively analyzed at each condition. a) Ethidium bromide staining and b) FITC signal scan. 20% native polyacrylamidgel.

At denaturation conditions of 79°C for 3 min (*Figure 4.3*, lane 1) signals at 20 and 35 bp were detectable but were very weak. Further incubation at 79°C for additional 5 min (*Figure 4.3*, lane 2) increased the intensity of both signals with a more pronounced signal at 35 bp. An additional incubation at the same conditions (*Figure 4.3*, lane 3) increased both signals only slightly. Incubation in 0.15 M NaOH solution (*Figure 4.3*, lane 4) led to a pronounced signal at 20 bp and no detectable signal at 35 bp. Additional 5 min of incubation at the same conditions (*Figure 4.3*, lane 5) showed the opposite, with a signal at 35 bp and no detectable signal at 20 bp. This observation is conform with the manufacturer´s informations admitting that small amounts of the biotin-template can be released after incubation at alkaline conditions. However, due to the good harvest rate the denaturation of all labeled TFOs from the templates used in this study was performed at alkaline condition by the addition of 0.15 M NaOH for 5 min. Before further use the isolated TFOs had to be titrated to a neutral pH-value by the addition of 10 x TFO-Binding Buffer and 1.25 M acetic acid.

4.2.2. Labeling Efficiency

The labeling efficiency was calculated as the ratio of preTFO amount in the primer extension mix and the amount of I-125-labeled TFOs at the end of the reaction.

The primer extension reaction mix described in **3.2.8** using 5 pmol of preTFO, 5 pmol of template and 2.5 MBq of I-125-dCTP led to an average total activity of ~ 370 kBq in TFOs labeled with a single I-125-dC at the terminal 3'-position. According to the calculation formulas shown in **3.2.9** this equaled a labeling efficiency of ~ 90% and a total amount of I-125-labeled TFO of ~ 4.5 pmol, respectively. In addition, the influence of an increased amount of preTFO/template was examined. Therefore, a maximum of 100 pmol of preTFO/template per reaction mix was tested. This increase of preTFO led to a total amount of I-125-labeled TFO of approximately 11 pmol and 11% labeling efficiency. Thus a 20-fold increase of preTFO/template amount resulted in an approximate doubling of I-125-labeled TFO. At the same time, however, the total amount of unlabeled TFO at the end of the reaction was more than 170-fold (0.5 pmol to 89 pmol) increased. Due to this unfavorable ratio of labeled to unlabeled TFO the primer extensions in the present work were performed with the reaction mixture described in the first place.

4.2.3. TFO Triplex Formation after I-125 Labeling

After primer extension the I-125-labeled TFOs were examined *in vitro* for their triplex forming capabilities.

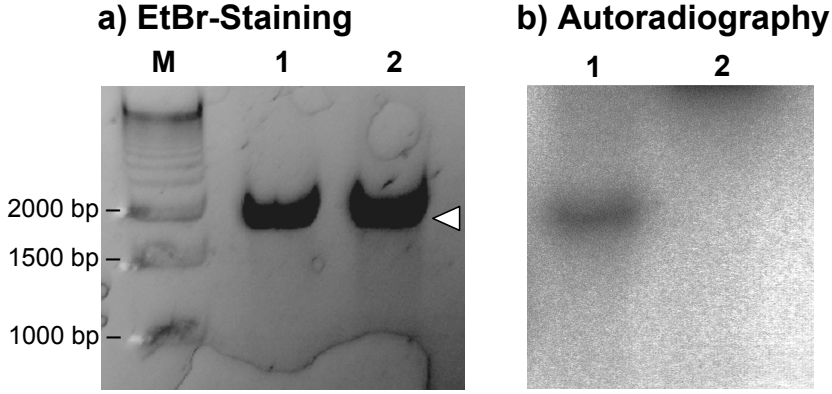

Figure 4.4.: Triplex formation of I-125-labeled TFO-BCL2, visualized via **a)** gel electrophoresis combined with **b)** autoradiography. 3.5% polyacrylamidgel. **Lane 1**: I-125-labeled TFO + ~ 0.4 μg target fragment (1695 bp, ◁). **Lane 2**: Non-sense sample containing a non complementary I-125-labeled TFO + ~ 0.4 μg target fragment (1695 bp, ◁).

The gel electrophoresis (*Figure 4.4* a) combined with the autoradiographic analysis (*Figure 4.4* b) confirmed successful triplex formation for TFOs after I-125 labeling with the specific DNA target (*Figure 4.4* a, lane 1 and b, lane 1). Due to the target length of 1695 bp an EMSA is not possible as a band shift caused by DNA triplex formation would not be pronounced enough for being visualized. However, the signal in the autoradiography revealed that the I-125-labeled TFO had bound to its specific target sequence

(*Figure 4.4* b, lane 1). As expected the non-complementary I-125-labeled TFO failed to form a triplex with the target fragment, having led to no detectable autoradiographic signal (*Figure 4.4* b, lane 2).

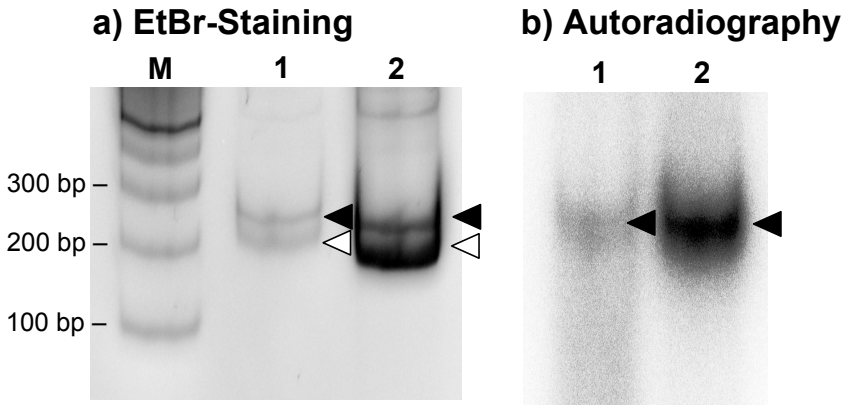

Figure 4.5.: Triplex formation of I-125-labeled TFO-BCL2 with varying target concentrations, visualized via **a)** electrophoretic mobility shift assay combined with **b)** autoradiography. 12% polyacryamidgel. **Lane 1**: I-125-labeled TFO + 1.6 μg target fragment (212 bp). **Lane 2**: I-125-labeled TFO + 4.9 μg target fragment (212 bp). **M**: Marker. A band shift and an autoradiographic signal, respectively, reflects a DNA triplex formation (◀). Target fragment (◁).

EMSA with the same TFO but with a much smaller target fragment (*Figure 4.5*, ◁, 212 bp), used at two different concentrations (lane 1, 1.6 μg; lane 2, 4.9 μg), revealed the successful DNA triplex formation by a band shift. The detected band shift in *Figure 4.5* a, lane 1 and 2 (◀) was additionally confirmed by the signals in the autoradiographic assay in *Figure 4.5* b, lane 1 and 2 (◀), showing successful binding of I-125-labeled TFO to its target. The variation in signal strength in the EtBr staining and the autoradiography was in good accordance with the different amounts of target fragments loaded in the reaction mixes (1.6 μg lane 1, 4.9 μg lane 2).

4.3. DNA Double-Strand Break Analysis *in vitro*

To demonstrate that I-125-labeled TFO induced DSBs within the binding region, a 1695 bp target fragment with a specific binding site for TFO-GAPDH was used for analysis. After 143 days at -80°C for decay accumulation the DNA triplex was analyzed on an agarose gel and visualized with EtBr staining (**3.2.4**) and southern blotting (**3.2.13**). The TFO binding site and induced breakage fragments of I-125-TFO-GAPDH are displayed in *Figure 4.6*.

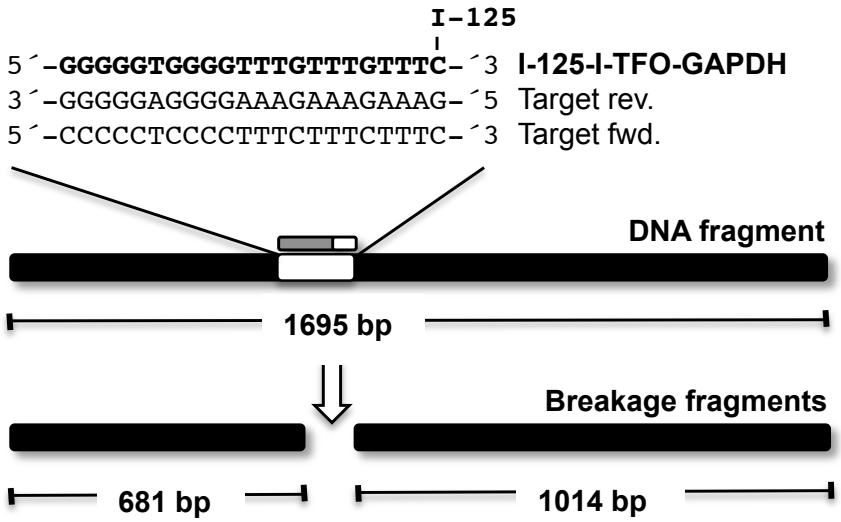

Figure 4.6.: Schematic diagram of the 1695 bp long DNA fragment containing the target sequence for TFO-GAPDH and the two expected breakage fragments of 681 bp and 1014 bp length. The TFO is I-125-labeled at the 3'-terminal cytosine and binds to the polypurine target sequence in reverse Hoogsteen orientation.

The results of the DSB analysis revealed that the I-125-TFO-GAPDH induced a single DSB within the 1695 bp target fragment (*Figure 4.7* a, ◁) resulting in the two expected breakage fragments of 1014 bp and 681 bp (*Figure 4.7* a, ◀). No DNA breakage was observed for the non-binding, non-specific, non-sense I-125-labeled TFO (*Figure 4.7* a, lane 2). Southern blot analysis (*Figure 4.7* b) verified that the observed breakage fragments originated from the target fragment (*Figure 4.7* b, lane 1). The southern blot probes were P-32-labeled PCR amplificates of the region up- and downstream of the TFO target site (**3.2.12**). The two detected bands at 500 bp and below did not show a southern-blot signal and are likely to be unspecific amplificates from the PCR of the target fragment.

The breakage efficiency in the target fragment was calculated as the sum of the band intensities of the two breakage fragments to the sum of the intensities of all three fragments according to Sedelnikova et al. [117] leading to a percentage of breaks of $\sim$ 40% after 143 days of decay accumulation ($\sim$ 1.9x10^{11} decays/pmol target DNA).

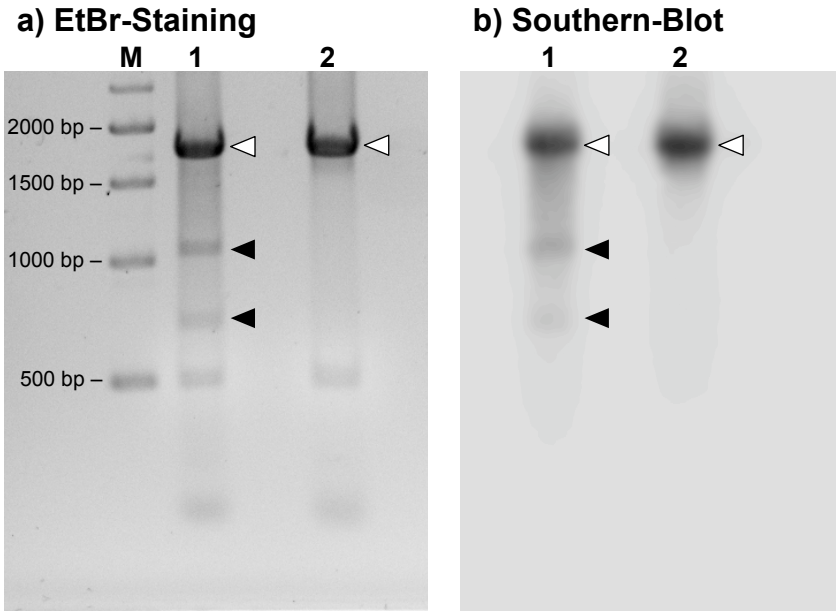

Figure 4.7.: DSB analysis of a 1695 bp DNA fragment (◁) containing the target sequence for TFO-GAPDH. The samples were separated in a 1% agarose gel and visualized by **a)** ethidium bromide staining and **b)** southern blotting. **M**: Marker. **Lane 1**: Target fragment + I-125-TFO-GAPDH. **Lane 2**: Non-sense sample containing the target fragment + non-binding I-125-TFO. Breakage fragments (◄) of 1041 and 681 bp length. Figure according to Dahmen and Kriehuber [23]

That equaled $\sim$ 1.9x10^{11} decays in 6 x 10^{11} molecules (0.31 decays/molecule). At $\sim$ 40% breaks this would be $\sim$ 1.2 DSB/decay. Taken into account that the molar ratio TFO:DNA target in the reaction was 2:1 (**3.2.13**), the number of DSB per decay was reduced to $\sim$ 0.6 DSB/decay because only half of the TFOs could bind to the DNA target at all.

4.4. Biokinetic of TFOs in SCL-II Cells

To elucidate the biokinetic behavior of TFOs, and to verify that the chosen transfection method (**3.2.15.1**) was able to get TFOs directly into the cell nucleus as well as to investigate whether the transfected TFOs persist for a longer period in the nucleus, biokinetic studies were performed in SCL-II cells. Therefore SCL-II cells were transfected with Alexa488-labeled TFOs and then whole cells and isolated nuclei samples were analyzed in the flow cytometer after certain time points during the 72 h post transfection. All samples whose measured fluorescence exceeded a defined threshold were defined as TFO positive cells and TFO positive nuclei, respectively. The threshold was set on the background fluorescence measured in sham transfected negative control samples (*Figure 4.8*). It should be kept in mind, however, that due to the sensitivity limit of the flow cytometry [148], cells or nuclei that are defined as TFO negative can still contain a certain amount of TFOs.

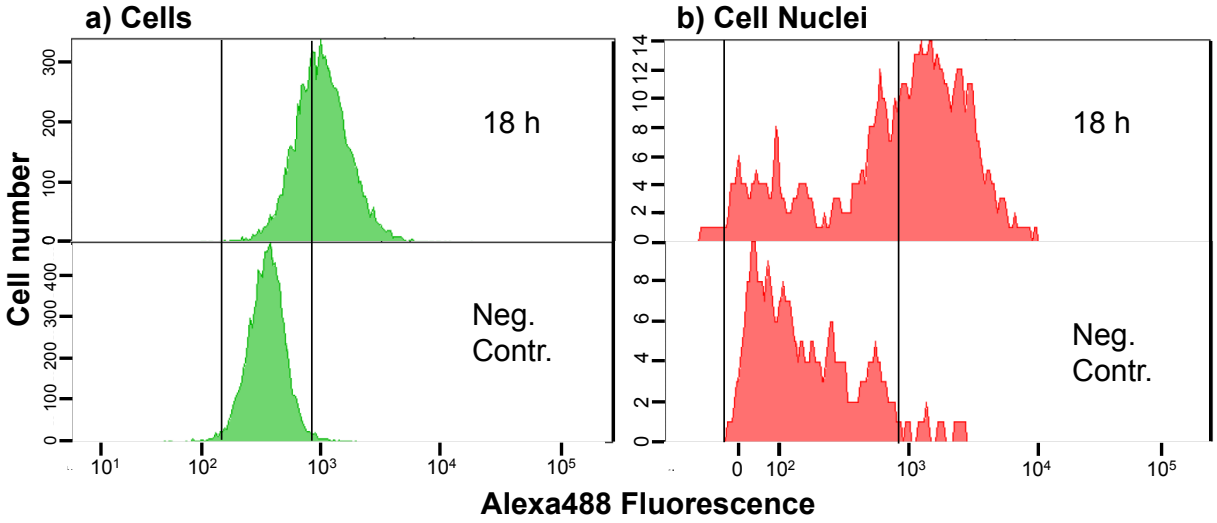

Figure 4.8.: Flow cytometric histogram of SCL-II cell analysis after transfection with an Alexa488-labeled TFO. Threshold setting (vertical black lines) for **a)** cells and **b)** nucleic samples on basis of the background fluorescence in sham transfected negative controls. Number of cells and cell nuclei, respectively, plotted against the Alexa488 fluorescence. The integral signal in the isolated nuclei shows stronger signal in comparison to the analyzed cells due to analysis at higher signal amplification.

The flow cytometric analysis showed that Alexa488-labeled TFOs were distributed throughout the cells immediately after transfection. One h post-transfection TFOs could be detected in whole cell samples and in isolated nuclei (*Figure 4.9*). A transfection efficiency of 85% ± 1.5% in whole cells and 75% ± 15.4% in isolated cell nuclei was observed. Within the first 6 h post-transfection a significant loss of TFO positive cell nuclei down to ~ 21% ± 8.1% occurred, followed by an almost constant fraction of TFO positive nuclei up to 24 h. After 30 h post transfection a slow decline of TFO positive

nuclei was detected continuing until 72 h. The TFO positive cells did not show a significant alteration for 30 h after transfection, followed by a significant decrease of TFO positive cells up to 72 h post transfection. The percentage of apoptotic/ necrotic cells did not change significantly throughout the entire test period.

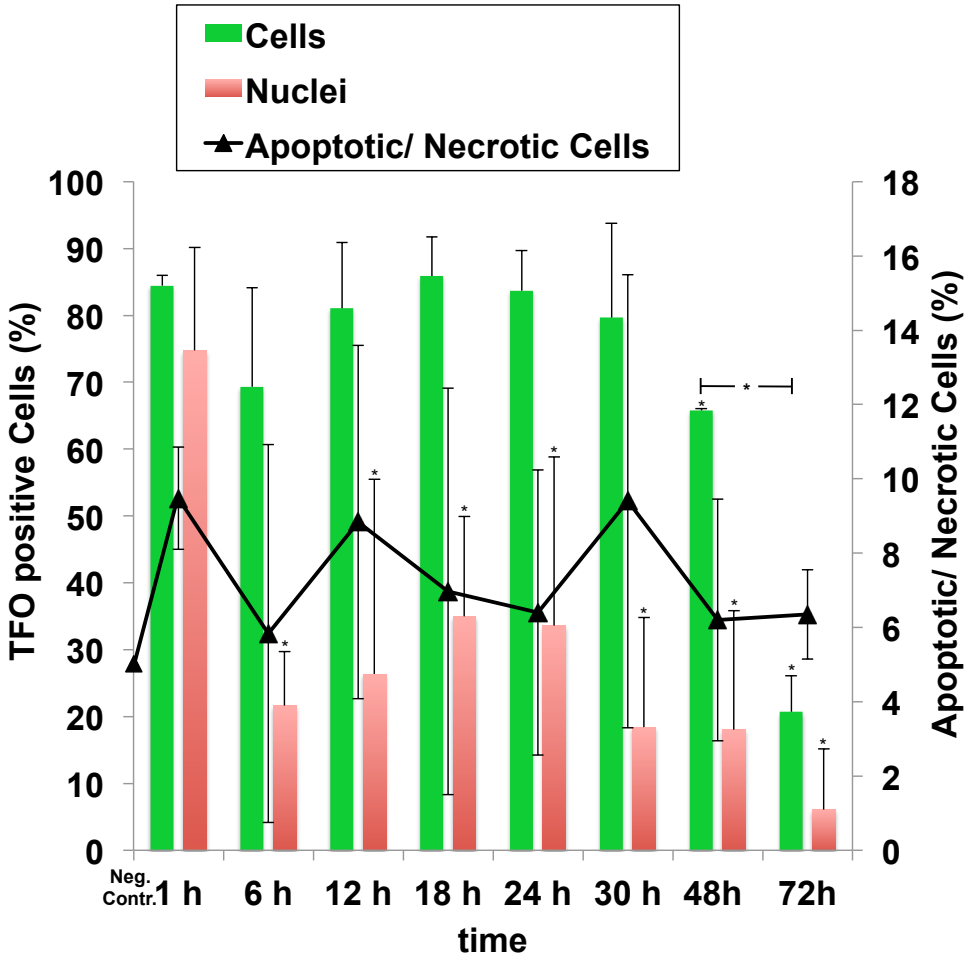

Figure 4.9.: Flow cytometric analysis of SCL-II cells after transfection with Alexa488-labeled TFO (n=3). Cell and nucleic samples were prepared for flow cytometric analysis after different time points (1 h - 72 h). Percent of TFO positive cells (green bar, left axis) and cell nuclei (red bars, left axis) plotted against time after transfection. Fraction of apoptotic/ necrotic cells in TFO transfected cells (black line, right axis) plotted against time after transfection. Error bars indicate the standard error of the mean (SEM) of n=3 independent experiments. (*p-value < 0.05; when not indicated differently samples were compared to 1 h sample)

Beside the flow cytometric analysis transfected SCL-II cells were also microscopically examined via live cell imaging.

The live cell imaging was performed in 20 cells per experiment for 22 h, while pictures were taken every 2 h of the individual cells. The images were analyzed by comparing the percentage of cells showing TFO signals in the cytoplasm only (*Figure 4.10*, 6 h/20 h, right pictures) to cells showing signal both in the cytoplasm as well as in the nucleus (*Figure 4.10*, 6 h/20 h, left pictures). The analysis revealed that the percentage of both

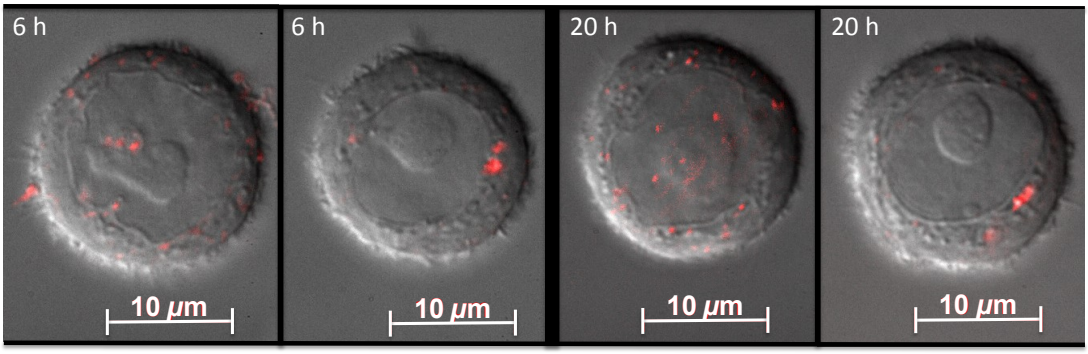

Figure 4.10.: Live cell images of SCL-II cells 6 h and 20 h after transfection with Alexa594-labeled TFOs (red). For visualization the SCl-II cells were kept in a microscope incubation chamber, enabling live cell images. (DIC overlay with fluorescence microscopy; Zeiss Plan-Apochromat 100x/1.40 Oil DIC, Texasred T7 Filter)

cell groups was almost constant throughout the whole testing period. The percentage of cells with TFOs in the cytoplasm only was 79% ± 3%. Cells with TFO signals in the cytoplasm and nucleus showed on average a percentage of 21% ± 3%. Additionally, it has to be stated that none of the cells with TFO signal in the cytoplasm and the nucleus retained the nuclear signal throughout the 22 h of observation. Interestingly, a steady loss or gain of TFO signal in the nucleus was detected. The longest period of time with a constant TFO signal in the nucleus was detected for 14 h (*Figure 4.11*). After 16 h the nucleus was not perfectly visible but after 18 h the TFO signal was located in the cytoplasm only, not in the nucleus anymore. The average signal in the nucleus was detectable for approximately 4 h.

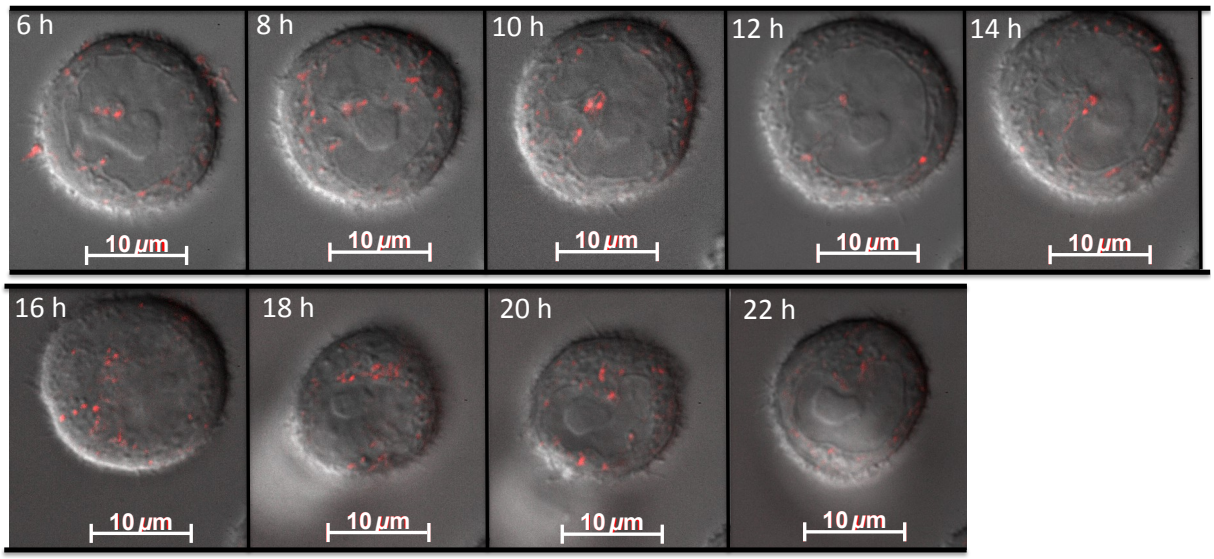

Figure 4.11.: Live cell images of a single SCL-II cell after transfection with Alexa594-labeled TFOs (red). Time period of 22 h with pictures taken every two hours. (DIC overlay with fluorescence microscopy; Zeiss Plan-Apochromat 100x/1.40 Oil DIC, Texasred T7 Filter)

4.5. Induction of DNA Double-Strand Breaks

The 53BP1 assay was performed in addition to the CFA (**4.6.1**) and was used to visualize and quantify the DSBs in SCL-II cells after transfection with I-125-TFO-GAPDH, I-125-TFO-MBS and I-125-TFO-QRT (*Figure 4.12*). For the subsequent decay accumulation cells were stored at -150°C. Cells transfected with the corresponding unlabeled TFO served as negative controls.

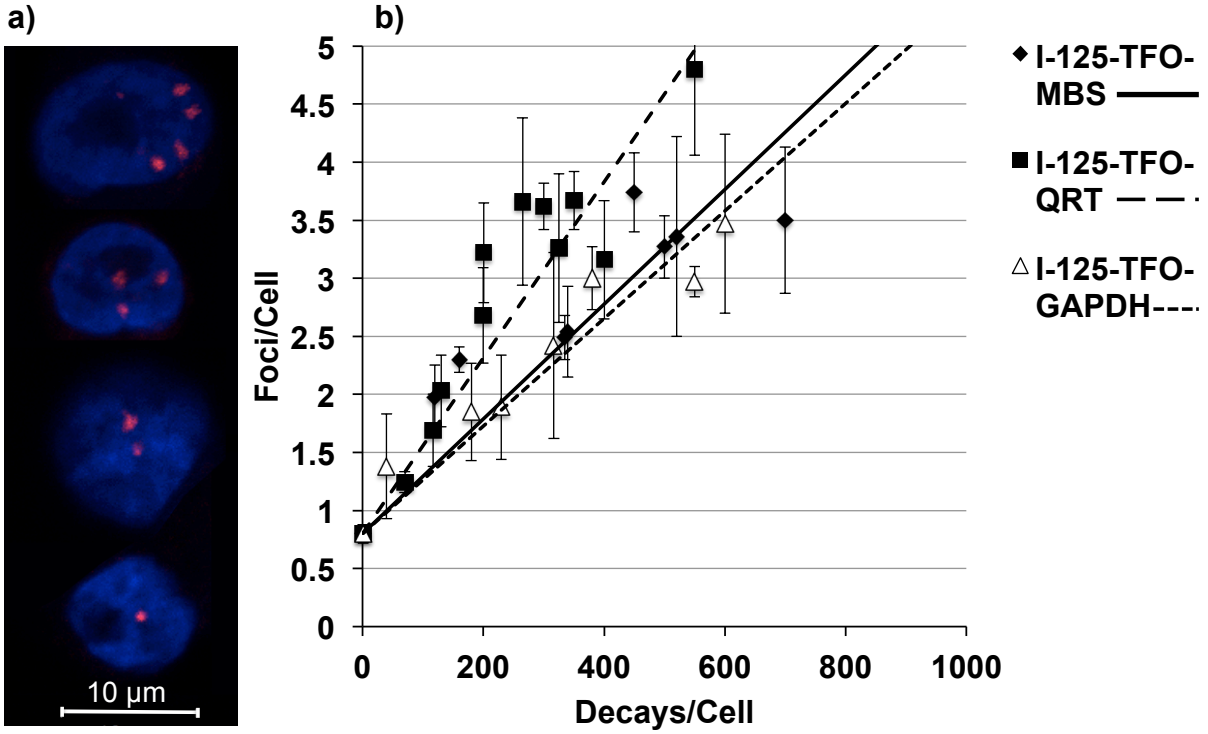

Figure 4.12.: DSB detection as 53BP1 foci in SCL-II cells after transfection with I-125-TFOs. **a)** Microscopic visualization of DSBs in SCL-II cells by 53BP1-antibody staining (DSBs, red) and DAPI staining (Nucleus, blue). **b)** 53BP1 foci on average per SCL-II cell plotted against accumulated decays/cell after the transfection with I-125-TFO-MBS (◆, —), I-125-TFO-QRT (■, – – –) and I-125-TFO-GAPDH (△, - - - -). Negative controls (not displayed) were transfected with the corresponding unlabeled TFO and showed on average ~ 0.8 foci/cell. The experimental points were fitted with linear multi target trend lines. Figure according to Dahmen and Kriehuber [23]

The negative controls showed with increasing storage time at -150°C an increase of foci/cell. Within the first days of storage the foci/cell increased from 0.5 foci/cell to a maximum of 1 focus/cell, where they remained constant for the rest of the storage period (⌀~ 0.8 foci/cell). The transfection with the single-binding-site TFO-GAPDH, which has its target sequence in the *GAPDH* gene, led to a linear increase of foci signals ($y = 0.0046x + 0.8$; $R^2 = 0.89$) reaching 3 foci/cell at approximately 480 accumulated decays/cell. The cells transfected with the multi-binding-site I-125-TFO-MBS, which possesses approximately 7000 targets in the whole genome, showed a very similar increase of foci numbers ($y = 0.0049x + 0.8$; $R^2 = 0.71$) reaching 3 foci/cell at ap-

proximately 450 accumulated decays/cell. In contrast, I-125-TFO-QRT, which targets ~ 370.000 putative target sequences induced a more pronounced increase of foci per decay (y = 0.0076x + 0.8; R^2 = 0.86) with 3 foci/cell at ~ 300 accumulated decays/cell resulting in ~ 1.5 fold stronger foci induction per decay.

Beside the quantification of the 53BP1 foci at different amounts of accumulated decays/cell (*Figure 4.12*), also the percentage of cells harboring a certain quantity of foci at a dedicated amount of accumulated decays/cell was determined (~ 330 decays/cell, *Figure 4.13*).

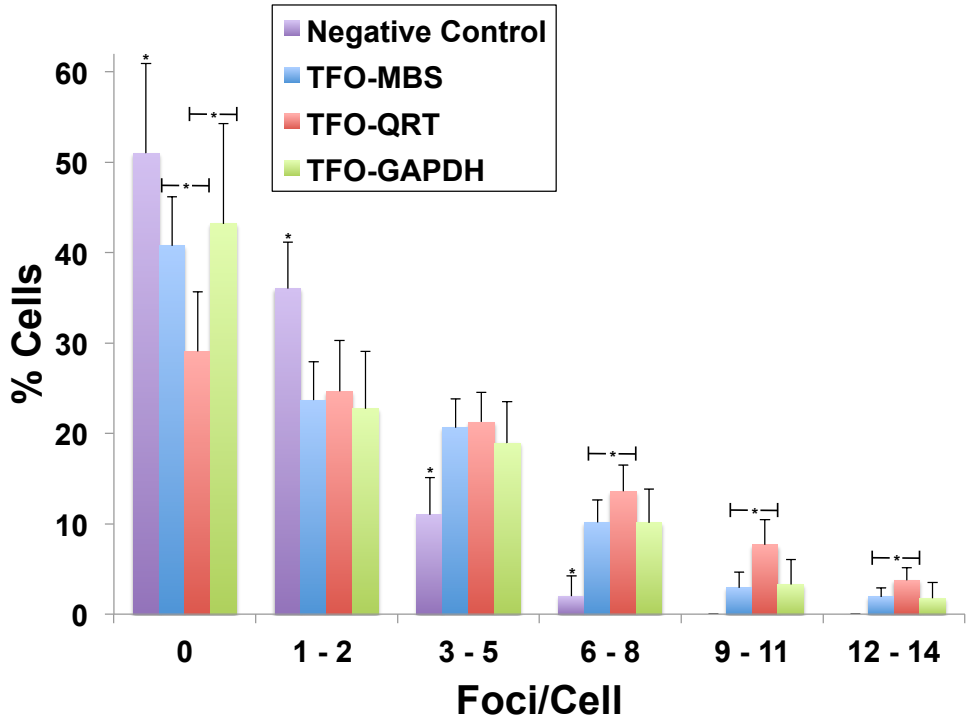

Figure 4.13.: Frequencies of 53BP1 foci in SCL-II cells after transfection with I-125-TFO-MBS (blue, n=3), I-125-TFO-QRT (red, n=3) and I-125-TFO-GAPDH (green, n=3); Negative controls (purple, n=3). The foci frequencies were determined after decay accumulation in the cells up to ~ 330 decays/cell. The bars show the percentage of cells (y-axis) containing the indicated number of foci (x-axis). Error bars indicate the standard error of the mean (SEM) of n=3 independent experiments. (*p-value < 0.05)

The negative controls contained in 51% ± 10% of the cells no foci. In 40% ± 5% and 43% ± 11% of the cells transfected with I-125-TFO-MBS and I-125-TFO-GAPDH, respectively, no foci were found. In cells transfected with I-125-TFO-QRT only 28% ± 6% of the cells contained no foci. A number of foci ranging from 1 - 2 foci/cell was detected in 36% ± 5% of the negative controls and in ~ 24% of cells after transfection with each individual of the three TFOs. Approximately 20% ± 4% of the cells contained 3 - 5 foci/cell regardless which TFO was used, whereas 11% ± 4% of the negative controls showed 3-5 foci/cell. In 10% ± 3% of I-125-TFO-MBS and I-125-TFO-GAPDH transfected cells and in 14% ± 3% of the I-125-TFO-QRT transfected cells an amount

of 6 - 8 foci/cell was found, which equaled an $\sim$ 1.4-fold higher percentage in the I-125-TFO-QRT transfected cells. Only 2% $\pm$ 2% of the negative controls contained 6 foci/cell or more. At 9 - 11 and 12 - 14 foci/cell the I-125-TFO-QRT displayed a $\sim$ 2-fold higher percentage of cells when compared to the I-125-TFO-MBS and I-125-TFO-GAPDH transfected cells.

4.6. Cell Killing

4.6.1. Cell Killing of SCL-II Cells after Transfection with I-125-labeled TFO

The CFA was performed to determine the cytotoxicity of I-125-labeled TFOs in respect to number and quality of the targeted TFO binding sites. For decay accumulation samples were stored at -150°C.

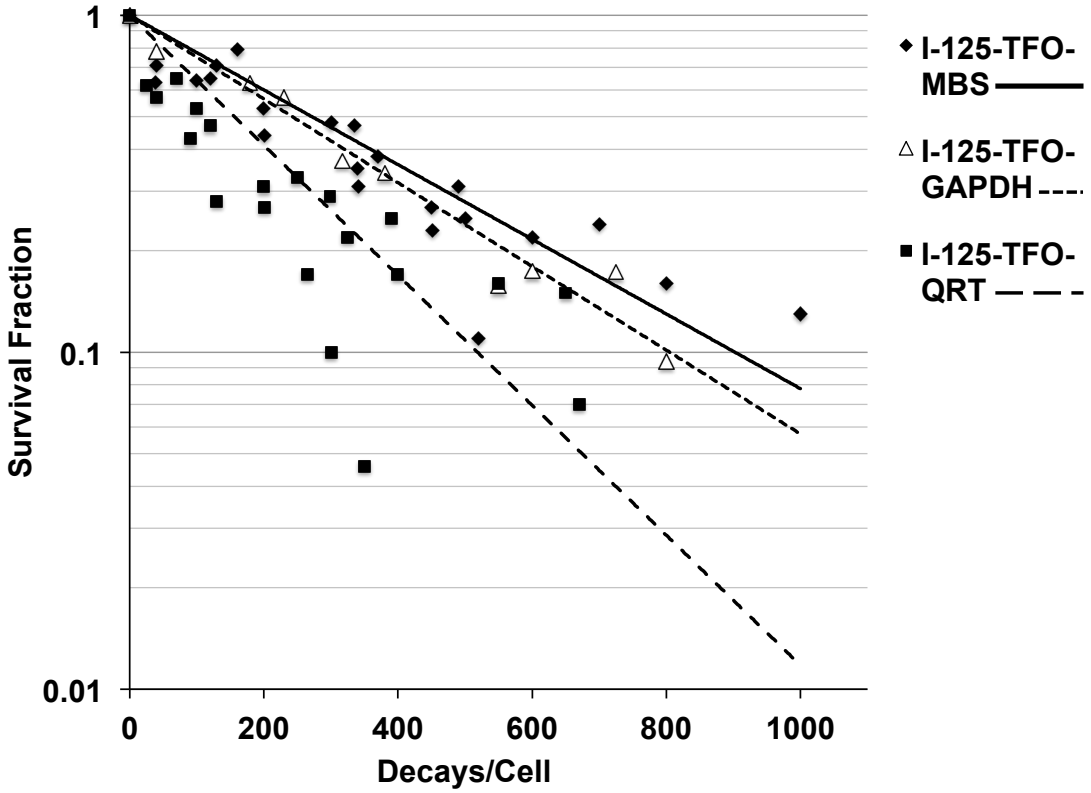

Figure 4.14.: Cell survival curves of SCL-II cells after transfection with I-125-TFO-MBS (◆, —), I-125-TFO-GAPDH (△, - - - -) or I-125-TFO-QRT (■, – – –). Surviving fraction is plotted against the amount of accumulated decays/cell. For decay accumulation the transfected samples were stored at -150°C. The data points were best fitted with the exponential multi target model of cell survival. Figure according to Dahmen and Kriehuber [23]

The CFA of SCL-II cells showed a reduced cell survival in respect to accumulated decays/cell for all three investigated I-125-labeled TFOs (*Figure 4.14*). The survival data were best fitted by using the straight exponential model of cell survival. The survival curve of I-125-TFO-GAPDH ($y = e^{-0.0029x}; R^2$ = 0.96) and I-125-TFO-MBS ($y = e^{-0.0026x}; R^2$ = 0.76) showed a D_{37} value of $\sim$ 350 respectively $\sim$ 390 decays/cell. I-125-TFO-GAPDH binds to a single site in the *GAPDH* gene only and the I-125-TFO-MBS binds to $\sim$ 7000 target sites in the whole genome [121]. I-125-TFO-QRT, as well a multiple target binding TFO applying the highest overall target number ($\sim$ 370,000

putative binding regions [133]) of all tested TFOs, induced a pronounced reduction of cell survival ($y = e^{-0.0044x}; R^2$ = 0.44), showing a D_{37} value of ~ 220 decays/cell, resulting in an almost 2-fold increase of cell killing when compared to I-125-TFO-GAPDH and I-125-TFO-1 Cyt 34.

4.6.2. Cell Killing of SCL-II Cells after (I-125)IdU incorporation

In order to compare the cyotoxicity of I-125-labeled TFOs with DNA incorporated I-125, CFAs of SCL-II cells after (I-125)5-Iodo-2´-deoxyuridine ((I-125)IdU) incorporation were carried out. The thymidine analogon used as a carrier for I-125 was incorporated during S-phase into the DNA. Therefore most of the decays occured in the DNA. After incorporation of (I-125)IdU cells were stored for decay accumulation at -150°C.

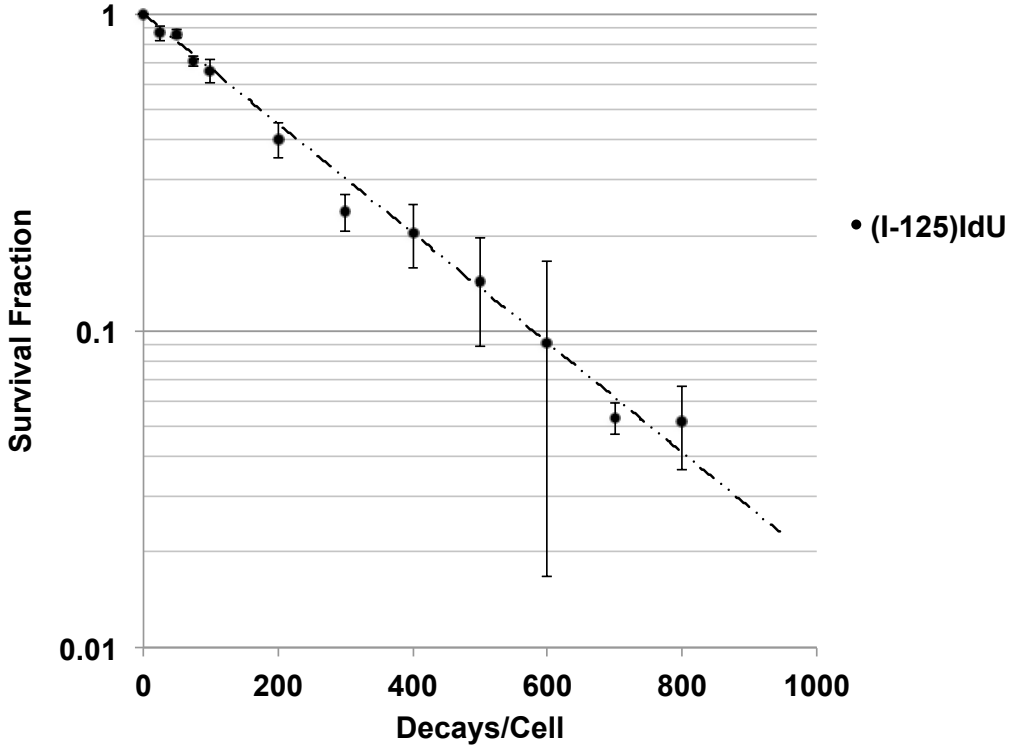

Figure 4.15.: Cell survival curve of SCL-II cells after incorporation of (I-125)IdU (n=3). Survival fraction is plotted against the number of accumulated decays/cell. For decay accumulation the samples were stored at -150°C. The data points were best fitted with the straight exponential single multi target model of cell survival. Error bars indicate the standard error of the mean (SEM) of n=3 independent experiments.

The SCL-II cells showed a pronounced reduction of cell survival ($y = e^{-0.0041x}; R^2$ = 0.98) after incorporation of (I-125)IdU in relation to the accumulated decays. The D_{37} value was reached at ~ 239 decays/cell and at more than 575 decays/cell the survival fraction was below 0.1. The data were best fitted using the exponential multi target model of

cell survival, resulting in a linear shaped survival curve, characteristic for high-LET radiation.

4.6.3. Cell Killing of SCL-II Cells after γ-Irradiation

SCL-II cells were γ-irradiated in T25 cell culture flasks at doses of 1, 2, 3, 4, 6, 8 and 10 Gy (**3.2.2**). The aim was to generate a dose dependent survival curve after gamma irradiation for comparison with the survival data after Auger irradiation (**4.6.1**).

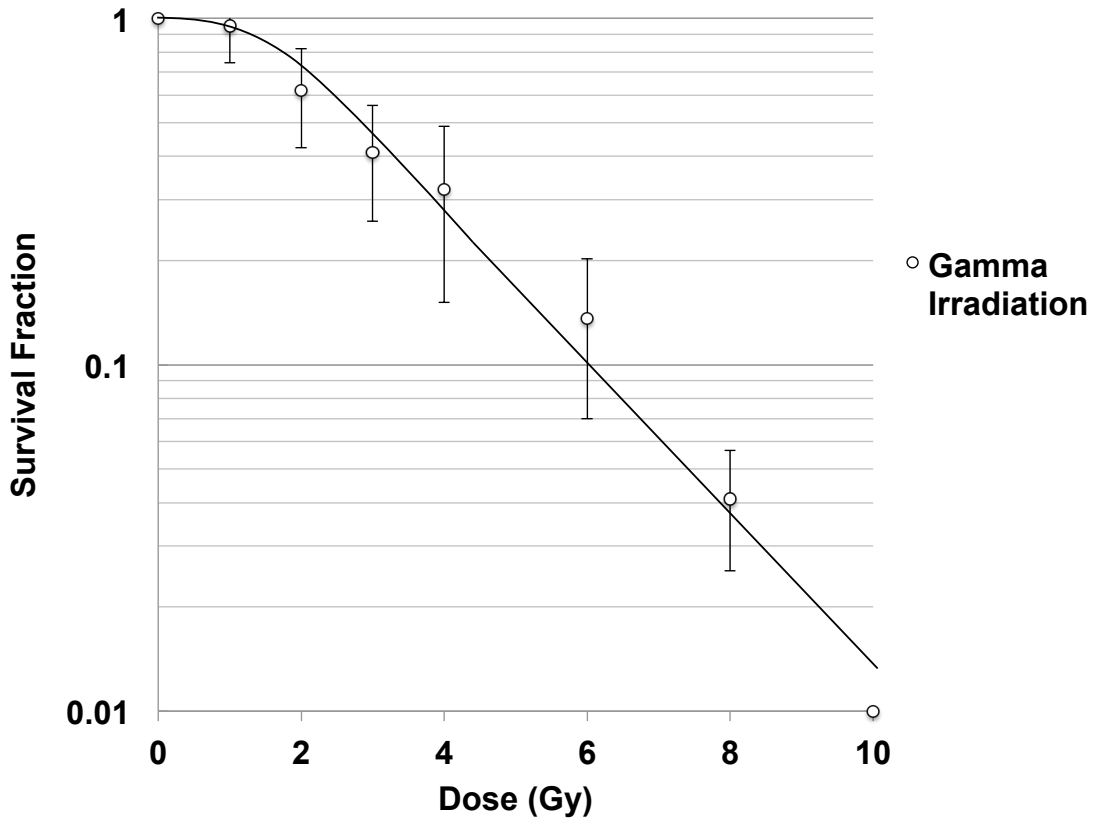

Figure 4.16.: Cell survival curves of SCL-II cells after gamma irradiation (n=3). Survival fraction plotted against the applied dose. The experimental points were fitted with the two-component model of cell survival. Error bars indicate the standard error of the mean (SEM) of n=3 independent experiments.

SCL-II cells showed a typical low-LET type of survival curve after gamma irradiation (Cs-137, 0.7 Gy/min). The survival data were fitted best using the two-component model of cell survival (D_q = 1.5, D_0 = 2 Gy, n = 2). The D_{37} value was reached at approximately 3.5 Gy (*Figure 4.16*). At 7.4 Gy the survival fraction was below 0.1. Higher doses led to a linear decrease of the survival fraction until no surviving cells ($\leq$ 0.01) could be detected at 10 Gy. The shape of the survival curve was, with the initial slope at low-dose, characteristic for low-LET radiation.

In order to allow a comparison of all survival data (*Figure 4.17*) the applied doses for I-125-TFO and (I-125)IdU transfected cells were determined with Point-Kernel calculations after Humm et al. [58] for SCL-II cells with a cell nucleus diameter of 10 μm. These led to an estimated dose of 3.5 mGy per decay of I-125. The I-125 data were best fitted with the exponential multi target model of cell survival and the data after γ-irradiation with the two-component model. All I-125 irradiated cells displayed a linear and more pronounced decrease in cell survival when compared to the γ-irradiated cells. The cytotoxic effect of DNA incorporated (I-125)IdU was very similar to the multi-binding-site I-125-TFO-QRT.

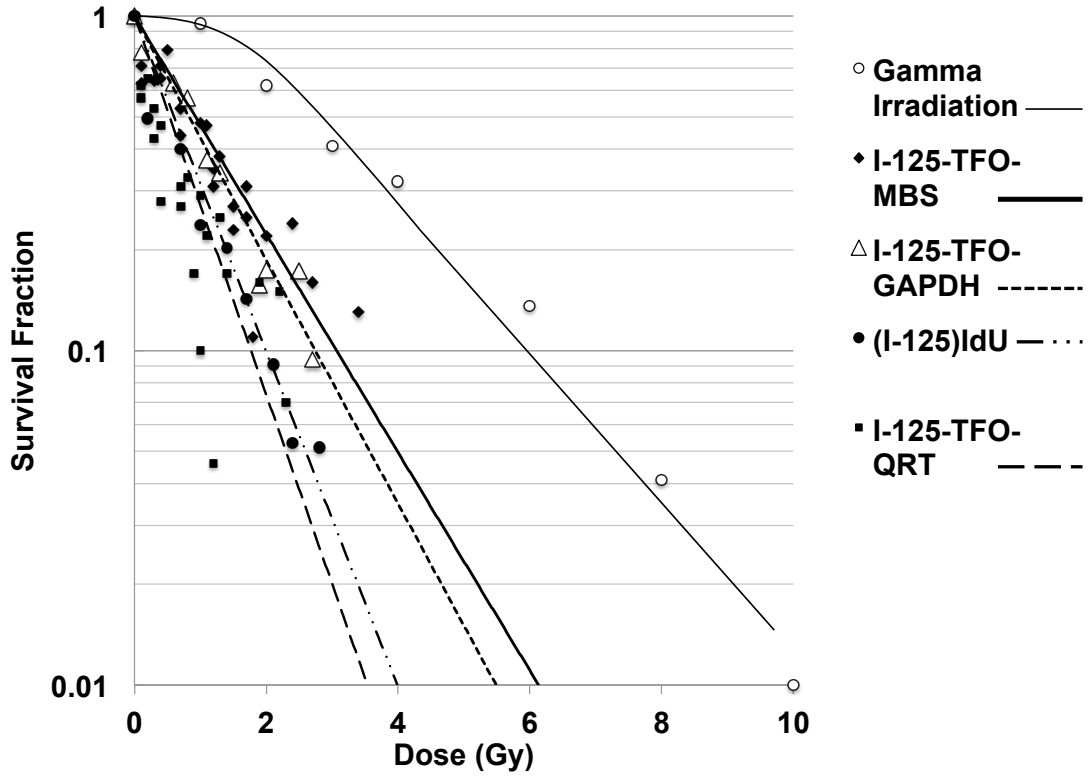

Figure 4.17.: Cell survival curves of SCL-II cells after transfection with I-125-TFO-MBS (◆, —), I-125-TFO-GAPDH (△, - - - -) and I-125-TFO-QRT (■, – – –). Incorporation of (I-125)IdU (•,– · · –) and Gamma Irradiation (○, —). Survival fraction plotted against the applied dose. Point-Kernel dose calculation for I-125-TFO-MBS, I-125-TFO-GAPDH, I-125-TFO-QRT and (I-125)IdU transfected cells after Humm et al. [58] for SCL-II cells with a cell nucleus diameter of 10 μm; 1 decay ~ 3.5 mGy

4.7. Relative Gene Expression Analysis

The relative gene expression analysis was performed by qRT-PCR (**3.2.20**) of RNA isolates from SCL-II cells after transfection with I-125-labeled TFOs (**3.2.15.1**). Prior to RNA isolation the transfected cells were stored for decay accumulation until ~ 300 accumulated decays/cell were obtained. The aim of the study was to determine the effect of I-125-labeled TFOs on the gene expression of the respective targeted gene. Three different TFOs were designed, specific for the genes *GAPDH*, *BRCA1* and *BCL2*.

4.7.1. *GAPDH* Gene Expression

TFO-GAPDH was designed to bind within the *GAPDH* gene. The target sequence is located in the promoter region, 422 bp upstream of the *GAPDH* sequence (*Figure 4.18* b). The relative gene expression of *GAPDH* showed a significant 1.7-fold down-regulation in I-125-TFO-GAPDH transfected SCL-II cells in comparison to the negative control cells which were transfected with non-labeled TFO-GAPDH (*Figure 4.18* a). When compared to I-125-TFO-QRT the I-125-TFO-GAPDH transfected cells showed a

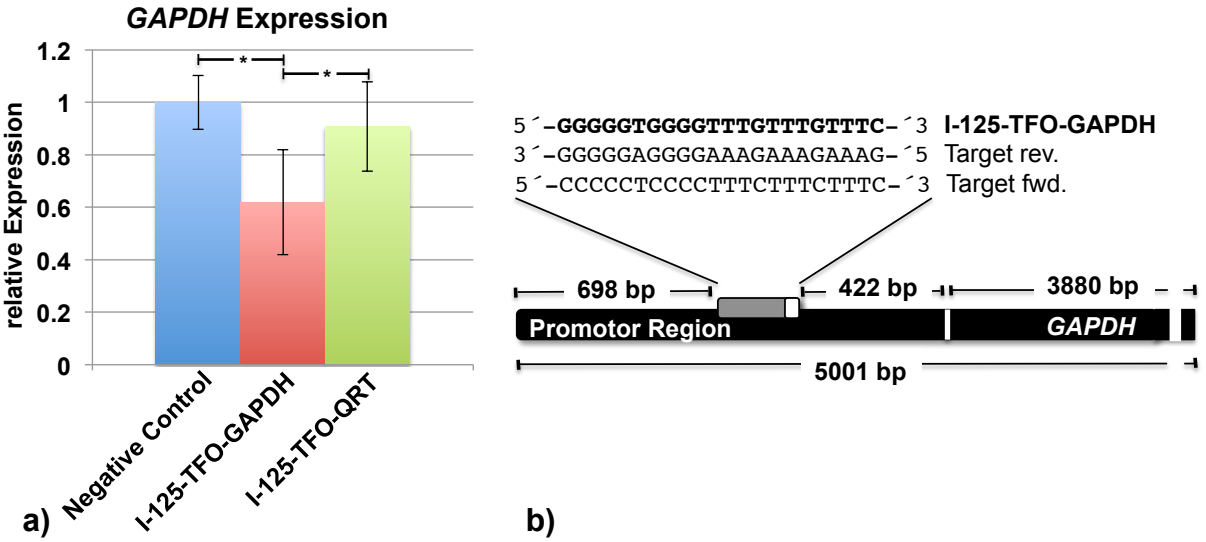

Figure 4.18.: a) Relative gene expression of *GAPDH* after transfection with I-125-TFO-GAPDH (n=7), I-125-TFO-QRT (n=3) and unlabeled TFO-GAPDH (n=3) as negative control. The (I-125-)TFO-GAPDH binds to a single target sequence in the *GAPDH* gene. I-125-TFO-QRT binds to multiple targets in the whole human genome. b) Schematic diagram of the TFO-GAPDH target sequence and its location in the *GAPDH* gene. Error bars indicate the standard error of the mean (SEM) of n independent experiments. (*p-value < 0.05). Figure according to Dahmen and Kriehuber [23]

significant 1.4-fold down-regulation of *GAPDH* expression. In contrast, the I-125-TFO-

QRT transfected cells displayed a non-significant 1.1-fold reduced expression when compared to the negative control.

4.7.2. *BRCA1* Gene Expression

TFO-BRCA1 was designed to bind within the *BRCA1* gene. The target sequence is located on the forward strand within the region of intron 19 at 6820 bp upstream of the stop codon (*Figure 4.19* b). The relative gene expression of *BRCA1* showed no significant alteration in I-125-TFO-BRCA1 transfected SCL-II cells when compared to the negative control cells, which were transfected with non-labeled TFO-BRCA1 (*Figure 4.19* a). In contrast SCL-II cells transfected with I-125-TFO-QRT showed a significant,

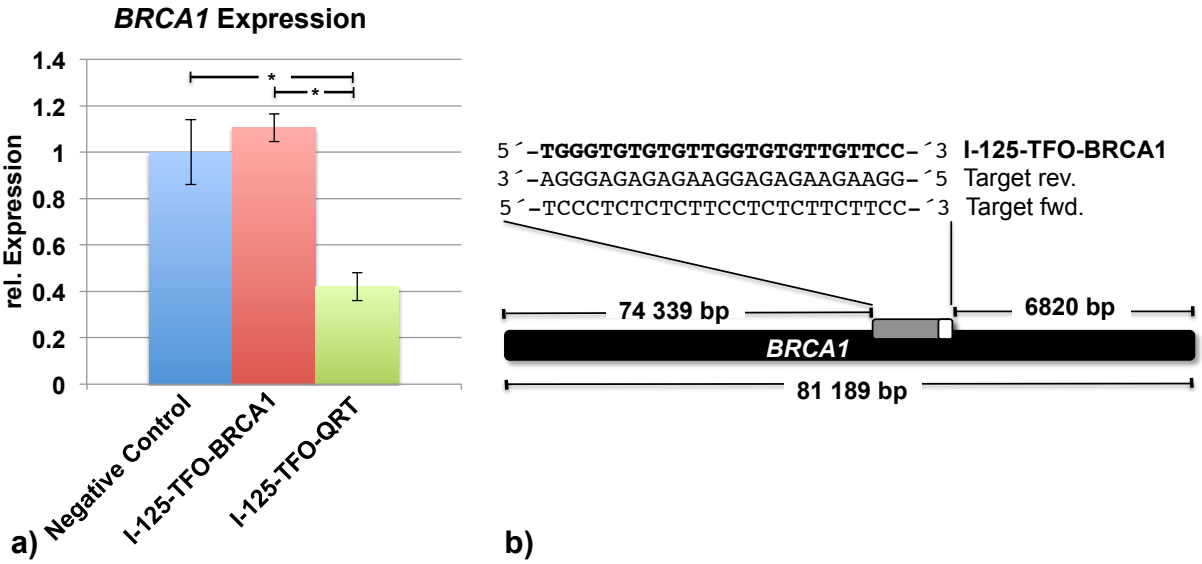

Figure 4.19.: a) Relative gene expression of *BRCA1* after transfection with I-125-TFO-BRCA1 (n=4), I-125-TFO-QRT (n=3) and unlabeled TFO-BRCA1 (n=3) as negative control. The (I-125-)TFO-BRCA1 binds to a single target sequence in the *BRCA1* gene. I-125-TFO-QRT binds to multiple targets in the whole human genome. b) Schematic diagram of the TFO-BRCA1 target sequence and its location in the *BRCA1* gene. Error bars indicate the standard error of the mean (SEM) of n independent experiments. (*p-value < 0.05)

more than two-fold down-regulation of the *BRCA1* expression. Compared to the negative control as well as to the I-125-TFO-BRCA1 transfected cells.

4.7.3. *BCL2* Gene Expression

TFO-BCL2 was designed to bind within the *BCL2* gene. The target sequence is located on the forward strand within the region of intron 2 at 5422 bp downstream of the *BCL2* promoter region (*Figure 4.20* b). The relative gene expression of *BCL2* in

I-125-TFO-BCL2 transfected cells showed a significant, almost two-fold up-regulation when compared to the negative controls, transfected with non-labeled TFO-BCL2 (*Figure 4.20* a). In contrast the *BCL2* expression in SCL-II cells transfected with I-125-TFO-QRT was approximately reduced to one fourth of the expression in the negative controls and compared to the I-125-TFO-BCL2 transfected cells the *BCL2* expression was almost reduced by the factor of 10.

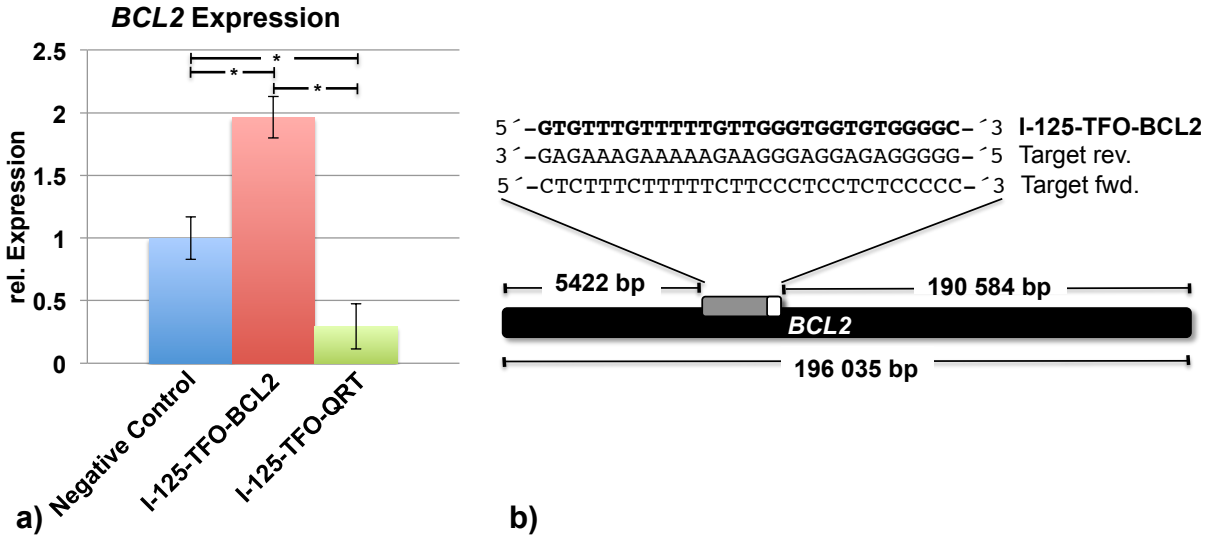

Figure 4.20.: a) Relative gene expression of *BCL2* after transfection with I-125-TFO-BCL2 (n=8), I-125-TFO-QRT (n=3) and unlabeled TFO-BCL2 (n=3) as negative control. The (I-125-)TFO-BCL2 binds to a single target sequence in the *BCL2* gene. I-125-TFO-QRT binds to multiple targets in the whole human genome. b) Schematic diagram of the TFO-BCL2 target sequence and its location in the *BCL2* gene. Error bars indicate the standard error of the mean (SEM) of n independent experiments. (*p-value < 0.05)

4.8. Induction of Micronuclei

The micronucleus assay was performed to determine to what extent I-125-TFO-induced DSBs were translated into chromosomal damage. Therefore, SCL-II cells were transfected with I-125-TFO-GAPDH, I-125-TFO-QRT or I-125-TFO-MBS and stored for accumulation of ~ 300, ~ 400, ~ 500 and ~ 600 decays/cell at -150°C. Cells transfected with the corresponding unlabeled TFO served as negative controls. Additionally, the MN induction after γ-irradiation was analyzed.

4.8.1. I-125-TFO-GAPDH Induced Micronuclei

SCL-II cells transfected with I-125-TFO-GAPDH showed a total amount of MN per 100 binuclear cells ranging between ~ 14 ± 6.6 at ~ 300 decays/cell and 8 ± 7.5 micronuclei at ~ 600 decays/cell (*Figure 4.21*). Only at ~ 300 and ~ 400 decays/cell the detected number of MN per 100 binuclear cells was significantly increased when compared to the negative controls with on average 4.8 ± 2 MN.

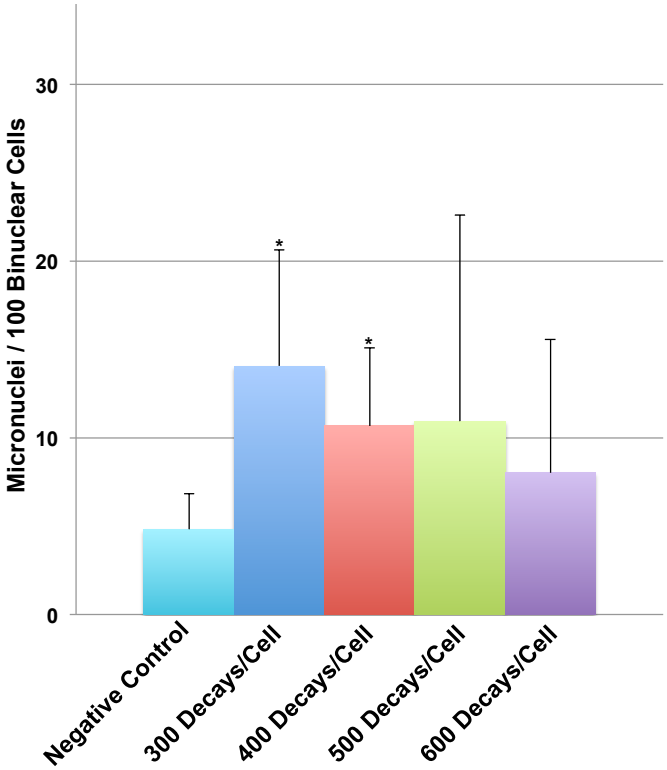

Figure 4.21.: Micronuclei in SCL-II cells after transfection with I-125-TFO-GAPDH (n=3). Before analysis decays were accumulated by storage at -150°C to ~ 300, ~ 400, ~ 500 and ~ 600 decays/cell. Total amount of micronuclei per 100 binuclear cells plotted against the accumulated decays/cell. Error bars indicate the standard error of the mean (SEM) of n=3 independent experiments. t-Test irradiated cells vs. non irradiated negative control (*p-value < 0.05)

4.8.2. I-125-TFO-QRT Induced Micronuclei

SCL-II cells transfected with I-125-TFO-QRT contained at each decays/cell significantly more MN than the negative control harboring on average 2.4 ± 1 MN per 100 binuclear cells (*Figure 4.22*). At ~ 300 decays/cell the cells contained on average 21.4 ± 2.2 MN per 100 binuclear cells but showed a decreasing number of MN with increasing decays/cell. The most pronounced decrease was observed at ~ 400 decays/cell with the MN amount dropping to 12.3 ± 11.2 MN per 100 binuclear cells, and further decreasing to a minimum of 7.6 ± 6.9 MN at ~ 600 decays/cell.

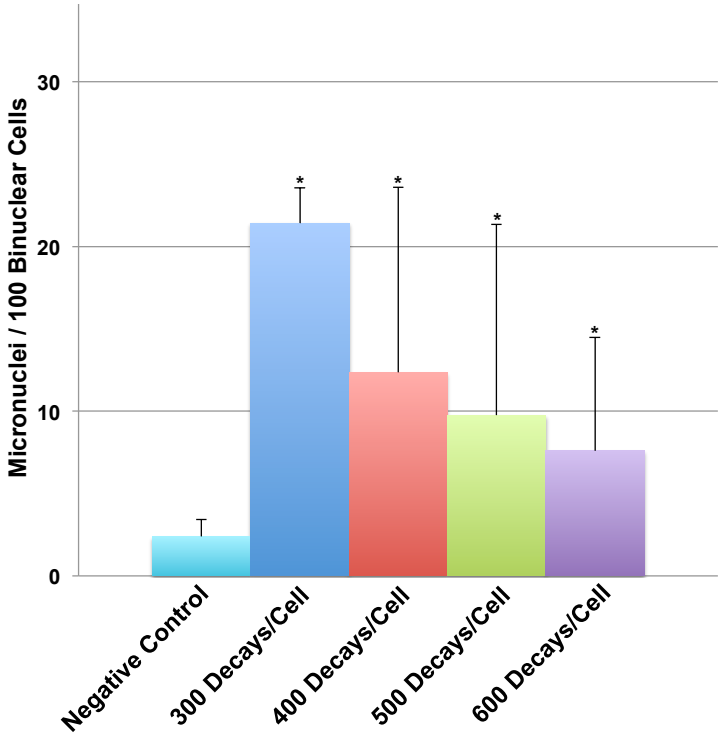

Figure 4.22.: Micronuclei in SCL-II cells after transfection with I-125-TFO-QRT (n=2). Before analysis decays were accumulated by storage at -150°C to ~ 300, ~ 400, ~ 500 and ~ 600 decays/cell. Total amount of micronuclei per 100 binuclear cells. Error bars indicate the standard error of the mean (SEM) of n=2 independent experiments. t-Test irradiated cells vs. non irradiated negative control (*p-value < 0.05)

4.8.3. I-125-TFO-MBS Induced Micronuclei

SCL-II cells transfected with TFO-MBS contained at each decays/cell significantly more MN than the negative control harboring on average 3.4 ± 2.8 MN per 100 binuclear cells (*Figure 4.23*). The total amount of MN was almost constant between ~ 300 to ~ 500 decays/cell with MN numbers from 13.8 ± 6.3 MN to 13.1 ± 11.4 MN. The highest amount of MN was detected after ~ 600 decays/cell with 20.5 ± 14.5 MN per 100 binuclear cells.

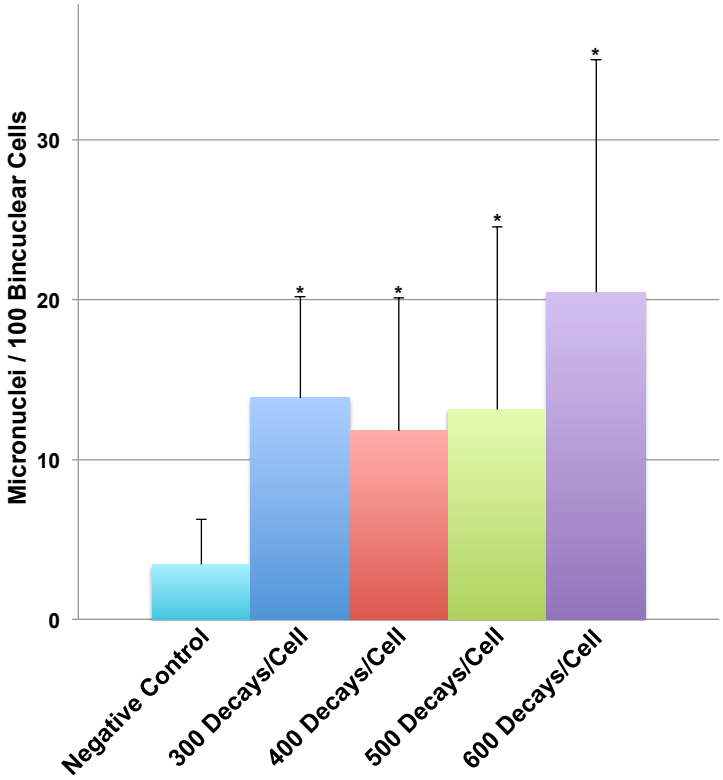

Figure 4.23.: Micronuclei in SCL-II cells after transfection with I-125-TFO-MBS (n=3). Before analysis decays were accumulated by storage at -150°C to ~ 300, ~ 400, ~ 500 and ~ 600 decays/cell. Total amount of micronuclei per 100 binuclear cells. Error bars indicate the standard error of the mean (SEM) of n=3 independent experiments. t-Test irradiated cells vs. non irradiated negative control (*p-value < 0.05)

4.8.4. γ-Irradiation Induced Micronuclei

SCL-II cells after γ-irradiation at doses of 0.5, 1, 1.5, 2, 4 and 6 Gy contained at each dose significantly more MN than the negative control harboring on average 1.4 ± 0.6 MN per 100 binuclear cells (*Figure 4.24*). Across all doses tested, the MN content constantly increased with 2.6 ± 0.6 MN at 0.5 Gy on average up to a maximum of 18.7

± 7.7 MN at 6 Gy. The most pronounced increase was observed between 1 to 1.5 Gy and 2 to 4 Gy.

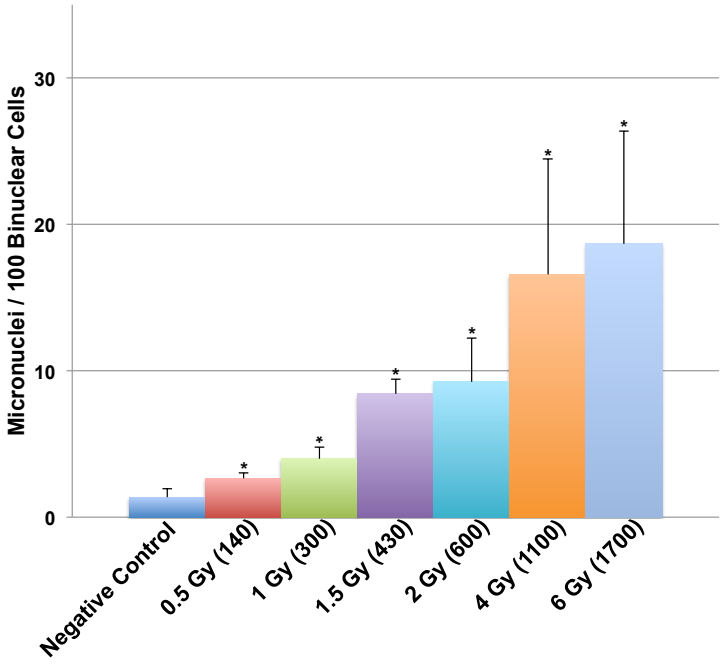

Figure 4.24.: Micronuclei in SCL-II cells after γ-irradiation (n=3). Before analysis cells were γ-irradiated at doses of 0.5, 1, 1.5, 2, 4 and 6 Gy. In parentheses is the number of corresponding I-125 decays determined with Point-Kernel calculations after Humm et al [58] for SCL-II cells with a cell nucleus diameter of 10 μm. Total amount of micronuclei per 100 binuclear cells. Error bars indicate the standard error of the mean (SEM) of n=3 independent experiments. t-Test irradiated cells vs. non irradiated negative control (*p-value < 0.05)

4.8.5. Comparison of I-125-TFO Induced Micronuclei

To demonstrate the different MN inducing potentials of the analyzed I-125-TFOs and γ-irradiation, the MN data were directly compared. In order to guarantee comparability between the three I-125-TFOs and the γ-irradiated samples, each data set was standardized against the negative controls.

By comparing the MN values of the I-125-TFOs at each decays/cell no significant difference could be detected (*Figure 4.25*). However, there is a tendency that I-125-TFO-QRT induces more MN than I-125-TFO-MBS and I-125-TFO-GAPDH at $\sim$ 300 decays/cell, whereas at $\sim$ 600 decays/cell I-125-TFO-MBS appears to induce a higher amount of MN compared to the two other I-125-TFOs.

In comparisson to the γ-irradiated cells only I-125-TFO-QRT induces a significantly higher number of MN at 300 decays/cell. At all other doses no significant differences

between the amount of I-125-TFO induced MN and γ-irradiation induced MN could be detected.

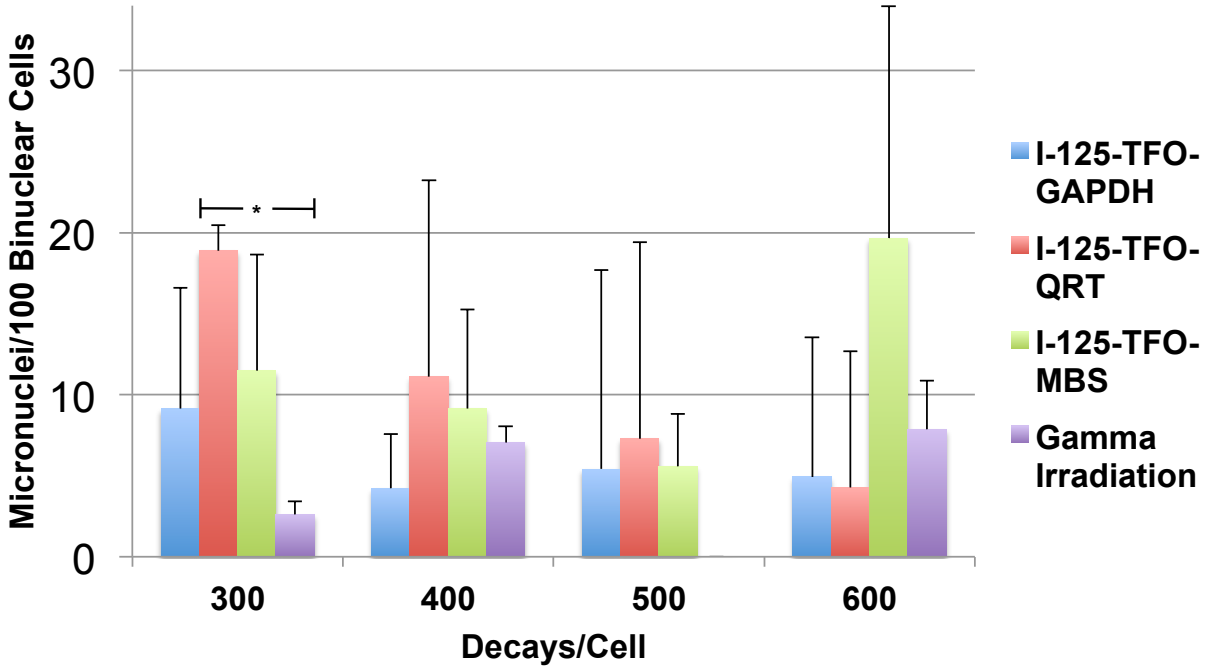

Figure 4.25.: Micronuclei after γ-irradiation (n=3) or transfection with I-125-TFO-GAPDH (n=3), I-125-TFO-QRT (n=2) and I-125-TFO-MBS (n=3). Before analysis decays were accumulated by storage at -150°C to ~ 300, ~ 400, ~ 500 and ~ 600 decays/cell. For γ-irradiation the corresponding decays were calculated with Point-Kernel calculations after Humm et al. [58] for SCL-II cells with a cell nucleus diameter of 10 μm. Total amount of micronuclei per 100 binuclear cells. Data standardized against negative controls. Error bars indicate the standard error of the mean (SEM) of n independent experiments. (*p-value < 0.05)

4.9. Cell Cycle Analysis of SCL-II Cells

The aim was to analyze the cell cycle of SCL-II cells at different time points (0 - 48 h) after transfection with I-125-labeled TFOs, to detect possible cell cycle arrests or perturbations. SCL-II cells transfected with the corresponding unlabeled TFO were used as negative controls. Prior to cell cycle analysis the transfected cells were stored for accumulation of decays at -150°C. In each experiment and for all investigated TFOs, experiments were carried out at ~ 300 accumulated decays/cell. Cells were thawed, taken into cell culture and analyzed at times indicated, except the 0 h samples where cells were thawed and immediately analyzed as described in **3.2.17.1**.

4.9.1. Cell Cycle Analysis after I-125-TFO-GAPDH Transfection

SCL-II cells transfected with I-125-TFO-GAPDH showed an almost similar distribution of cells in the cell cycle phases at 0 h post irradiation[1], compared to the negative control (*Figure 4.26*). Approximately 40% ± 8% of the cells were in G_2/M-, 20% ± 10% in S- and 40% ± 2% in G_1/G_0-phase. Within the next 8 h the I-125-TFO-GAPDH transfected

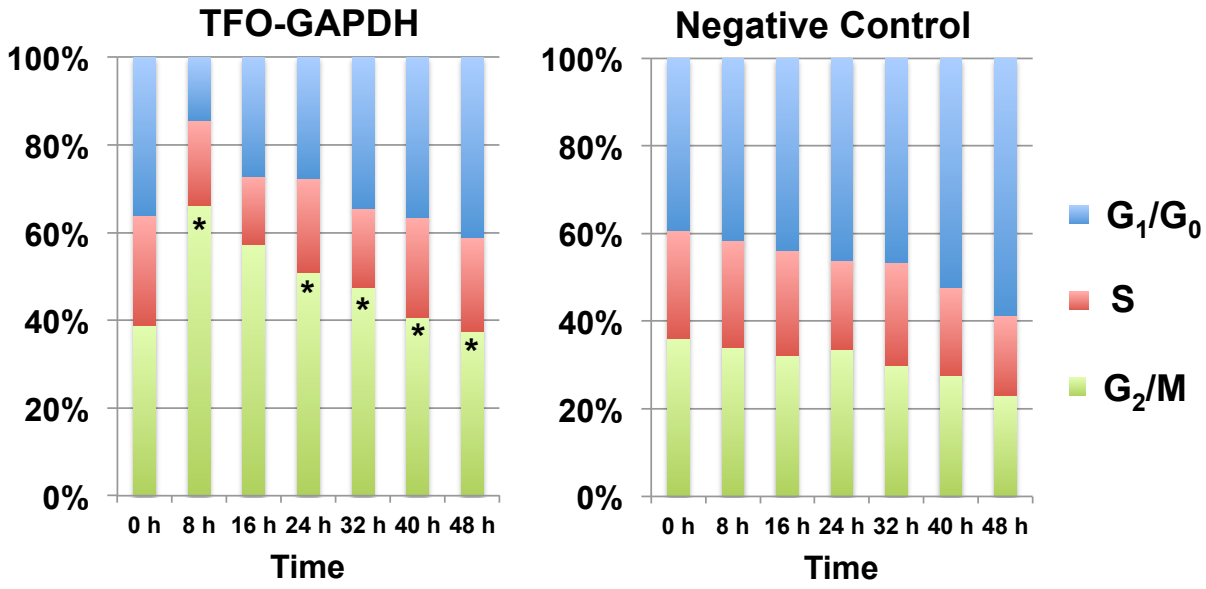

Figure 4.26.: Fluorescence cytometric analysis of SCL-II cells at different time points after irradiation with I-125-TFO-GAPDH and accumulated ~ 300 decays/cell (n=3). As negative controls served cells transfected with equivalent but unlabeled TFO. Percentage of cells in different cell cycle phases G_1/G_0, S and G_2/M (y-axis) is plotted against time after irradiation (x-axis). (*p-value < 0.05; t-Test irradiated sample vs. negative control)

cells showed a significantly increased percentage of G_2/M-phase cells from 40% ± 8% to 65% ± 8% whereas the negative control cells remained at almost constant percentages of 30% ± 7%. During the following 40 h the ratio of G_2/M-phase cells in the I-125-TFO-GAPDH transfected cells remained significantly increased in comparison to the negative controls but at the same time they showed a constant decrease to a percentage of 37% ± 4% G_2/M-phase cells after 48 h. Finally a fraction of ~ 14% remained in G_2/M-phase when compared to the negative control G_2/M fraction. The negative controls showed no significant changes throughout the period of measurement.

1 Irradiation refers to the time point of cell recultivation after -150°C storage for accumulation of ~ 300 decays/cell.

4.9.2. Cell Cycle Analysis after I-125-TFO-QRT Transfection

SCL-II cells transfected with I-125-TFO-QRT (*Figure 4.27*) showed a similar distribution of cells in the cell cycle phases at 0 h post irradiation, compared to the negative control. Approximately 30% ± 6% of the cells were in G_2/M-, 30% ± 4% in S- and ~ 40% ± 10% in G_1/G_0-phase. A significant increase of G_2/M-phase cells was observed in I-125-TFO-QRT transfected cells 8 h after irradiation, reaching a maximum of 70% ± 13% at 16 h post irradiation. Within the next 32 h the percentage of G_2/M-phase cells dropped to 40% ± 5% at 48 h but remained significantly increased when compared to the negative controls. At 48 h a fraction of approximately 17% of the I-125-TFO-QRT transfected cells still remained in a G_2/M-phase arrest. The negative control cells did not show any significant change within the surveyed 48 h.

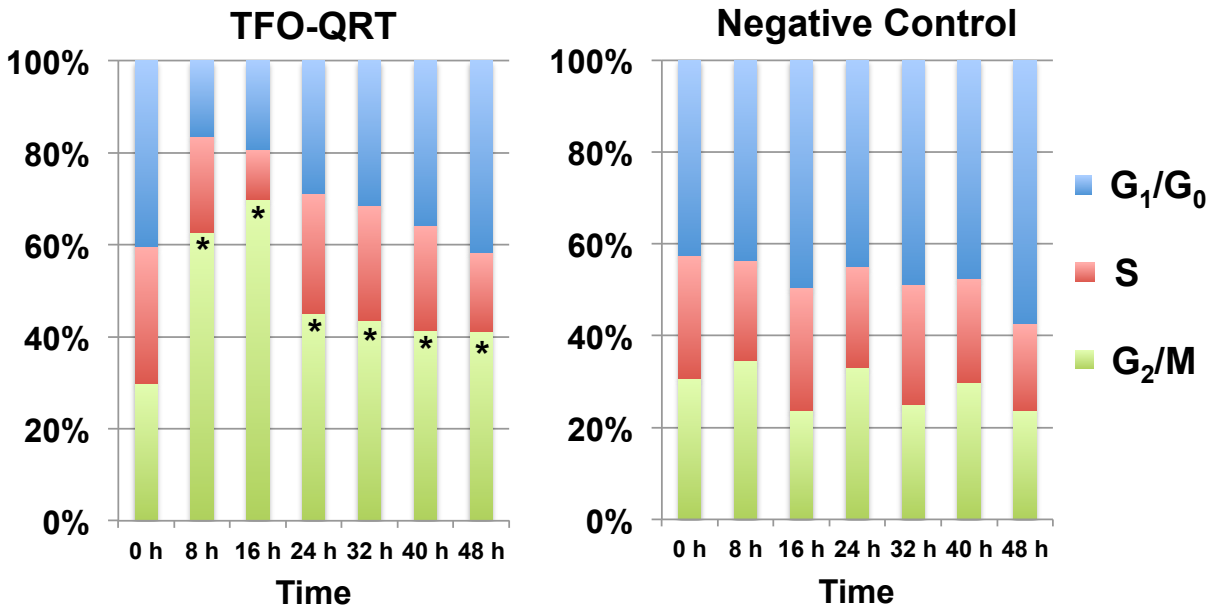

Figure 4.27.: Fluorescence cytometric analysis of SCL-II cells at different time points after irradiation with I-125-TFO-QRT and accumulated ~ 300 decays/cell (n=3). As negative controls served cells transfected with equivalent but unlabeled TFO. Percentage of cells in different cell cycle phases G_1/G_0, S and G_2/M (y-axis) is plotted against time after irradiation (x-axis). (*p-value < 0.05; t-Test irradiated sample vs. negative control)

4.9.3. Cell Cycle Analysis after I-125-TFO-MBS Transfection

SCL-II cells transfected with I-125-TFO-MBS showed that at 0 h 30% ± 5% of the cells were in G_2/M-phase whereas 40% ± 10% were in G_1/G_0-phase of the cell cycle and 30% ± 5% in S-phase (*Figure 4.28*). There was no significant difference in cell cycle distribution when compared to the negative controls at 0 h. At 8 h the percentage of

G_2/M-phase cells increased significantly to 60% ± 5%. Also at 24, 32 and 40 h after irradiation the percentage of cells in G_2/M-phase remained significantly increased in comparison to the negative controls. That fraction, however, decreased over time until it nearly reached control level at 48 h.

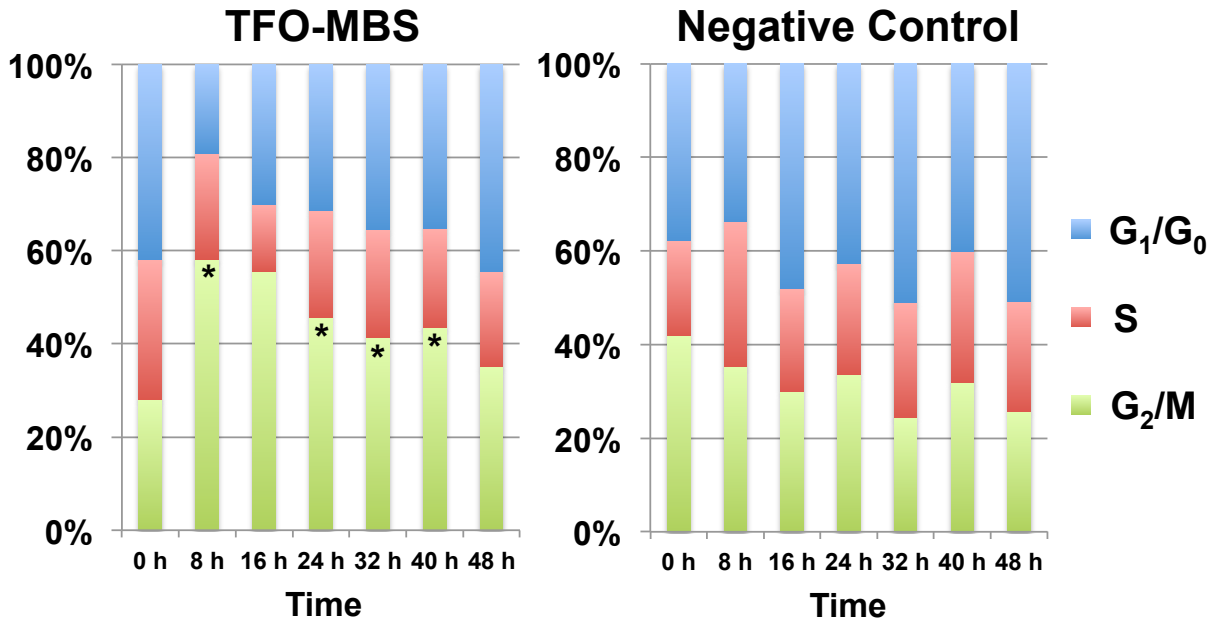

Figure 4.28.: Fluorescence cytometric analysis of SCL-II cells at different time points after irradiation with I-125-TFO-MBS and accumulated ~ 300 decays/cell (n=3). As negative controls served cells transfected with equivalent but unlabeled TFO. Percentage of cells in different cell cycle phases G_1/G_0, S and G_2/M (y-axis) is plotted against time after irradiation (x-axis). (*p-value < 0.05; t-Test irradiated sample vs. negative control)

5. Discussion

5.1. *In Vitro* DNA Triplex Formation and Binding Assay

The sequence of all TFOs investigated, were determined with the TFO target sequences search tool provided by http://spi.mdanderson.org/tfo/about.php, except the two multi-binding site TFOs[1]. Although all TFOs were designed to the following special criteria of a minimum length of 15 bp, a guanine content of minimum 50%, no pyrimidine interrupts and the purine sequence located on one strand (**3.2.6**), a triplex formation could only be verified by EMSA *in vitro* for 42% of all examined TFOs (*Table 4.1*). Therefore it can be concluded that a stable triplex DNA formation can not be predicted by the sequence of TFOs only. This conclusion is supported by TFO stability experiments performed by Beal and Dervan [9]. Therefore, the confirmation of DNA triplex formation of every TFO with its specific target sequence by EMSA or a equivalent method is strongly recommended.

5.2. I-125 Labeling of TFOs

The establishment of the I-125 labeling reaction was one of the most important but also delicate steps of the present work. The labeling reaction was performed following the primer extension method described by Panyutin et al. [97]. However, distinct and very important modifications of the reaction were necessary at some delicate key steps discussed in the following sections.

The first attempts to separate the labeled TFO from its complementary DNA template were done by heat denaturation as proposed by Panyutin et al. [97]. To achieve this, a temperature was chosen which was significantly above the melting temperature (Tm) of the TFO ($\sim 72°C$) but still low enough to avoid the breakup of the biotin-streptavidine bond (Tm biotin-streptavidine $> 81.1°C$ [43]) when connecting the biotin template to the

1 **TFO-MBS** was designed and previously investigated by Sedelnikova et al. [121]. **TFO-QRT** was not originally designed as DNA triplex forming but to interfere with DNA quadruplex structures. The *in vitro* verification of quadruplex structures is still in progress.

streptavidine magnetic particles. Extensive experiments revealed that at the chosen denaturation temperature of 79°C, which was the best compromise between Tm of TFO and assumed biotin-streptavidine stability, it was not possible to denature the TFO from the template with a sufficient yield but induced a breakage of the biotin-streptavidine bond (*Figure 4.3*, lanes 1-3). Although Gonzales et al. [43] determined a Tm for the biotin-streptavidine bond between 81.1°C and 108°C our findings are more in accordance with Holmberg at al. who described that heating of a biotin-streptavidine bond in aqueous solution to 70°C is sufficient to efficiently break the bond [54]. As the biotin-streptavidine bond is stable throughout a wide pH range [54] it turned out that the denaturation of the TFO from the template by adding NaOH to apply alkaline conditions is much more suitable. This approach led to the desired denaturation with a high elution efficiency as can be seen in *Figure 4.3*, lane 4. However, if the denaturation at alkaline conditions is continued for more than 10 min the biotin-streptavidine bond is broken too (*Figure 4.3*, lane 5). Finally we were able to achieve a labeling efficiency of $\sim$ 90% I-125-labeled TFOs in relation to the inserted amount of preTFOs in the reaction-mix (**4.2.2**). This corresponded to a total amount of labeled TFOs of $\sim$ 4.5 pmol and $\sim$ 0.5 pmol unlabeled TFO in one labeling reaction. In contrast, Panyutin et al. reached a maximum yield of only 10% labeled TFOs with their strategy [97]. Further testing with a 20-fold increase of preTFO concentration in the labeling reaction-mix led to an almost two-fold increased amount of labeled TFO. But at the same time the actual labeling efficiency was reduced almost 10-fold to $\sim$ 11% I-125-labeled TFOs. Moreover, the amount of unlabeled TFOs (preTFO) still included in the reaction mix of $\sim$ 89 pmol was significantly increased compared to the former labeling reaction strategy containing only $\sim$ 0.5 pmol preTFOs. In some DNA triplex formation experiments (data not given) evidence arose that an increased amount of unlabeled TFOs in a triplex forming reaction mix is able to inhibit the target binding of the labeled TFOs, possibly in a sort of competitive inhibition. This finding led to the important conclusion that the amount of unlabeled TFOs in the reaction mix is an inhibitory factor with regard to TFO target binding. The concentration of unlabeled TFOs should therefore be kept as low as possible to allow maximum DNA triplex formation with the respective I-125-labeled TFO.

The triplex forming ability of TFOs after labeling with I-125 could be confirmed (*Figure 4.4, 4.5*). The I-125-labeled TFOs investigated bound to their specific target sequence in the 1695 bp and 212 bp DNA target fragment *in vitro*. Triplex verification was performed with EMSA (for target fragments < 300 bp) or agarose gel electrophoresis (for larger targets) combined with autoradiography. To ensure that the band shift in the EMSA (*Figure 4.5* a, ◄) is predominantly due to binding of I-125-labeled TFOs the

EMSA gels were additionally analyzed via autoradiography (*Figure 4.5* b). A band shift in the EMSA and a corresponding signal in the autoradiography ensured the triplex forming abilities of the I-125-labeled TFOs. The autoradiographic analysis was also used by Panyutin et al. [96] to verify triplex formation of I-125-labeled TFOs. To additionally confirm the binding specificity of the TFO, they varied the binding conditions (pH value) until no triplex formation could be detected anymore. In the present work the binding specificity was underlined by the use of a non-complementary TFO, which, as expected, failed to form a DNA triplex structure (*Figures 4.4* b, lane 2). A non-specific binding of TFOs to the target fragments can therefore be neglected *in vitro*.

5.3. DNA Double-Strand Break Analysis *in vitro*

One of the main aims of the present work was to show that an I-125-labeled TFO is able to induce a DSB at a defined specific sequence in a DNA target fragment. The results of the DSB analysis (**4.3**) showed that after an accumulation time of 143 days approximately 40% of the target strand broke into two defined breakage fragments of the expected size (*Figure 4.7*, ◄). These findings are in good agreement with the results of Sedelnikova et al. [117], who described 50% TFO-induced DSB in plasmid DNA after 136 days of decay accumulation, using 6-aminopyrazolo[3,4-*d*]pyrimidine-4(*3H*)-one-(8-aza-7-deazaguanine) (PPG) modified TFOs. This modification enhances the triplex formation [10], and leads to 100% target binding of the TFOs at equimolar ranges of TFO and plasmid DNA [117]. That might explain the higher DSB percentage in comparison with the present work.

It could be shown that after exposure of the DNA target to non-specific I-125-labeled TFOs no distinct breakage fragments were detectable (*Figure 4.7*, lane 2). This finding underlines the results of Panyutin et al. [101] who found also that the effect of unbound I-125-TFOs is only of minor nature.

Beside the percentage of induced DSBs ($\sim$ 40%), we additionally determined the DSB/decay rate and found that approximately 0.6 DSBs were induced per decay of bound I-125-TFO. This result is slightly different from the results of Panyutin et al. [101], who found 0.46 DSB/decay. The higher DSB/decay value obtained in the present work might be induced as a non-directed side effect by unbound I-125-TFOs in the reaction. In addition, Panyutin et al. [101] found an induction of 0.17 DSB/decay for free I-125-TFOs. Consequently, 0.46 DSB/decay for bound TFOs and 0.17 DSB/decay for free TFO, equals a total of 0.63 DSB/decay, which is close to the DSB/decay rate of 0.6

DSB/decay determined in the present work. Moreover, a DSB ratio of 0.6 DSB/decay fits in the coherence of I-125 target distance and DSB induction, investigated by several other groups [114, 81, 7, 64]. These groups determined approximately 1 DSB/decay for I-125 directly incorporated in the DNA and with increasing distance to the binding site a decrease to 0.10 DSB/decay for unbound I-125.

On the agarose gel of the DSB analysis (*Figure 4.7* a, lanes 1 and 2) one more band at 500 bp appears, representing a possible hint for non-specifically induced breaks. However, our explanation is, that this is an unspecific amplificate from the PCR of the target fragment [110]. It can be excluded that this fragment originates from the target as there was no corresponding signal detected in the southern blot (*Figure 4.7* b) using probes specific for the target and the breakage fragments, respectively.

5.4. Biokinetic of TFOs in SCL-II Cells

In the present work it was a major goal to investigate the biokinetics of TFOs in the cellular environment. It should be elucidated how efficient TFOs can be transferred into cells, where TFOs are localized and to determine the persistence of TFOs in the cellular environment.

The biokinetic studies confirmed that the applied transfection protocol caused an initial efficient transfer of TFOs into the cytoplasm and cell nucleus (*Figure 4.9*). The substantial loss of more than $\sim$ 50% TFO positive nuclei detected in the first 6 h after transfection matches the results of Forsha et al. [36] who found after an initial accumulation of fluorescence-labeled oligonucleotides, which are analogues of TFOs, in the nucleus, a pronounced loss of fluorescence signal. That loss was caused by a translocation of oligonucleotides from the nucleus into the cytoplasm. Additionally to a possible translocation process the loss of TFO positive nuclei could also be due to a degradation of TFOs. Degradation processes cannot be generally excluded but are unlikely since Sedelnikova et al. [118] confirmed triplex stability in HeLa cells for at least 48 h. This could be also demonstrated during earlier studies using FRET analysis technique (Kriehuber, personal communication). Since cells were proliferating, the observed significant decrease of TFO positive cells and the smooth decline of TFO positive nuclei 48 h and 72 h post-transfection is probably due to further dilution of the fluorescence signal, caused by cell division. However, TFO signals were detectable throughout the experiment (0 - 72 h). Moreover, it has to be kept in mind that a cell is defined as TFO negative, if the fluorescence signal drops below the set threshold.

However, it is very likely that there is a certain amount of TFO molecules left in the cells, due to the detection limit in flow cytometry. This limit depends on reagents, staining, and instrument parameters and for the most common procedures and reagents the sensitivity limit is ~ 2000 molecules [148]. It is therefore more than likely that there is a reasonable quantity of TFOs left in cells that are methodology defined as TFO negative.

The results of the live cell imaging confirmed the dynamic characteristic of TFO location in the cells. Cells harboring TFOs in the nucleus showed a high variation in signal intensity during the 22 h observation time (*Figure 4.11*). However, the overall amount of TFO-positive nuclei remained constant at ~ 21%, reflecting the flow cytometric results very well. The variation might be explained as all pictures were taken at the same focal plane and it is most likely that the TFOs were out of focus due to diffusion or transport processes. The average retention period of TFOs in the nuclei was 4 h, which is in good accordance with the microscopic analysis of Forsha et al. [36] who observed a translocation of oligonucleotides from the nucleus into the cytoplasm within approximately 5 h. However, it has to be recalled that microscopical analysis of fluorescence-labeled TFO is somehow difficult to interpret, since it is likely that the observed signals represent only large aggregations of TFOs. Single TFOs can not be observed by conventional microscopic techniques.

5.5. Induction of DNA Double-Strand Breaks

The 53BP1 assay was used to quantify the DNA DSBs, induced in SCL-II cells after transfection with different I-125-labeled TFOs with increasing decays/cell (**4.5**) and each 53BP1 focus was regarded as one DSB [115]. The single-binding-site I-125-TFO-GAPDH and the multi-binding-site I-125-TFO-MBS induced 3 foci/cell at similar accumulated decays of ~ 480 decays/cell and ~ 450 decays/cell, respectively. That observation is quite remarkable as a multiple-binding-site I-125-TFO with ~ 7000 targets in the genome is expected to induce more foci/cell. However this holds true only under the assumption that all possible target sequences are bound by the TFO. The employed transfection method delivered on average approximately $6x10^3$ ± 20% I-125-TFO per cell (free and DNA bound I-125-TFO) at a transfection efficiency of ~ 85%. According to that a 100% saturation of all 7000 putative targets with I-125-TFO is not possible. Due to this it can be concluded, that the multi-binding-site I-125-TFO-MBS is not able to unfold its maximum DSB inducing potential. This assumption is in good accordance with results of Sedelnikova et al. [121] and Panyutin et al. [102], who achieved higher

I-125-TFO concentrations of $\sim$ 1x10^7 I-125-TFOs per cell and observed a 1.9-fold increased induction of foci for a multi-binding-site I-125-TFO with $\sim$ 7000 targets compared to a single-binding-site I-125-TFO. It can be therefore concluded that a higher concentration of I-125-in the cell would probably lead to a stronger DSB induction of multi-binding-site I-125-TFO compared to single-binding-site I-125-TFOs. That explanation does also account for the relatively low foci induction of the multi-binding-site I-125-TFO-QRT. Although possessing > 40-times more putative targets than the other two I-125-TFO, only a 1.5-fold stronger foci induction could be observed.

A further question that might arise from the given data is, how can a single-binding-site TFO like I-125-TFO-GAPDH induce more than two foci/cell? For this TFO a maximum of 3.5 foci/cell was measured, which is likely to be a result of the measured background foci of 0.8 foci/cell plus an near-tetraploid fraction ($\sim$ 20 - 40%) of the SCL-II cell line [132] almost doubling the putative target number and therefore enabling a DSB content of more than 2.

The detected slight increase of foci/cell over storage time in the negative controls is in good accordance with the results of Fairbairn et al. who found an increase of DNA damage due to freezing of cells but only a minor further increase after longer time storage [30]. It can therefore be neglected that the increase of foci found in the I-125-TFO transfected cells is only due to the varying storage periods.

The analysis of the uniformity of TFO uptake by quantification of cells with no visible foci and cells with multiple foci revealed in the negative controls a fraction of 87% containing on maximum 2 foci/cell ($\varnothing\sim$ 0.8 foci/cell). That background DSB level is in good accordance with an average of $\sim$ 0.9 foci/cell and a maximum of 3 foci/cell detected by Sedelnikova et al. in non-radioactive TFO transfected negative controls [121]. For all three I-125-TFOs a cell fraction of $\sim$ 62% $\pm$ 5% did not contain more than 2 foci/cell, whereas $\sim$ 38% $\pm$ 5% of cells possessed at least 3 foci/cell or more. These percentages are in good correspondence to the observed transfection efficiency with approximately 34% $\pm$ 25% of cells containing TFOs in the nucleus. In conclusion, cells where the I-125-TFOs are located in the nucleus seem to represent the fraction of cells with the highest DNA damage.

Looking at the multi-binding-site I-125-TFO-MBS and single-binding-site I-125-TFO-GAPDH both inducing in $\sim$ 55% of cells not more than 8 foci/cell and in $\sim$ 40% no foci, the different target numbers were not clearly reflected. In this context the group of Panyutin at al. [102] reported a distribution of foci that was in good correspondence to the different target numbers of their investigated I-125-TFOs. Panyutin et al. showed for the multi-binding-site I-125-TFO a substantial percentage of cells containing between

20 and 30 foci/cell, whereas the single-binding-site I-125-TFO induced between 5 and 10 foci/cell only. This disagreement with the results of the present study might also be explained by the higher intracellular I-125-TFO concentration achieved by Panyutin et al.

However, 12% of I-125-TFO-QRT transfected cells contained on average between 9 and 14 foci/cell, which is twice more than that induced by the other two I-125-TFOs. This might be explained by the very high target number of > 300,000 putative targets per cell for I-125-TFO-QRT. The high target number allows numerous TFO-formation even at low intracellular concentrations of I-125-TFO-QRT.

5.6. Cell Killing

To study the cytotoxic effects of I-125-TFO-QRT, I-125-TFO-MBS and I-125-TFO-GAPDH on transfected SCL-II cells, cell survival experiments were carried out with different accumulated decays (*Figure 4.14*). Additionally, experiments after (I-125)IdU incorporation (*Figure 4.15*) and γ-irradiation (*Figure 4.16*) were performed, to allow the comparison between radiation qualities and different DNA localization of I-125.

The γ-irradiated cells showed, as described in the literature [12], the typical survival curve, with an initial slope in the low dose range, typical for sparsely ionizing radiation (low-LET) (*Figure 4.16*). In contrast to the γ-irradiated cells, the incorporation of (I-125)IdU into DNA led to the characteristic straight exponential survival curve described for densely ionizing radiation (high-LET) (*Figure 4.15*). Even at low numbers of accumulated decays and hence at low radiation doses the DNA incorporated I-125 caused pronounced cytotoxicity. Comparing the D_{37} value of the γ-irradiated cells of 3.5 Gy with the D_{37} value of the cells after (I-125)IdU incorporation of $\sim$ 0.83 Gy [2], revealed a > 4-fold stronger reduction of colony forming ability for the DNA incorporated Auger electron emitter I-125. This finding is in good agreement with the high relative biological effectiveness (RBE) for I-125 of up to $\sim$ 7 described in the literature [88]. In contrast when located extracellular or cytoplasmic, I-125 has an RBE of $\sim$ 1.3 - 1.4 as could be demonstrated by Ling et al. and Kassis et al. [76, 65] and induces survival curves more resembling to low-LET irradiation [65, 113].

The observed results of the CFA (*Figure 4.14*) corresponded very well to the results of the 53BP1 assay (*Figure 4.12*). I-125-TFO-QRT induced the highest DSB number

2 Point-Kernel dose calculation after Humm et al. [58] for SCL-II cells with a cell nucleus diameter of 10 μm.

and showed concordantly the strongest cytotoxicity of all three tested TFOs. I-125-TFO-QRT displays an almost twice as high cytotoxicity and a ~ 1.5-fold increased 53BP1 foci number/cell per decay when compared to I-125-TFO-GAPDH and I-125-TFO-MBS. This result is not unexpected as I-125-TFO-QRT possesses the highest target number in the genome of all three tested TFOs, with more than ~ 300,000 putative target sequences overall, and ~ 14,700 located in promotor and regulatory regions [133, 59]. In view of theses results one could conclude that the general cytotoxic effect of I-125-TFOs depends largely on the target quantity, hence number of putative targets and less on the localization or function of the targeted sequence. Interestingly, however, the single-binding-site I-125-TFO-GAPDH, binding in the promotor region of the *GAPDH* gene only, showed an almost as high cytotoxicity as the multi-binding-site I-125-TFO-MBS, the latter having ~ 7000 potential targets in the whole genome [121]. This could easily reflect the biological importance of the selected target gene and strongly suggests, that targeting one single essential target in the genome can be at least as cytotoxic as targeting multiple, but non-essential targets.

This hypothesis is supported by the work of Sedelnikova et al [121], who compared the cytotoxicity of the same I-125-TFO that was used in the present work, i.e. I-125-TFO-MBS (yet labeled with three I-125 molecules) to a single-binding-site I-125-TFO binding in the *HPRT* gene. This gene is part of the purine recycling pathway in human cells and was previously shown to be a non-essential gene for cells growing in culture [128]. By comparing the non-essential single-binding-site I-125-TFO-HPRT to a multi-binding-site TFO, Sedelnikova et al. [121] observed a 1.7 times higher cytotoxicity of the multi-binding-site I-125-TFO-MBS. In contrast, the observed strong cytotoxicity of the single target binding I-125-TFO-GAPDH in the present work might be explained by the crucial importance of *GAPDH* in glycolysis, which is essential for growing cells in culture [3].

Therefore, the question arises whether it is the target quantity or the target quality that determines the observed cytotoxicity. The obtained results allow conclusions in both directions. It was shown that a single-binding-site TFO (I-125-TFO-GAPDH) can be as cytotoxic as an multi-binding-site TFO (I-125-TFO-MBS), which is probably due to the target quality. However, the I-125-TFO-QRT, which possesses the highest target number, induced the most pronounced cytotoxic effect per decay, which in turn might indicate that the target quantity is of major importance. Considering that I-125-TFO-QRT induced almost twice as much 53BP1 foci per decay when compared to I-125-TFO-MBS and I-125-TFO-GAPDH it is highly probable that the amount of targets and hence induced DSB per decay is much more relevant for cell killing than the quality of the target.

It should also be mentioned that I-125-TFO-QRT was not originally designed to form DNA triplices but as an oligonucleotide with a high probability of forming secondary structures caused by the guanine motif contained in it [95]. It is well known that numerous genes possess guanine-rich sequences in promotor regions as well as in other regulatory and non-regulatory structures of the genomic DNA, which enables them to form various secondary structures, including guanine quadruplices [95]. We conclude therefore that the I-125-TFO-QRT binds within these regions as part of a quadruplex structure. The observed strong cytotoxicity can be explained by multiple binding and disruption of these sequences, leading to the enhanced cytotoxic effect of I-125-TFO-QRT. Finally we cannot determine with certainty that the observed cytotoxic effects are rather due to the quantity of TFO targets or if the proper localization of the TFOs is of major importance. As already mentioned, the induced effects are remarkable, considering the relatively low achieved concentrations of I-125-TFOs in the cells, but probably not pronounced enough to reflect more clearly the distinct TFO qualities. However, we assume more distinct effects at higher cellular I-125-TFO concentrations.

A question which might also arise from the present data is to what extent the measured cytotoxic and genotoxic effects are due to I-125-TFOs, which are not bound to their DNA targets. It is known that I-125 has to be in close proximity to the DNA to induce its pronounced cytotoxicity due to the numerous ejected low energy auger electrons. Nevertheless, I-125 emits also higher energy electrons with longer range as well as γ-irradiation [62], which might also damage cellular components and reduce colony forming ability. This has been investigated by Sedelnikova et al. [120] who found a measurable cytotoxic effect for unbound I-125-ODNs in the cell. However, the observed cytotoxicity was more than 3 orders of magnitude below the cytotoxic effect measured for incorporated (I-125)IdU and reached the D_{37} value at 1.3x10^4 decays/cell. Since this value is nearly 40-fold higher when compared to the D_{37} values determined for I-125-TFOs investigated in the present work, we assume that the effect of unbound I-125-TFO can be neglected in that context.

When comparing the survival data of I-125-TFO transfected cells to the transfection efficiency, it seems curious that over $\sim$ 90% of cells can be killed at a transfection efficiency of $\sim$ 85% and about $\sim$ 30% of TFOs in the nucleus. As already mentioned in **5.4**, however, the flow cytometry used for determination of the transfection efficiency has an approximate sensitivity limit of $\sim$ 2000 molecules [148]. Therefore we assume that the amount of TFO that cannot be detected in the flow cytometry due to a concentration below the detection limit is still high enough to induce a pronounced cytotoxic effect, when I-125-labeled TFO are used.

5.7. Relative Gene Expression Analysis

According to the existing literature, the approach of using a gene specific binding I-125-labeled TFO to manipulate a gene on the expression level, has not been applied before. Up to now I-125-labeled TFOs were investigated only with regard to TFO delivery and induction of gene specific DSBs [119, 116, 99] but without analyzing specific alterations of gene expression. In the present work three different I-125-TFOs binding within the genes *GAPDH*, *BRCA1* and *BCL2* were investigated. Additionally, the effect of the multi-binding-site I-125-TFO-QRT on all three genes was investigated. Before analysis transfected cells were stored at -150°C for accumulation of $\sim$ 300 decays/cell. 300 accumulated decays were chosen as it largely represents the average D_{37} value determined in the precedent CFAs (*Figure 4.14*).

The *GAPDH* gene was chosen as a TFO target due to its constant high expression level in the cell, and therefore allows good quantification of potential TFO-induced gene expression alteration. Targeting the *GAPDH* gene with the specific binding I-125-TFO-GAPDH resulted in a significant down-regulation of the *GAPDH* gene expression (*Figure 4.18*). We suggest that this reflects the DNA damage caused by *GAPDH* bound I-125-TFO-GAPDH and the subsequent decay of I-125. This interpretation is supported by the observed induction of site-specific DSBs in our *in vitro* studies (*Figure 4.7*), and the general geno- and cytotoxicity of I-125-TFO-GAPDH in the 53BP1 foci assay and the CFA (*Figure 4.12* and *4.14*). It also correlates very well with the findings of Sedelnikova et al. [119], who were able to show the induction of specific DSBs in the human *MDR1* gene in KB-V1 cells by a specific binding I-125-labeled TFO. Furthermore the results in the present work emphasize the high target specificity of I-125-TFO-GAPDH when compared to I-125-TFO-QRT, which possesses a much higher cytotoxicity (***4.14***), but barely affects the gene expression of *GAPDH*.

The target sequence of I-125-TFO-GAPDH is located in the promoter region 422 bp upstream of the *GAPDH* gene. From that it might be concluded that the decrease in gene expression is not due to the decay of I-125 and the subsequently caused DNA damage, but to a blockage of the promoter region by the TFO itself. The group of Cooney et al. [20] used an unlabeled TFO binding 115 bp upstream of the *c-myc* gene transcription origin, to successfully downregulate the gene expression. In the present work this effect can be ruled out as the negative controls contained TFO-GAPDH without the I-125 labeling, and no gene expression alterations could be detected in these samples.

BRCA1 is part of the cellular DNA damage response and plays an important role in cell cycle checkpoint activation and DNA damage repair [141]. A loss of function mutation of *BRCA1* increases the risk for breast or ovarian cancer [79].

A significant gene expression alteration of *BRCA1* in I-125-TFO-BCL2 transfected cells could not be detected (*Figure 4.19*). A possible explanation for the lack of any gene expression alteration might be the position of the primer pair that was used for the qRT-PCR. The amplified region for the qRT-PCR is located upstream of the TFO binding site. Hence it is possible that even though the I-125-TFO induced damage at its binding site, the region upstream of the TFO binding site was still transcribed and led therefore to an unaltered signal in the qRT-PCR. The primers, however, were positioned under the assumption that a damage induced anywhere within the gene sequence would cause a general stop of transcription as could be shown by Donahue at al. [28].

In contrast to I-125-TFO-BCL2 the multi-binding-site I-125-TFO-QRT induced a pronounced down-regulation of the *BRCA1* gene expression. It is likely that I-125-TFO-QRT caused widely spread damage to the genome, which might cause the observed down-regulation. That hypothesis is supported by the results of several groups who could show a significant downregulation of the BRCA1 mRNA level in human cancer cell lines after treatment with different DNA damaging agents such as UV irradiation [4, 31, 145].

The proto-oncogene *BCL2* was originally discovered as part of a t(14;18) chromosomal translocation leading to *BCL2* overexpression, frequently found in non-Hodgkin´s lymphomas [134]. Overexpression of *BCL2* also occurs in many other types of human tumors, including cancers of prostate, colon, and lung [107]. Therefore, *BCL2* represented a possible candidate gene for I-125-TFO based antigene radiotherapy [99].

Interestingly, in I-125-TFO-BCL2 transfected SCL-II cells a 2-fold upregulation of the *BCL2* gene expression was detected when compared to the negative control. In contrast to that, we initially expected a downregulation of the gene expression due to the complex DNA damage in the gene that is assumed to be caused by the *BCL2* bound I-125-TFO-BCL2. According to existing literature there has been no evidence so far that DNA damage induces an upregulation of *BCL2* gene expression, whereas a downregulation of *BCL2* after DNA damage could be shown in several studies [17, 35, 77]. A possible explanation for this observation might be drawn from the results of Varga et al. who showed that a DSB inserted at a predetermined location was able to induce complex DNA rearrangements such as inversions, deletions and translocations [135]. Therefore, it might be hypothesized that the site-specific I-125-TFO-BCL2 induced DSB led to a translocation of fragments or of the whole *BCL2* gene under the influence of a

stronger promotor, inducing the increased gene expression. This is supported by the location of the binding sequence of the used I-125-TFO-BCL2, which is in close vicinity of the known major breakpoint region (MBR) in the *BCL2* gene [19]. Breaks in this region lead to an increased translocation frequency of the *BCL2* gene under the influence of the IgH enhancer located on chromosome 14, resulting in an overexpression of *BCL2* [146]. Naturally, one has to bear in mind that the induced translocations are rare events happening only in a fraction of cells. As, however, the *BCL2* mRNA level in cells without the t(14;18) translocation is generally very low [122], it should be possible to detect also small increases in the mRNA level.

In contrast, the non-specific I-125-TFO-QRT led to a significant 4-fold downregulation of *BCL2* gene expression in transfected SCL-II cells. This multi-binding-site I-125-TFO is supposed to cause widely spread damage to the genome, which might lead to the observed downregulation. That would be in good agreement with findings of Chen et al. who detected a $\sim$ 5-fold downregulation of *BCL2* gene expression after induction of DNA damage in human leukemia cells after exposure to 10 Gy of X-rays [17].

5.8. Induction of Micronuclei

All three tested I-125-TFOs induced, between $\sim$ 300 and $\sim$ 400 decays/cell, a significantly increased number of MN when compared to the negative controls (*Figure 4.21*, *4.22* and *4.23*). Only I-125-TFO-MBS and I-125-TFO-QRT, both binding to multiple targets, induced also at higher decays/cell significantly increased MN numbers. The lack of a clear positive MN-dose-dependency in all three analyzed I-125-TFOs that has been shown after γ-irradiation (*Figure 4.24*) is striking. A possible explanation might be the rather short cytochalasin B incubation time of the cells after decay accumulation, in combination with a radiation induced G_2/M cell cycle arrest, that was confirmed thereupon (*Figure 4.26*, *4.27* and *4.28*). In consequence not all cells underwent cell division and since MN formation requests mitosis, cells have to undergo cell division at least once to form MN [34]. Ludwikow et al. detected a decrease in MN formation in CHO cells at higher doses of DNA incorporated (I-125)IdU, also assuming a connection between cell cycle perturbences and MN amount. They concluded that an increased cytochalasin B incubation before MN analysis should overcome the problem. However, an increase of the incubation period did not lead to a significant change in MN content [83]. In the present work an elongated cytochalasin B incubation up to 48 h did not make any difference in MN content either (data not shown). It is therefore more likely that the observed MN-dose-response is a consequence of the increasing cell killing at

higher doses (*Figure 4.14*) in combination with a constant fraction of non-transfected cells ($\sim$ 15%; transfection efficiency $\sim$ 85%) receiving no dose. Since the MN assay displays only living cells, the non-transfected cell fraction becomes more dominant the more the transfected cells are reduced by cell killing with increasing dose. This is supposed to create the appearance of a decreasing MN number with increasing dose. This assumption is additionally supported by the fact that the strongest MN decrease was induced by I-125-TFO-QRT, showing also the strongest cell killing effect of the analyzed I-125-TFOs.

The comparison of the I-125-TFOs with each other did not reveal significant differences of their MN inducing potential. Hence, the results of the 53BP1 assay, with I-125-TFO-QRT inducing $\sim$1.5-fold more 53BP1 foci, were not significantly reflected in the MN frequencies. However, there is experimental evidence that at $\sim$ 300 and $\sim$ 400 decays/cell a higher number of MN are observed for the two multi-binding I-125-TFO-QRT and I-125-TFO-MBS when compared to the single-binding-site I-125-TFO-GAPDH. Additionally I-125-TFO-QRT induced at $\sim$ 300 decays/cell significantly more MN than γ-irradiation. Therefore it is likely that the DSB inducing potential of a I-125-TFO is also reflected in chromosomal damage. This assumption is supported by the general acceptance that unrepaired or misrepaired DNA DSBs lead to the formation of chromosome aberrations [60].

5.9. Cell Cycle Analysis of SCL-II Cells

It is well known that exposure to ionizing radiation induces cell cycle delays in a variety of cells [87]. Such delays may appear in G_1-phase, G_2/M-phase or in S-phase of the cell cycle. Cell cycle arrests are highly conserved from yeast to mammalian cells and DNA damage as e.g. caused by ionizing radiation are potent causes for cell cycle arrests [87]. In the present work SCL-II cells either transfected with I-125-TFO-GAPDH, I-125-TFO-QRT or I-125-TFO-MBS displayed a pronounced cell cycle arrest in G_2/M-phase with approximately 60% of cells arrested in G_2/M, 8 h post irradiation[3]. These observations are in good agreement with results obtained by Xu et al. showing a transient G_2/M arrest in several tumor cell lines after irradiation with 6 Gy of γ-rays [142]. By 16 h post irradiation cells of I-125-TFO-GAPDH and I-125-TFO-MBS transfected samples began to reenter cell cycle whereas the I-125-TFO-QRT transfected cells displayed a further increasing fraction of G_2/M arrested cells. The more pronounced G_2/M

3 Irradiation refers to the time point of cell recultivation after -150°C storage for accumulation of $\sim$ 300 decays/cell.

arrest induced by I-125-TFO-QRT might be due to the number of potential target sequences of I-125-TFO-QRT in the genome and hence the resulting numerous DNA damages. Thus, it might be concluded that the more DNA damage is induced, the more pronounced is the G_2/M arrest. That assumption is supported by the general assumed dose and damage dependency of the cell cycle delay detected in various cell lines [143, 142].

With regard to the radiation quality the question arises whether Auger electron emitter are able to induce more pronounced cells cycle delay than γ-irradiation or α-particles. Lücke-Huhle et al. could show a G_2/M arrest of 45% at 8 h after $\sim$ 0.35 Gy of α-particles irradiation and $\sim$ 2 Gy of γ-irradiation, equaling an RBE of 5.7 [84]. Compared to the average G_2/M arrested fraction in the present work of 60% after 8 h post irradiation with $\sim$ 300 decays/cell, which equals a cell nucleus dose of $\sim$ 1 Gy[4], this would equal a RBE of $\sim$ 2.6 compared to γ-irradiation. It is obvious that this is only a rough estimation but nevertheless these RBEs would match very well the RBEs of the I-125-TFOs observed in the performed cell survival experiments displaying an RBE of 1.7 - 3 at a radiation dose to the cell nucleus of 1 Gy.

4 Point-Kernel dose calculation after Humm et al. [58] for SCL-II cells with a cell nucleus diameter of 10 μm.

6. Summary

The present work demonstrated that DNA triplex-forming oilgonucleotides (TFO) do bind to their specific targets in a sequence-specific manner. It could be shown that software-based design of TFOs as well as any chemical modification of TFOs e.g. such as adding I-125-labeled nucleotides or fluorochromes demands the experimental verification of the successful DNA triplex formation *in vitro*.

I-125-labeled TFOs are able to induce site-specific DSBs in DNA fragments *in vitro*. It could be further demonstrated that fluorochrome-labeled TFOs persist in a cellular environment for more than 72 h and that I-125-labeled TFOs cause putative site-specific DNA damage, leading to a decrease in cell survival and a corresponding increase of 53BP1 foci in the human SCL-II cell line. In that context the comparison of single-binding-site TFOs with multiple binding TFOs gave experimental evidence that the cytotoxicity of an AEE-labeled TFO seems to depend on target quantity as well as on target quality.

In addition, there is good evidence that I-125-labeled TFOs may not only target DNA by the formation of a DNA triplex structure but possess, with adopted base sequence, the potential to bind to guanine rich sequences as a part of a quadruplex structure. This significantly increases the potential of AEE-labeled TFOs to be used to introduce complex DNA lesions in cells and cell lines.

It could also be demonstrated that I-125-labeled TFOs targeting single genes can alter gene expression of the specifically targeted gene. Both, a specific down- as well as an upregulation of gene expression could be shown. It is likely that the influence on gene expression is due to the site-specific induction of DSBs.

The TFO based carrier system might be a very useful tool for future targeted cancer therapy approaches and, more recently, for basic DNA repair research.

7. Future Strategies

The future strategies are divided in short term tasks, which mostly comprise further improvement of the established methods or additional techniques for verification of the achieved results, and middle to long term tasks, which rather refer to potential fields the TFO based system could be used upon.

Short Term Tasks:

- Although we could determine the stability of TFOs in a cellular environment, there is evidence that TFOs are degraded to a certain extent. To increase TFO stability modifications of the employed oligonucleotides e.g with a phosphorothioate or phosphoramidate backbone should be examined to enhance cellular persistence.

- The labeling of TFOs with I-125 was well established and reached an efficiency of $\sim$ 90% but nevertheless we found indications that the remaining fraction of unlabeled TFOs can induce inhibitory effects on the DNA triplex formation with labeled TFOs. Therefore, the labeling reaction has to be optimized in a way to separate the labeled TFOs from unlabeled residues.

- One very important task for future research is to elucidate the amount of non-directed effects of I-125-labeled TFOs in the cell. Non-bound I-125-labeled TFOs might induce a certain degree of cytotoxicity and non-specific DNA damage, respectively, when located in the nucleus, as was shown by Sedlenikova et al. [120]. To quantify this effect I-125-TFOs with no obvious target in the genome, or the use of TFOs with a complementary oligonucleotide preventing DNA binding, shall be examined.

- Based on the results of the 53BP1 assay it seems that the obvious I-125-TFO induced effects become more distinct, when higher intracellular concentrations of I-125-TFOs are achieved. Thus one further task is to increase the efficiency of TFO delivery into the cells either by improving the technique used in the present study or by establishing a liposome-based method.

- Investigation of the I-125-TFO damaging potential on the chromatin level, without the limitations of the MN assay e.g. by using *In-Situ* Hybridisation techniques.

Middle to Long Term Tasks:

- Auger electron emitter labeled TFOs allow the site-specific induction of complex DNA lesions and are therefore an interesting tool for DNA-repair-research. Numerous structures such as promotors, exons and introns but also hetero- or euchromatic regions can be targeted in a sequence-specific manner. The repair mechanisms and repair efficiencies of such DNA structures in a cellular environment are at present barely understood. Therefore, addressing these topics using AEE-labeled TFOs will certainly be part of future studies.

- Interesting applications of AEE-labeled TFOs might also be in the field of molecular microbiology with focus on anti-infectives research. Bacteria resistant against most available antibiotics constitute a severe problem in clinical surgery and therapy [80]. In many cases single base mutations in the bacterial genome are sufficient to extend the resistance spectrum and to render the available antibiotics almost noneffective. An AEE-labeled TFO, specific for a sequence in the resistance gene of a bacterium might induce a downregulation and a reduced production of resistance factors. Combined with a regular antibiotic therapy this approach might increase therapeutic success in severe multi resistant bacterial inflammations.

8. Bibliography

[1] R. T. Abraham. Cell cycle checkpoint signaling through the ATM and ATR kinases. *Genes Dev*, 15(17):2177–2196, Sep 2001.

[2] S. J. Adelstein, A. I. Kassis, L. Bodei, and G. Mariani. Radiotoxicity of iodine-125 and other auger-electron-emitting radionuclides: background to therapy. *Cancer Biother Radiopharm*, 18(3):301–316, Jun 2003.

[3] B. Alberts. Cell biology: the endless frontier. *Mol Biol Cell*, 21(22):3785, Nov 2010.

[4] J. L. Andres, S. Fan, G. J. Turkel, J. A. Wang, N. F. Twu, R. Q. Yuan, K. Lamszus, I. D. Goldberg, and E. M. Rosen. Regulation of BRCA1 and BRCA2 expression in human breast cancer cells by DNA-damaging agents. *Oncogene*, 16(17):2229–2241, Apr 1998.

[5] P. Auger. Sur les rayons β secondaires produits dans un gaz par des rayons X. *Comptes Rendues Hebdomadaires des Seances de l'Academie des Sciences*, 177:169–171, 1923.

[6] O. T. Avery, C. M. Macleod, and M. McCarty. Studies on the chemical nature of the substance inducing transformation of pneumococcal types : Induction of transformation by a desoxyribonucleic acid fraction isolated from pneumococcus type III. *J Exp Med*, 79(2):137–158, Feb 1944.

[7] P. Balagurumoorthy, X. Xu, K. Wang, S. J. Adelstein, and A. I. Kassis. Effect of distance between decaying 125I and DNA on Auger-electron induced double-strand break yield. *Int J Radiat Biol*, Jun 2012.

[8] P. A. Beal and P. B. Dervan. Second structural motif for recognition of DNA by oligonucleotide-directed triple-helix formation. *Science*, 251(4999):1360–1363, Mar 1991.

[9] P. A. Beal and P. B. Dervan. The influence of single base triplet changes on the stability of a pur.pur.pyr triple helix determined by affinity cleaving. *Nucleic Acids Res*, 20(11):2773–2776, Jun 1992.

[10] E. S. Belousov, I. A. Afonina, I. V. Kutyavin, A. A. Gall, M. W. Reed, H. B. Gamper, R. M. Wydro, and R. B. Meyer. Triplex targeting of a native gene in permeabilized intact cells: covalent modification of the gene for the chemokine receptor CCR5. *Nucleic Acids Res*, 26(5):1324–1328, Mar 1998.

[11] E. J. Bernhard, A. Maity, R. J. Muschel, and W. G. McKenna. Effects of ionizing radiation on cell cycle progression. a review. *Radiat Environ Biophys*, 34(2):79–83, Jun 1995.

[12] R. P. Bird and H. J. Burki. Survival of synchronized Chinese hamster cells exposed to radiation of different linear-energy transfer. *Int J Radiat Biol Relat Stud Phys Chem Med*, 27(2):105–120, Feb 1975.

[13] S. L. Broitman, D. D. Im, and J. R. Fresco. Formation of the triple-stranded polynucleotide helix, poly(A.A.U). *Proc Natl Acad Sci U S A*, 84(15):5120–5124, Aug 1987.

[14] T. Brown. *Current Protocols in Immunology*. John Wiley and Sons, Inc., 2001.

[15] M. H. Caruthers, N. T. Thuong, U. Asseline, T. Monteney-Garestier, J. Goodchild, P. S. Miller, C. A. Stein, B. Rayner, C. Malvy, J. Paoletti, B. Lebleu, C. Paoletti, J. L. Imbach, C. Hélène, J. J. Toulmé, D. G. Knorre, V. V. Vlassov, V. F. Zarytova, P. B. Dervan, L. M. Neckers, and G. Zon. *Oligodeoxynucleotides: antisense inhibitors of gene expression.* CRC Press Inc, 1989.

[16] P. P. Chan and P. M. Glazer. Triplex DNA: fundamentals, advances, and potential applications for gene therapy. *J Mol Med (Berl)*, 75(4):267–282, Apr 1997.

[17] M. Chen, J. Quintans, Z. Fuks, C. Thompson, D. W. Kufe, and R. R. Weichselbaum. Suppression of Bcl-2 messenger RNA production may mediate apoptosis after ionizing radiation, tumor necrosis factor alpha, and ceramide. *Cancer Res*, 55(5):991–994, Mar 1995.

[18] A. J. Cheng and M. W. Van Dyke. Monovalent cation effects on intermolecular purine-purine-pyrimidine triple-helix formation. *Nucleic Acids Res*, 21(24):5630–5635, Dec 1993.

[19] M. L. Cleary and J. Sklar. Nucleotide sequence of a t(14;18) chromosomal breakpoint in follicular lymphoma and demonstration of a breakpoint-cluster region near a transcriptionally active locus on chromosome 18. *Proc Natl Acad Sci U S A*, 82(21):7439–7443, Nov 1985.

[20] M. Cooney, G. Czernuszewicz, E. H. Postel, S. J. Flint, and M. E. Hogan. Site-specific oligonucleotide binding represses transcription of the human c-myc gene in vitro. *Science*, 241(4864):456–459, Jul 1988.

[21] D. Coster and L. De Kronig. New type of auger effect and its influence on the x-ray spectrum. *Physica*, 2:13–24, 1935.

[22] R. Dahm. Discovering DNA: Friedrich Miescher and the early years of nucleic acid research. *Hum Genet*, 122(6):565–581, Jan 2008.

[23] V. Dahmen and R. Kriehuber. Cytotoxic effects and specific gene expression alterations induced by I-125-labeled triplex-forming oligonucleotides. *Int J Radiat Biol*, 88(12):972–979, Dec 2012.

[24] T. de Bizemont, G. Duval-Valentin, J. S. Sun, E. Bisagni, T. Garestier, and C. Hélène. Alternate strand recognition of double-helical DNA by (T,G)-containing oligonucleotides in the presence of a triple helix-specific ligand. *Nucleic Acids Res*, 24(6):1136–1143, Mar 1996.

[25] D. Deckbar, P. A. Jeggo, and M. Loebrich. Understanding the limitations of radiation-induced cell cycle checkpoints. *Crit Rev Biochem Mol Biol*, 46(4):271–283, Aug 2011.

[26] V. C. Diculescu, A.-M. Chiorcea-Paquim, R. Eritja, and A. M. Oliveira-Brett. Thrombin-Binding Aptamer Quadruplex Formation: AFM and Voltammetric Characterization. *J Nucleic Acids*, 2010, 2010.

[27] S. Diviacco, V. Rapozzi, L. Xodo, C. Hélène, F. Quadrifoglio, and C. Giovannangeli. Site-directed inhibition of DNA replication by triple helix formation. *FASEB J*, 15(14):2660–2668, Dec 2001.

[28] B. A. Donahue, S. Yin, J. S. Taylor, D. Reines, and P. C. Hanawalt. Transcript cleavage by RNA polymerase II arrested by a cyclobutane pyrimidine dimer in the DNA template. *Proc Natl Acad Sci U S A*, 91(18):8502–8506, Aug 1994.

[29] G. T. Emery. Perturbation of nuclear decay rates. *Annu Rev Nucl Sci*, 22:165–202, 1972.

[30] D. W. Fairbairn, W. A. Reyes, R. Van Grigsby, and K. L. O'Neill. Laser scanning microscopic analysis of DNA damage in frozen tissues. *Cancer Lett*, 76(2-3):127–132, Jan 1994.

[31] S. Fan, N. F. Twu, J. A. Wang, R. Q. Yuan, J. Andres, I. D. Goldberg, and E. M. Rosen. Down-regulation of BRCA1 and BRCA2 in human ovarian cancer cells exposed to adriamycin and ultraviolet radiation. *Int J Cancer*, 77(4):600–609, Aug 1998.

[32] A. F. Faruqi, M. M. Seidman, D. J. Segal, D. Carroll, and P. M. Glazer. Recombination induced by triple-helix-targeted DNA damage in mammalian cells. *Mol Cell Biol*, 16(12):6820–6828, Dec 1996.

[33] G. Felsenfeld, D. R. Davies, and A. Rich. Formation of a three-stranded polynucleotide molecule. *J Am Chem Soc*, 79(8):2023–2024, April 1957.

[34] M. Fenech and A. Morley. Solutions to the kinetic problem in the micronucleus assay. *Cytobios*, 43(172-173):233–246, 1985.

[35] H. W. Findley, L. Gu, A. M. Yeager, and M. Zhou. Expression and regulation of Bcl-2, Bcl-xl, and Bax correlate with p53 status and sensitivity to apoptosis in childhood acute lymphoblastic leukemia. *Blood*, 89(8):2986–2993, Apr 1997.

[36] S. J. Forsha, I. V. Panyutin, R. D. Neumann, and I. G Panyutin. Intracellular traffic of oligodeoxynucleotides in and out of the nucleus: effect of exportins and DNA structure. *Oligonucleotides*, 20(6):277–284, Dec 2010.

[37] J. C. François, T. Saison-Behmoaras, and C. Hélène. Sequence-specific recognition of the major groove of DNA by oligodeoxynucleotides via triple helix formation. footprinting studies. *Nucleic Acids Res*, 16(24):11431–11440, Dec 1988.

[38] M. D. Frank-Kamenetskii and S. M. Mirkin. Triplex DNA structures. *Annu Rev Biochem*, 64:65–95, 1995.

[39] M. J. Fulwyler. Status quo in flow-through cytometry. *J Histochem Cytochem*, 22(7):605–606, Jul 1974.

[40] D. M. Gadbois, H. A. Crissman, A. Nastasi, R. Habbersett, S. K. Wang, D. Chen, and B. E. Lehnert. Alterations in the progression of cells through the cell cycle after exposure to alpha particles or gamma rays. *Radiat Res*, 146(4):414–424, Oct 1996.

[41] M. M. Garner and A. Revzin. A gel electrophoresis method for quantifying the binding of proteins to specific DNA regions: application to components of the Escherichia coli lactose operon regulatory system. *Nucleic Acids Res*, 9(13):3047–3060, Jul 1981.

[42] C. Giovannangéli, M. Rougée, T. Garestier, N. T. Thuong, and C. Hélène. Triple-helix formation by oligonucleotides containing the three bases thymine, cytosine, and guanine. *Proc Natl Acad Sci U S A*, 89(18):8631–8635, Sep 1992.

[43] M. González, C. E. Argaraña, and G. D. Fidelio. Extremely high thermal stability of streptavidin and avidin upon biotin binding. *Biomol Eng*, 16(1-4):67–72, Dec 1999.

[44] J. R. Goñi, X. de la Cruz, and M. Orozco. Triplex-forming oligonucleotide target sequences in the human genome. *Nucleic Acids Res*, 32(1):354–360, 2004.

[45] J. R. Goñi, J. M. Vaquerizas, J. Dopazo, and M. Orozco. Exploring the reasons for the large density of triplex-forming oligonucleotide target sequences in the human regulatory regions. *BMC Genomics*, 7:63, 2006.

[46] V. Gottifredi and C. Prives. The S phase checkpoint: when the crowd meets at the fork. *Semin Cell Dev Biol*, 16(3):355–368, Jun 2005.

[47] A. L. Guieysse, D. Praseuth, J. C. Francois, and C. Hélène. Inhibition of replication initiation by triple helix-forming oligonucleotides. *Biochem Biophys Res Commun*, 217(1):186–194, Dec 1995.

[48] E. J. Hall and A. J. Giaccia. *Radiobiology for the Radiobiologist*. Lippincott Williams & Wilkins, sixth edition, 2006.

[49] J. A. Heddle. A rapid in vivo test for chromosomal damage. *Mutat Res*, 18(2):187–190, May 1973.

[50] C. Hélène. The anti-gene strategy: control of gene expression by triplex-forming-oligonucleotides. *Anticancer Drug Des*, 6(6):569–584, Dec 1991.

[51] H. Hertz. Ueber den Einfluss des ultravioletten Lichtes auf die elektrische Entladung. *Annalen der Physik*, 267(8):983–1000, 1887.

[52] R. Higuchi, G. Dollinger, P. S. Walsh, and R. Griffith. Simultaneous amplification and detection of specific DNA sequences. *Biotechnology (N Y)*, 10(4):413–417, Apr 1992.

[53] R. M. Hoffman. In vitro sensitivity assays in cancer: a review, analysis, and prognosis. *J Clin Lab Anal*, 5(2):133–143, 1991.

[54] A. Holmberg, A. Blomstergren, O. Nord, M. Lukacs, J. Lundeberg, and M. Uhlén. The biotin-streptavidin interaction can be reversibly broken using water at elevated temperatures. *Electrophoresis*, 26(3):501–510, Feb 2005.

[55] K. Hoogsteen. The structure of crystals containing a hydrogen-bonded complex of 1-methylthymine and 9-methyladenine. *Acta Cryst*, 12, May 1959.

[56] R. W. Howell. Radiation spectra for Auger-electron emitting radionuclides: report No. 2 of AAPM Nuclear Medicine Task Group No. 6. *Med Phys*, 19(6):1371–1383, 1992.

[57] R. W. Howell. Auger processes in the 21st century. *Int J Radiat Biol*, 84(12):959–975, Dec 2008.

[58] J. L. Humm, R. W. Howell, and D. V. Rao. Dosimetry of Auger-electron-emitting radionuclides: report no. 3 of AAPM Nuclear Medicine Task Group No. 6. *Med Phys*, 21(12):1901–1915, Dec 1994.

[59] J. L. Huppert and S. Balasubramanian. G-quadruplexes in promoters throughout the human genome. *Nucleic Acids Res*, 35(2):406–413, 2007.

[60] G. Iliakis, H. Wang, A. R. Perrault, W. Boecker, B. Rosidi, F. Windhofer, W. Wu, J. Guan, G. Terzoudi, and G. Pantelias. Mechanisms of DNA double strand break repair and chromosome aberration formation. *Cytogenet Genome Res*, 104(1-4):14–20, 2004.

[61] G. Iliakis, Y. Wang, J. Guan, and H. Wang. DNA damage checkpoint control in cells exposed to ionizing radiation. *Oncogene*, 22(37):5834–5847, Sep 2003.

[62] A. I. Kassis. The amazing world of auger electrons. *Int J Radiat Biol*, 80(11-12):789–803, 2004.

[63] A. I. Kassis and S. J. Adelstein. Radiobiologic principles in radionuclide therapy. *J Nucl Med*, 46 Suppl 1:4S–12S, Jan 2005.

[64] A. I. Kassis, R. S. Harapanhalli, and S. J. Adelstein. Comparison of strand breaks in plasmid DNA after positional changes of Auger electron-emitting iodine-125. *Radiat Res*, 151(2):167–176, Feb 1999.

[65] A. I. Kassis, K. S. Sastry, and S. J. Adelstein. Kinetics of uptake, retention, and radiotoxicity of 125IUdR in mammalian cells: implications of localized energy deposition by Auger processes. *Radiat Res*, 109(1):78–89, Jan 1987.

[66] M. B. Kastan and D. S. Lim. The many substrates and functions of ATM. *Nat Rev Mol Cell Biol*, 1(3):179–186, Dec 2000.

[67] M. B. Kastan, Q. Zhan, W. S. el Deiry, F. Carrier, T. Jacks, W. V. Walsh, B. S. Plunkett, B. Vogelstein, and AJ Fornace, Jr. A mammalian cell cycle checkpoint pathway utilizing p53 and GADD45 is defective in ataxia-telangiectasia. *Cell*, 71(4):587–597, Nov 1992.

[68] R. Kriehuber, K. Kadenbach, F. Schultz, and D. G. Weiss. Study on cell survival, induction of apoptosis and micronucleus formation in SCL-II cells after exposure to the auger electron emitter (99m)Tc. *Int J Radiat Biol*, 80(11-12):875–880, 2004.

[69] R. Kriehuber, M. Riedling, M. Simkó, and D. G. Weiss. Cytotoxicity, genotoxicity and intracellular distribution of the auger electron emitter (65)Zn in two human cell lines. *Radiat Environ Biophys*, 43(1):15–22, May 2004.

[70] R. Kriehuber and M. Simkó. Apoptosis induction and micronucleus formation after exposure to the Auger electron emitter zinc-65 in a human cell line. *Acta Oncol*, 39(6):699–706, 2000.

[71] A. Krishan. Rapid flow cytofluorometric analysis of mammalian cell cycle by propidium iodide staining. *J Cell Biol*, 66(1):188–193, Jul 1975.

[72] T. Le Doan, L. Perrouault, D. Praseuth, N. Habhoub, J. L. Decout, N. T. Thuong, J. Lhomme, and C. Helene. Sequence-specific recognition, photocrosslinking and cleavage of the dna double helix by an oligo-[alpha]-thymidylate covalently linked to an azidoproflavine derivative. *Nucleic Acids Res*, 15(19):7749–7760, Oct 1987.

[73] C. M. Lederer, V. S. Shirley, E. Browne, J. M. Dairiki, R. E. Doebler, A. A. Shihiab-Eldin, L. J. Jardine, J. K. Tuli, and A. B. Burn. Table of isotopes, seventh edition. *Wiley, New York*, 343:528–529, 1978.

[74] J.B. LePecq and C. Paoletti. A fluorescent complex between ethidium bromide and nucleic acids. Physical-chemical characterization. *J Mol Biol*, 27(1):87–106, Jul 1967.

[75] A. G. Letai, M. A. Palladino, E. Fromm, V. Rizzo, and J. R. Fresco. Specificity in formation of triple-stranded nucleic acid helical complexes: studies with agarose-linked polyribonucleotide affinity columns. *Biochemistry*, 27(26):9108–9112, Dec 1988.

[76] C. C. Ling, W. X. Li, and L. L. Anderson. The relative biological effectiveness of I-125 and Pd-103. *Int J Radiat Oncol Biol Phys*, 32(2):373–378, May 1995.

[77] J. Lips and B. Kaina. DNA double-strand breaks trigger apoptosis in p53-deficient fibroblasts. *Carcinogenesis*, 22(4):579–585, Apr 2001.

[78] M. N. Lipsett. Complex formation between polycytidylic acid and guanine oligonucleotides. *J Biol Chem*, 239:1256–1260, Apr 1964.

[79] E. T. Liu. Oncogenes, breast cancer, and chemoprevention. *J Cell Biochem Suppl*, 17G:161–166, 1993.

[80] D. M. Livermore. Fourteen years in resistance. *Int J Antimicrob Agents*, 39(4):283–294, Apr 2012.

[81] P. N. Lobachevsky and R. F. Martin. DNA strand breakage by 125I-decay in a synthetic oligodeoxynucleotide–2. Quantitative analysis of fragment distribution. *Acta Oncol*, 35(7):809–815, 1996.

[82] P. N. Lobachevsky and R. F. Martin. Iodine-125 decay in a synthetic oligodeoxynucleotide. II. The role of auger electron irradiation compared to charge neutralization in DNA breakage. *Radiat Res*, 153(3):271–278, Mar 2000.

[83] G. Ludwików, F. Ludwików, and K. J. Johanson. Kinetics of micronuclei induced by 125idu in cells of two lines. *Radiat Res*, 138(1):70–78, Apr 1994.

[84] C. Luecke-Huhle, W. Comper, L. Hieber, and M. Pech. Comparative study of G2 delay and survival after 241 Americium-alpha and 60 Cobalt-gamma irradiation. *Radiat Environ Biophys*, 20(3):171–185, 1982.

[85] J. Lukas, C. Lukas, and J. Bartek. Mammalian cell cycle checkpoints: signalling pathways and their organization in space and time. *DNA Repair (Amst)*, 3(8-9):997–1007, 2004.

[86] V. I. Lyamichev, S. M. Mirkin, and M. D. Frank-Kamenetskii. Structures of homopurine-homopyrimidine tract in superhelical DNA. *J Biomol Struct Dyn*, 3(4):667–669, Feb 1986.

[87] A. Maity, W. G. McKenna, and R. J. Muschel. The molecular basis for cell cycle delays following ionizing radiation: a review. *Radiother Oncol*, 31(1):1–13, Apr 1994.

[88] G. M. Makrigiorgos, A. I. Kassis, J. Baranowska-Kortylewicz, K. D. McElvany, M. J. Welch, K. S. Sastry, and S. J. Adelstein. Radiotoxicity of 5-[123I]iodo-2'-deoxyuridine in V79 cells: a comparison with 5-[125I]iodo-2'-deoxyuridine. *Radiat Res*, 118(3):532–544, Jun 1989.

[89] R. F. Martin and W. A. Haseltine. Range of radiochemical damage to DNA with decay of iodine-125. *Science*, 213(4510):896–898, Aug 1981.

[90] M.W. McDonell, M.N. Simon, and F.W. Studier. Analysis of restriction fragments of T7 DNA and determination of molecular weights by electrophoresis in neutral and alkaline gels. *J Mol Biol*, 110(1):119–146, Feb 1977.

[91] S. M. Mirkin, V. I. Lyamichev, K. N. Drushlyak, V. N. Dobrynin, S. A. Filippov, and M. D. Frank-Kamenetskii. DNA H form requires a homopurine-homopyrimidine mirror repeat. *Nature*, 330(6147):495–497, 1987.

[92] A. Munshi, M. Hobbs, and R. M. Meyn. *In Vitro Assays*. Springer, 2005.

[93] H. Nikjoo, D. Emfietzoglou, and D. E. Charlton. The Auger effect in physical and biological research. *Int J Radiat Biol*, 84(12):1011–1026, Dec 2008.

[94] S. B. Noonberg, J. C. François, T. Garestier, and C. Hélène. Effect of competing self-structure on triplex formation with purine-rich oligodeoxynucleotides containing ga repeats. *Nucleic Acids Res*, 23(11):1956–1963, Jun 1995.

[95] M. I. Onyshchenko, T. I. Gaynutdinov, E. A. Englund, D. H. Appella, R. D. Neumann, and I. G. Panyutin. Quadruplex formation is necessary for stable PNA invasion into duplex DNA of BCL2 promoter region. *Nucleic Acids Res*, 39(16):7114–7123, Sep 2011.

[96] I. G. Panyutin and R. D. Neumann. Sequence-specific DNA double-strand breaks induced by triplex forming 125I labeled oligonucleotides. *Nucleic Acids Res*, 22(23):4979–4982, Nov 1994.

[97] I. G. Panyutin and R. D. Neumann. Sequence-specific DNA breaks produced by triplex-directed decay of iodine-125. *Acta Oncol*, 35(7):817–823, 1996.

[98] I. G. Panyutin and R. D. Neumann. The potential for gene-targeted radiation therapy of cancers. *Trends Biotechnol*, 23(10):492–496, Oct 2005.

[99] I. G. Panyutin, O. A. Sedelnikova, V. N. Karamychev, and R. D. Neumann. Antigene radiotherapy: targeted radiodamage with 125I-labeled triplex-forming oligonucleotides. *Ann N Y Acad Sci*, 1002:134–140, Dec 2003.

[100] I. G. Panyutin, T. A. Winters, L. E. Feinendegen, and R. D. Neumann. Development of DNA-based radiopharmaceuticals carrying Auger-electron emitters for anti-gene radiotherapy. *Q J Nucl Med*, 44(3):256–267, Sep 2000.

[101] I. V. Panyutin, A. N. Luu, I. G. Panyutin, and R. D. Neumann. Strand breaks in whole plasmid DNA produced by the decay of (125)I in a triplex-forming oligonucleotide. *Radiat Res*, 156(2):158–166, Aug 2001.

[102] I. V. Panyutin, O. A. Sedelnikova, W. M. Bonner, I. G. Panyutin, and R. D. Neumann. Dna damage produced by 125I-triplex-forming oligonucleotides as a measure of their successful delivery into cell nuclei. *Ann N Y Acad Sci*, 1058:140–150, Nov 2005.

[103] E. Pomplun. Auger electron spectra–the basic data for understanding the Auger effect. *Acta Oncol*, 39(6):673–679, 2000.

[104] E. Pomplun and G. Sutmann. Is coulomb explosion a damaging mechanism for (125)IUdR? *Int J Radiat Biol*, 80(11-12):855–860, 2004.

[105] E. H. Postel, S. J. Flint, D. J. Kessler, and M. E. Hogan. Evidence that a triplex-forming oligodeoxyribonucleotide binds to the c-myc promoter in HeLa cells, thereby reducing c-myc mRNA levels. *Proc Natl Acad Sci U S A*, 88(18):8227–8231, Sep 1991.

[106] T. S. Rao, R. H. Durland, D. M. Seth, M. A. Myrick, V. Bodepudi, and G. R. Revankar. Incorporation of 2'-deoxy-6-thioguanosine into G-rich oligodeoxyribonucleotides inhibits G-tetrad formation and facilitates triplex formation. *Biochemistry*, 34(3):765–772, Jan 1995.

[107] J. C. Reed. Mechanisms of Bcl-2 family protein function and dysfunction in health and disease. *Behring Inst Mitt*, 97(97):72–100, Oct 1996.

[108] M. Riley and B. Maling. Physical and chemical characterization of two- and three-stranded adenine-thymine and adenine-uracil homopolymer complexes. *J Mol Biol*, 20(2):359–389, Sep 1966.

[109] M. Rougée, B. Faucon, J. L. Mergny, F. Barcelo, C. Giovannangeli, T. Garestier, and C. Hélène. Kinetics and thermodynamics of triple-helix formation: effects of ionic strength and mismatches. *Biochemistry*, 31(38):9269–9278, Sep 1992.

[110] W. Rychlik, W. J. Spencer, and R. E. Rhoads. Optimization of the annealing temperature for DNA amplification in vitro. *Nucleic Acids Res*, 18(21):6409–6412, Nov 1990.

[111] W. A. Saffran, M. Goldenberg, and C. R. Cantor. Site-directed psoralen crosslinking of DNA. *Proc Natl Acad Sci U S A*, 79(15):4594–4598, Aug 1982.

[112] F. Sanger and A. R. Coulson. A rapid method for determining sequences in DNA by primed synthesis with DNA polymerase. *J Mol Biol*, 94(3):441–448, May 1975.

[113] K. S. Sastry, R. W. Howell, and D. V. Rao. Dosimetry of Auger emitters: physical and phenomenological approaches. *Taylor & Francis*, pages 27–38, 1988.

[114] A. Schmidt and G. Hotz. The occurrence of double-strand breaks in coliphage T1-DNA by iodine-125 decay. *Int J Radiat Biol Relat Stud Phys Chem Med*, 24(3):307–313, Sep 1973.

[115] L. B. Schultz, N. H. Chehab, A. Malikzay, and T. D. Halazonetis. p53 binding protein 1 (53BP1) is an early participant in the cellular response to DNA double-strand breaks. *J Cell Biol*, 151(7):1381–1390, Dec 2000.

[116] O. A. Sedelnikova, V. N. Karamychev, I. G. Panyutin, and R. D. Neumann. Sequence-specific gene cleavage in intact mammalian cells by 125i-labeled triplex-forming oligonucleotides conjugated with nuclear localization signal peptide. *Antisense Nucleic Acid Drug Dev*, 12(1):43–49, Feb 2002.

[117] O. A. Sedelnikova, A. N. Luu, V. N. Karamychev, I. G. Panyutin, and R. D. Neumann. Development of DNA-based radiopharmaceuticals carrying Auger-

electron emitters for antigene radiotherapy. *Int J Radiat Oncol Biol Phys*, 49(2):391–396, Feb 2001.

[118] O. A. Sedelnikova, I. G. Panyutin, A. N. Luu, and R. D. Neumann. The stability of DNA triplexes inside cells as studied by iodine-125 radioprinting. *Nucleic Acids Res*, 27(19):3844–3850, Oct 1999.

[119] O. A. Sedelnikova, I. G. Panyutin, A. N. Luu, M. W. Reed, T. Licht, M. M. Gottesman, and R. D. Neumann. Targeting the human mdr1 gene by 125I-labeled triplex-forming oligonucleotides. *Antisense Nucleic Acid Drug Dev*, 10(6):443–452, Dec 2000.

[120] O. A. Sedelnikova, I. G. Panyutin, A. R. Thierry, and R. D. Neumann. Radiotoxicity of Iodine-125-labeled oligodeoxyribonucleotides in mammalian cells. *J Nucl Med*, 39(8):1412–1418, Aug 1998.

[121] O. A. Sedelnikova, I. V. Panyutin, R. D. Neumann, W. M. Bonner, and I. G. Panyutin. Assessment of DNA damage produced by 125I-triplex-forming oligonucleotides in cells. *Int J Radiat Biol*, 80(11-12):927–931, 2004.

[122] Y. Shen, J. Iqbal, J. Z. Huang, G. Zhou, and W. C. Chan. BCL2 protein expression parallels its mRNA level in normal and malignant B cells. *Blood*, 104(9):2936–2939, Nov 2004.

[123] C. J. Sherr and J. M. Roberts. Inhibitors of mammalian G1 cyclin-dependent kinases. *Genes Dev*, 9(10):1149–1163, May 1995.

[124] M. Shimada and M. Nakanishi. Response to DNA damage: why do we need to focus on protein phosphatases? *Front Oncol*, 3:8, 2013.

[125] T. Simonsson. G-quadruplex DNA structures–variations on a theme. *Biol Chem*, 382(4):621–628, Apr 2001.

[126] E. M. Southern. Detection of specific sequences among DNA fragments separated by gel electrophoresis. *J Mol Biol*, 98(3):503–517, Nov 1975.

[127] G. G. Steel. *Basic clinical radiobiology*. Little, Brown and Company, 1993.

[128] J. T. Stout and C. T. Caskey. HPRT: gene structure, expression, and mutation. *Annu Rev Genet*, 19:127–148, 1985.

[129] J. S. Sun, T. Garestier, and C. Hélène. Oligonucleotide directed triple helix formation. *Curr Opin Struct Biol*, 6(3):327–333, Jun 1996.

[130] M. Takasugi, A. Guendouz, M. Chassignol, J. L. Decout, J. Lhomme, N. T. Thuong, and C. Hélène. Sequence-specific photo-induced cross-linking of the two strands of double-helical DNA by a psoralen covalently linked to a triple helix-forming oligonucleotide. *Proc Natl Acad Sci U S A*, 88(13):5602–5606, Jul 1991.

[131] N. T. Thuong and C. Hélène. Sequence-specific recognition and modification of double-helical DNA by oligonucleotides. *Angew. Chem. Int. Ed.*, 32:666–690, 1993.

[132] W. Tilgen, P. Boukamp, D. Breitkreutz, R. T. Dzarlieva, M. Engstner, D. Haag, and N. E. Fusenig. Preservation of morphological, functional, and karyotypic traits during long-term culture and in vivo passage of two human skin squamous cell carcinomas. *Cancer Res*, 43(12 Pt 1):5995–6011, Dec 1983.

[133] A. K. Todd, M. Johnston, and S. Neidle. Highly prevalent putative quadruplex sequence motifs in human DNA. *Nucleic Acids Res*, 33(9):2901–2907, 2005.

[134] Y. Tsujimoto and C. M. Croce. Analysis of the structure, transcripts, and protein products of bcl-2, the gene involved in human follicular lymphoma. *Proc Natl Acad Sci U S A*, 83(14):5214–5218, Jul 1986.

[135] T. Varga and P. D. Aplan. Chromosomal aberrations induced by double strand DNA breaks. *DNA Repair (Amst)*, 4(9):1038–1046, Aug 2005.

[136] D. Vlieghe, L. Van Meervelt, A. Dautant, B. Gallois, G. Précigoux, and O. Kennard. Parallel and antiparallel (G.GC)2 triple helix fragments in a crystal structure. *Science*, 273(5282):1702–1705, Sep 1996.

[137] M. A. Walicka, S. J. Adelstein, and A. I. Kassis. Indirect mechanisms contribute to biological effects produced by decay of DNA-incorporated iodine-125 in mammalian cells in vitro: double-strand breaks. *Radiat Res*, 149(2):134–141, Feb 1998.

[138] G. Wang, D. D. Levy, M. M. Seidman, and P. M. Glazer. Targeted mutagenesis in mammalian cells mediated by intracellular triple helix formation. *Mol Cell Biol*, 15(3):1759–1768, Mar 1995.

[139] J. F. Ward, W. F. Blakely, and Joner E. L. Mammalian cells are not killed by DNA single-strand breaks caused by hydroxyl radicals from hydrogen peroxide. *Radiat Res*, 103(3):383–92, Sep 1985.

[140] J. D. Watson and F. H. Crick. The structure of DNA. *Cold Spring Harb Symp Quant Biol*, 18:123–131, 1953.

[141] J. Wu, L. Y. Lu, and X. Yu. The role of BRCA1 in DNA damage response. *Protein Cell*, 1(2):117–123, Feb 2010.

[142] B. Xu, S.-T. Kim, D.-S. Lim, and M. B. Kastan. Two molecularly distinct G(2)/M checkpoints are induced by ionizing irradiation. *Mol Cell Biol*, 22(4):1049–1059, Feb 2002.

[143] M. Yamada and T. T. Puck. Action of radiation on mammalian cells. IV. Reversible mitotic lag in the S3 HeLa cell produced by low doses of x-rays. *Proc Natl Acad Sci U S A*, 47:1181–1191, Aug 1961.

[144] S. L. Young, S. H. Krawczyk, M. D. Matteucci, and J. J. Toole. Triple helix formation inhibits transcription elongation in vitro. *Proc Natl Acad Sci U S A*, 88(22):10023–10026, Nov 1991.

[145] R. Yuan, S. Fan, J. A. Wang, Q. Meng, Y. Ma, D. Schreiber, I. D. Goldberg, and E. M. Rosen. Coordinate alterations in the expression of BRCA1, BRCA2, p300, and Rad51 in response to genotoxic and other stresses in human prostate cancer cells. *Prostate*, 40(1):37–49, Jun 1999.

[146] J. J. Yunis, G. Frizzera, M. M. Oken, J. McKenna, A. Theologides, and M. Arnesen. Multiple recurrent genomic defects in follicular lymphoma. A possible model for cancer. *N Engl J Med*, 316(2):79–84, Jan 1987.

[147] U. Zimmermann, U. Friedrich, H. Mussauer, P. Gessner, K. Haemel, and V. Sukhorukov. Electromanipulation of mammalian cells: Fundamentals and application. *IEEE Transactions on Plasma Science*, 28(1), Feb 2000.

[148] H. Zola. High-sensitivity immunofluorescence/flow cytometry: detection of cytokine receptors and other low-abundance membrane molecules. *Curr Protoc Cytom*, Chapter 6:Unit 6.3, Nov 2004.

A. Curriculum Vitae

Der Lebenslauf ist in der Online-Version aus Gründen des Datenschutzes nicht enthalten.

B. Erklärung

Erklärung
Hiermit erkläre ich, gem. § 6 Abs. (2) f) der Promotionsordnung der Fakultäten für Biologie, Chemie und Mathematik zur Erlangung der Dr. rer. nat., dass ich das Arbeitsgebiet, dem das Thema „I-125-labeled Triplex-Forming-oligonucleotides: Studies on intracellular distribution, cytotoxicity and on gene expression alterations of target genes “ zuzuordnen ist, in Forschung und Lehre vertrete und den Antrag von Herrn Volker Dahmen befürworte und die Betreuung auch im Falle eines Weggangs, wenn wichtige Gründe dem entgegenstehen, weiterführen werde.

Essen, den _____	_____	_____
	Name d. wissenschaftl. Betreuers/Mitglieds der Universität Duisburg-Essen	Unterschrift d. wissenschaftl. Betreuers/Mitglieds der Universität Duisburg-Essen

Erklärung
Hiermit erkläre ich, gem. § 7 Abs. (2) c) + e) der Promotionsordnung der Fakultäten für Biologie, Chemie und Mathematik zur Erlangung des Dr. rer. nat., dass ich die vorliegende Dissertation selbständig verfasst und mich keiner anderen als der angegebenen Hilfsmittel bedient habe.

Essen, den _____	_____
	Unterschrift des Doktoranden

Erklärung
Hiermit erkläre ich, gem. § 7 Abs. (2) d) + f) der Promotionsordnung der Fakultäten für Biologie, Chemie und Mathematik zur Erlangung des Dr. rer. nat., dass ich keine anderen Promotionen bzw. Promotionsversuche in der Vergangenheit durchgeführt habe und dass diese Arbeit von keiner anderen Fakultät/Fachbereich abgelehnt worden ist.

Essen, den _____	_____
	Unterschrift des Doktoranden